On adaptive control and particle filtering in the automatic administration of medicinal drugs

Nicolò Malagutti

A thesis submitted for the degree of
Doctor of Philosophy at
The Australian National University

October 2013

This thesis is the result of my own original work during the period of my PhD degree at the Australian National University. All references to external sources and collaborations with colleagues have been duly acknowledged where applicable.

The following is a list of journal and conference publications which I have authored while I was enrolled in the PhD program at the Australian National University. A large part of the materials presented in this thesis is related to these publications.

Journal publications

- Bagnoli P, Malagutti N, Gastaldi D, Marcelli E, Lui E, Cercenelli L, Costantino ML, Plicchi G, Fumero R; "Computational finite-element model of cardiac torsion"; International Journal of Artificial Organs, 34(1):44-53, 2011.
- Malagutti N, Dehghani A, Kennedy RA; "Robust Control Design for Automatic Regulation of Blood Pressure"; IET Control Technology and Applications 9:387-396, 2012.
- Malagutti N; "Particle filter-based robust adaptive control for closed-loop administration of sodium nitroprusside"; International Journal of Computational Surgery; submitted July 2013, final version submitted October 2013, pending publication.
- Malagutti N; "Open-loop real-time estimation of propofol pharmacokinetics-pharmacodynamics using particle filtering"; Medical & Biological Engineering & Computing; submitted October 2013, pending review.

Conference publications

- Malagutti N, Dehghani A, Kennedy RA; "Safety issues in adaptive control systems for automatic administration of vasoactive drugs"; Proceedings of 18th IFAC World Congress, Milan, Italy, August 2011

- Malagutti N, Dehghani A, Kennedy RA; "Improved Robust Performance in a System for Automatic Administration of a Vasoactive Drug"; Proceedings of International Conference on Bio-inspired Systems and Signal Processing (BIOSTEC BIOSIGNALS) 2012, Vilamoura, Portugal, February 2012

- Malagutti N, Dehghani A, Kennedy RA; "A Robust Multiple-Model Adaptive Control System for Automatic Delivery of a Vasoactive Drug"; Proceedings of the 9th IASTED International Conference on Biomedical Engineering (BioMed), Innsbruck, Austria, February 2012

- Malagutti N, Dehghani A, Kennedy RA; "An approach to controlled drug infusion via tracking of the time-varying dose-response"; Proceedings of the 34th Annual International Conference of the IEEE Engineering in Medicine and Biology Society (IEEE EMBS), San Diego, CA, USA, September 2012

- Malagutti N, Hassani V, Dehghani A; "An adaptive multi-controller architecture using particle filtering"; Proceedings of the 4th Australian Control Conference (AuCC), Sydney, Australia, November 2012

Nicolò Malagutti
25 October 2013

Each problem that I solved became a rule which served afterwards to solve other problems.
- Rene Descartes.

Acknowledgments

I would like to take the opportunity to express my gratitude to my supervisory panel at the Australian National University for their guidance and advice throughout the PhD program. In apologising for my repeat offender behaviour when it comes to forcing long meetings, I thank Prof. Rod Kennedy and Prof. Brian Anderson for their patience and useful suggestions over many conversations about my research, even when these involved lengthy expositions of obscure biomedical topics. Thank you also to Dr Arvin Dehghani for facilitating my admission into the PhD program, Dr Parastoo Sadeghi, for her assistance with finding my research legs during the early stages of my work, and the Head of School, Prof. Thushara Abhaypala, for his help with ensuring that I always had an adequate workspace.

A truly special thank you goes to Dr Jochen Trumpf, who more than anyone else supported my research endeavour through a very difficult time. I would not have completed this thesis if it hadn't been for his frank advice and probing questions, and an uncommon generosity with his time.

I would also like to acknowledge the contribution of Dr Vahid Hassani of Istituto Superior Tecnico – Lisbon, with whom I developed a friendly and insightful collaboration in 2012, leading to the research work featured in Chapter 4 of this thesis. Vahid offered results and conceptual insights from his prior experience with the RM-MAC and RAC-EKF methodologies, which played an instrumental role in refining the RAC-PF concept.

My sincere thanks also go to the academics and Universities who hosted me on academic visits during my program: Prof. Antonio Pascoal from Istituto Superior Tecnico Lisbon, Prof. Maria Laura Costantino from Politecnico di Milano, Dr. Emanuela Marcelli from Universita degli Studi di Bologna and Prof. Bob Bitmead of the University of Southern California, for opening their doors to a clueless student and offering stimulating ideas and conversations. I also wish to thank the Computational Surgery International Network for their generous invitation to contribute to their symposium on haemodynamic management in December 2012.

Last but not least, I would like to thank my family: my wife Anne, my parents Marina and Marzio and my brother Tobia, for their encouragement, love and support throughout this academic journey and, in general, through life.

Abstract

Automatic feedback methodologies for the administration of medicinal drugs offer undisputed potential benefits in terms of cost reduction and improved clinical outcomes. However, despite several decades of research, the ultimate safety of many—it would be fair to say most—closed-loop drug delivery approaches remains under question and manual methods based on clinicians' expertise are still dominant in clinical practice. Key challenges to the design of control systems for these applications include uncertainty in pharmacological models, as well as intra- and interpatient variability in the response to drug administration. Pharmacological systems may feature nonlinearities, time delays, time-varying parameters and non-Gaussian stochastic processes.

This dissertation investigates a novel multi-controller adaptive control strategy capable of delivering safe control for closed-loop drug delivery applications without impairing clinicians' ability to make an expert assessment of a clinical situation. Our new feedback control approach, which we have named Robust Adaptive Control with Particle Filtering (RAC-PF), estimates a patient's individual response characteristic in real-time through particle filtering and uses the Bayesian inference result to select the most suitable controller for closed-loop operation from a bank of candidate controllers designed using the robust methodology of μ synthesis. The work is presented as four distinct pieces of research. We first apply the existing approach of Robust Multiple-Model Adaptive Control (RMMAC), which features robust controllers and Kalman filter estimators, to the case-study of administration of the vasodepressor drug sodium nitroprusside and examine benefits and drawbacks. We then consider particle filtering as an alternative to Kalman filter-based methods for the real-time estimation of pharmacological dose-response, and apply this to the nonlinear pharmacokinetic-pharmacodynamic model of the anaesthetic drug propofol. We ultimately combine particle filters and robust controllers to create RAC-PF, and test our novel approach first in a proof-of-concept design and finally in the case of sodium nitroprusside.

The results presented in the dissertation are based on computational studies, including extensive Monte-Carlo simulation campaigns. Our findings of improved parameter estimates from noisy observations support the use of particle filtering as a viable tool for real-time Bayesian inference in pharmacological system identification. The potential of the RAC-PF approach as an extension of RMMAC for closed-loop control of a broader class of systems is also clearly highlighted, with the proposed new approach delivering safe control of acute hypertension through sodium nitroprusside infusion when applied to a very general population response model. All approaches presented are generalisable and may be readily adapted to other drug delivery instances.

Contents

List of Figures

List of Tables

Chapter 1

Introduction

1.1 General overview of the research problem and its significance

Feedback systems are a fundamental part of the functioning of living organisms. A myriad of mechanical, electrical and chemical feedback loops exist and interact synergically to ensure *homeostasis*, that is, the preservation of appropriate (physiological) conditions for the survival and operation of complex biological entities. Examples of feedback systems in the human body include the regulation of blood pressure and flow in the cardiovascular system to ensure tissue perfusion, the light-dependent muscle reflex controlling the correct aperture of the pupil and the secretion of the hormone insulin by the pancreas to regulate the metabolism of glucose (an analysis of these and other physiological feedback examples can be found in Khoo [1999]). In many cases, the disruption of physiological feedback determines a state of disease. In the context of the previously cited examples, incorrect cardiovascular regulation may lead to a range of conditions, such as hypertension or cardiac decompensation; pupil reflex alteration may result in photophobia; and insulin secretion deficiencies are associated with type 1 diabetes. Medical intervention may be directed at restoring these loops, either by removing the cause of the disruption or by creating artificial loops to support or replace a missing function. A possible type of intervention is the administration of medicinal drugs, which we will consider as the overarching theme of this dissertation.

The process of administering a drug can itself be considered a closed-loop process. This may not be immediately apparent, as it is a common experience that a drug is taken with the expectation of achieving a pre-determined therapeutic effect. Even in cases of such open-ended administration, a clinical re-evaluation after the therapy would represent the event closing the therapeutic loop (a second course of the drug could be prescribed, for example, if required). In less trivial drug administration instances, however, actual titration processes are required, by which a dose is selected and adjusted over time depending on the observed effect on the patient. Most commonly, the role of the feedback controller is carried out by a clinical operator (such as a doctor or a nurse), who may employ their experience to combine the available qualitative and quantitative information about the patient's condition and

come to an appropriate dosing decision. In some cases, even the patient themselves may act as the controller, see, e.g., patient-controlled analgesia for pain management (Nikolajsen and Haroutiunian [2011]). There are drug administration instances, however, in which automatic feedback control may be deemed useful. Such applications typically involve patient monitoring and administration control over an extended period of time—where the ongoing presence of a clinician may be impractical—and/or in settings where human error may pose a significant risk. We cite here three of the most studied drug administration problems, which will be discussed in greater detail in the next section:

The administration of drugs to control cardiovascular parameters in the critical setting, e.g., vasodepressors to reduce blood pressure. Critical patients may exhibit frequent changes in their baseline condition and response characteristic, requiring ongoing monitoring and adjustment of the administered dose to ensure that a suitable target blood pressure is maintained while avoiding potentially dangerous hypotensive effects which could result from overadministration.

The administration of drugs which cause the loss of consciousness (hypnotic drugs) in the context of surgical procedures. The required administration profile may vary according to several factors, including the patient's individual rate of metabolic destruction of the drug, the intensity of the nociceptive stimuli and the duration of the procedure. Close monitoring and control of drug administration is required so that patients do not experience awareness of the procedure, but at the same time do not suffer from extended recovery times and/or other undesired effects of excessively deep anaesthesia.

The administration of insulin to diabetic patients. Insulin promotes the removal of glucose from the bloodstream and must be administered in patients with impaired glucose metabolism to prevent high glucose concentration (hyperglycemia) peaks to occur following food intake, as these may cause terminal damage to organs and tissues. Excessively low glucose concentrations (hypoglycemia) must also be avoided as they may be extremely debilitating to the point of sending the body into shock. Insulin dosing must be carefully managed throughout the life of the patient in order to maintain glucose level in the physiological range in the face of daily variations in meal times, content and sizes, as well as metabolic activity.

The problem of designing fully automatic solutions for closed-loop drug administration applications poses several relevant challenges. The relationship between the administered drug dose and the observed response can be described in terms of so-called pharmacokinetic-pharmacodynamic models, which are usually developed from population studies. When considering a population model, differences in the actual response may exist across individuals (interpatient variability) and even within one patient over time, as their condition evolves (intrapatient variability). In

many cases, this variability may be considerable. Dose-response models may also include nonlinearities and stochastic effects, including from non-Gaussian processes. Furthermore, the medical nature of the control task may impose strict constraints in terms of safety and performance requirements. In control engineering terms, the specifications of the drug administration problem as described translate into the problem of designing a feedback control architecture which should ensure closed-loop stability (robustness) and deliver the necessary performance in the face of parametric and non-parametric plant uncertainties of potentially large magnitude for a general class of systems, including time-varying systems.

The significance of this research lies first and foremost in its potential clinical impact. Successful implementation of closed-loop administration of medicinal drugs has the potential to improve patient outcomes through more reliable and accurate dosing, and a reduction in the risk of adverse events from incorrect administration or human error. Automatic systems taking care of repetitive dosing tasks would also allow for human resources to be more efficiently allocated to expert decisions, especially in environments where staffing may be an issue, thus reducing healthcare costs (Bailey and Haddad [2005]).

Beyond clinical applications, the methodological challenges associated with the engineering problem relate to the topic of robust adaptive control (RAC). RAC is defined as a feedback system capable of forcing an unknown time-varying plant to meet performance requirements while retaining adequate robustness properties and has been dubbed as akin to the *Holy Grail* of control engineering (Ioannou [2008]) due to its putative ability to solve a very broad range of control problems. RAC has been an active area of research for several decades and solutions have been proposed for selected categories of systems. One recently developed such methodology, which will be considered in this thesis, is Robust Multiple-Model Adaptive Control (RMMAC) (Fekri [2005]), a multi-controller architecture devised for RAC of linear-Gaussian plants. Although this thesis primarily focuses on the biomedical engineering problem, some of the methods adopted whilst seeking an approach suited to the more general drug delivery problem may provide an extension to existing RAC methodologies such as RMMAC.

1.2 A historical review of automatic drug delivery

The idea of devising systems for automatic closed-loop drug delivery is by no means new. The following subsections expand on the already mentioned key areas of research found in the literature. For each, we describe the control methods used and the results achieved.

Cardiovascular control

Cardiovascular control deals with the regulation of haemodynamic signals. A common application is the control of mean arterial pressure in patients experiencing

perioperative hypertension. This is achieved through the infusion of vasodepressor drugs such as sodium nitroprusside. Methods for closed-loop delivery of sodium nitroprusside were proposed as early as the late 1970s. Initially based on simple PID controllers (Sheppard [1980]), the approaches evolved to various adaptive control methods including self-tuning regulators (Mansour and Linkens [1989]), model reference adaptive control (Pajunen et al. [1990]) and multiple model adaptive control (He et al. [1986]; Martin et al. [1987]). A device reporting success in clinical trials in the late 1980s, named the IVAC Titrator, received market authorisation by the American Food and Drugs Administration but enjoyed little commercial success and was soon withdrawn from the market (Bequette [2007]). Later approaches based on adaptive predictive control (Yu et al. [1992]) and fuzzy logic (Ying and Sheppard [1994]) were also proposed, but these did not develop into a new device. The standard clinical practice for the management of perioperative hypertension is still based on manual control of drug infusion to this day (Varon and Marik [2008]).

In the last decade, joint control of blood pressure and flow using multiple drugs has been proposed, either with methods based on model predictive control (Rao et al. [2003]) or approaches based on fuzzy logic methods (Hoeksel et al. [1999]), which adopt rule-based control actions mimicking the clinicians' decision processes. While there is a clinical benefit in jointly controlling blood pressure and flow, there are also significant challenges given by the limited availability of dose-response models describing drug interactions and the very low accuracy of blood flow measurements. Uemura et al. [2006] have taken a different approach and sought to estimate a patient's cardiovascular response parameters such as vascular resistance and target those parameters through drugs, arguing that this could decouple the joint control problem. Their approach has a superior grounding in physiology but uses basic PI control for implementation and does not take into account the uncertainty in the model estimate arising from (potentially large) measurement errors. While all of the cited approaches have reported some successes in small research trials, to the author's knowledge, none are currently employed on a larger scale or have been developed into a commercial technology.

Control of anaesthesia

Anaesthesia control concerns the administration of a pharmacological agent to promote adequate insensitivity to external stimuli and pain, and loss of consciousness in patients undergoing surgery. Anaesthetic drugs may be administered in gaseous or intravenous form. Early attempts to achieve closed-loop control of gaseous anaesthetic were based on the assumption that exhaled drug concentrations would correlate with blood concentrations. The approaches were initially based on PID control (Ritchie et al. [1987]), and later improved by adopting adaptive predictive control (Jee and Roy [1992]). While these methods could achieve feedback regulation of blood drug concentrations, differences amongst individual patients in the concentration-effect relationship (pharmacodynamics) meant that the actual anaesthetic effect would not be dependable.

Direct measures of anaesthetic effect have since been developed, particularly brain activity-derived measures obtained from real-time processing of electroencephalographic signals. A commonly found measure in the literature is the proprietary *Bispectral Index* (BIS) developed by Aspect Medical Systems (Norwood, MA, USA) (Glass et al. [1997]). BIS-based anaesthesia monitors have become fairly widespread in operating theatres, where they assist anaesthesiologists in assessing the hypnotic state of patients. It has been proposed that BIS could be used as a target signal and a basis for closed-loop administration systems. Approaches based on PID control (Absalom et al. [2002]), adaptive control (Struys et al. [2001]) and, more recently, fuzzy logic control (Bailey and Haddad [2005]) have been developed. Generally good performance has been reported in tracking desired BIS values, including in some clinical trials (see e.g., Hemmerling et al. [2013]). Some unresolved issues remain, however. A key challenge lies in the fact that for the same measured BIS, depth of anaesthesia may vary amongst patients (Russell [2007]), and, as such, BIS is used by practitioners as a "guide" rather than a quantitative measure. This may only be resolved through proprietary research into improving the specificity of BIS (Russell [2013]). From a control perspective, methods based on BIS-only measurements may suffer from the converse problem of concentration only-measurements, whereby variability in pharmacokinetics may lead to inadequate transients (e.g., overshooting seen in Bailey and Haddad [2005]) as control actions are calibrated on an "average" model of drug distribution. Adaptive control based on combined pharmacokinetic-pharmacodynamic models could overcome this problem (this has been attempted in Gentilini et al. [2001] for gaseous drug isoflurane). However, non-gaseous anaesthetic agents (such as intravenous propofol) have become predominant in recent years and, for these, real-time blood concentration measurements remain difficult and inaccurate (Miekisch et al. [2008]). No automatic closed-loop devices are currently approved for the control of anaesthesia.

Glucose control in type 1 diabetes

The automatic infusion of insulin in diabetic patients has also received considerable research attention. As mentioned, the pancreas of type 1 diabetes patients cannot produce insulin and these patients must receive a carefully managed insulin infusion regimen to maintain normoglycemia. Unlike the previously cited examples, the control of insulin administration is a chronic application for life-long support of patients.

Research into closed-loop glycaemic control also started around the early 1980s, with a device for in-hospital research use (glycaemic clamping), named the Biostator, which was loosely based on a fixed administration rate for insulin and proportional control of dextrose infusion (Clemens et al. [1982]). Further developments in this field of application were stymied for many years by the absence of adequate sensor technologies for continuous glucose monitoring, which were not introduced until the mid 1990s (see Girardin et al. [2009] for a review of currently available approaches). A variety of algorithms have been proposed in recent years, including PID control

(Steil et al. [2006]), adaptive control (Eren-Oruklu et al. [2009]), model predictive control (Magni [2012]) and neural networks (El-Jabali [2005]). For detailed reviews on available control algorithms we refer the reader to Lunze et al. [2013] and El Youssef et al. [2009]. These methodologies have been tested in computational studies (in-silico) and through a number of small-scale clinical in-vivo trials where they are used to control wearable insulin pumps (see, e.g., Hovorka et al. [2011]). While these experimental results have been positive, the current state of the art of individualised insulin infusion technology remains limited to open-loop systems, in which the algorithms provide alerts and decision support but it is the patient or clinician who ultimately decides on going ahead with the infusion of a particular insulin dose. Lunze et al. [2013] cite safety reasons as pivotal to this and list a number of ongoing challenges in this application, including the presence of model disturbances in the form of metabolic changes (daytime/nighttime, rest/activity, etc.) and interindividual differences, the use of insulin alone as a single-input control action in a complex system, and the limited lifespan of available continuous blood glucose measurement sensors (currently limited to a few days and requiring frequent recalibration).

Robustness and verifiability: the missing pieces

The above review raises a number of relevant considerations, which have informed the development of this thesis. Firstly, it is remarkable that despite a long period of ongoing investigations and promising results in clinical research publications, closed-loop methods for automatic drug administration have not yet been embraced by the medical community and manual control remains, to date, the standard of care in the clinical setting. A number of barriers of a regulatory and financial nature have been named as delaying factors to the marketing of closed-loop technologies (as discussed in Bequette [2007]; Doyle et al. [2011]), but it is also evident that significant control challenges still exist. Indeed, Doyle et al. [2011] have concluded a recent review of the state of the art of biological systems control by stating that *"Success in the development of [...] closed-loop biomedical devices, will be contingent on the development of robust, verifiable advanced control algorithms"*.

The closed-loop methodologies applied to drug delivery problems have followed the historic developments of control approaches: traditional PID control initially, then adaptive control during the 1980s and 1990s, and model predictive control and fuzzy-logic/artificial intelligence methods in more recent years. The shift towards adaptive methods highlights, across the board, the critical nature of the challenge posed by variability in the dose-response process. It is also notable that robust control methods, also developed in the 1980s and 1990s (Zhou et al. [1995]), are rather unrepresented in the drug delivery literature, although there are a few exceptions (usually with limited or no clinical testing see e.g., Dumont et al. [2009] for closed-loop administration of propofol and Parker et al. [2000] for insulin control). We suggest that this may be due to the fact that robust approaches are traditionally single-controller and therefore unlikely to be able to deliver clinically adequate closed-loop performance in the presence of large population variability. In light of the absence of a definitive

solution for drug delivery problems, it appears natural that the viability of emerging new multi-controller robust adaptive control techniques, such as the previously cited RMMAC (Fekri [2005]), should be investigated.

Furthermore, the review highlights the importance of, and the challenges associated with, performing informative measurements in biological systems. Measurements are a fundamental part of feedback control system and this is a key reason why most contemplated closed-loop solutions relate to contexts where a high number of sensors can be connected to a patient in a protected environment (such as the operating room or intensive care ward). As recognised in Doyle et al. [2007], improved sensor technology would greatly advance feedback control for biological processes. In current practice, even when measurements are available, they may be infrequent, sparse with respect to the complexity of the underlying process, and/or affected by large measurement errors. The risk that these limitations may lead to an incorrect response from an adaptive feedback controller for drug delivery has not been well studied. Also, the use of adaptation algorithms which may be perceived as being too complex or "hidden" to the operator makes it difficult for the clinician to verify, in real-time, that the system is taking clinically appropriate action. These are major issues which, in our view, have limited clinicians' ability to place trust in automatic closed-loop drug administration systems as proposed thus far.[1]

1.3 Outline of the thesis and key contributions

This dissertation seeks to investigate a novel approach to the problem of closed-loop drug administration by addressing the key engineering drivers of robustness and verifiability, which translate into safety and transparency requirements from a medical perspective. The end result of this research is a methodology which we name Robust Adaptive Control with Particle Filtering (RAC-PF). RAC-PF is a multi-controller approach which features a bank of linear controllers computed using the $\mathcal{H}_\infty$ robust technique of μ synthesis to cater for nonparametric uncertainty as well as intrapatient and interpatient parametric variability in the dose-response characteristic for a particular drug. Controller selection is determined on the basis of the result of a Bayesian inference process conducted through a real-time particle filtering algorithm, which uses available measurement data to estimate the probability distribution of an individual patient's response parameters. The proposed advantages of such a system are a conservative approach to individualised therapy, owing to the use of robust control methods, and the fact that the probability distribution result delivered by the particle filter is available to the operator, thus making it possible to verify the dependability of the estimate of the individual response.

The research is presented as four distinct yet related items of work. These follow from each other as conceptual steps in the development of RAC-PF, but may be read individually if desired. The chapters of the thesis, their content and main

[1] These concerns have been expressed on multiple occasions in personal communications between the author and several specialist intensivists and anaesthesiologists.

contributions are described in the following.

Chapter 2 considers the problem of automatic administration of sodium nitroprusside and applies the RMMAC architecture to the feedback control of mean arterial pressure. In a simulation study which assumes a very general model for the dose-response characteristic, we present a comparison between RMMAC and two other adaptive control architectures taken from the literature. Key results of this chapter are evidence of undesirable closed-loop behaviour from past approaches when assumptions on time-varying parameters and the nature of baseline disturbances are relaxed, and a demonstration of the ability of RMMAC to deliver safer control.

Chapter 3 investigates the use of a particle filter for the real-time estimation of pharmacokinetic-pharmacodynamic model parameters in relation to the administration of the intravenous anaesthetic drug propofol. In a Monte-Carlo simulation study based on population models, we compare the quality of the inference achievable through a variety of measurements such as the bispectral index (BIS) and blood concentrations, including inaccurate concentration measurements. A key result of this chapter is the demonstration of the viability of particle filters for the purpose of conducting real-time Bayesian inference on pharmacological systems in the presence of measurement errors, including non-Gaussian-distributed errors. Our findings also indicate that the incorporation of breath propofol measurements in anesthesia management systems, despite the intrinsic inaccuracy of breath-based measurement techniques, would inform better individualised therapy than current BIS-only approaches.

Chapter 4 introduces the new RAC-PF methodology and applies it to a non-clinical test bench case: the feedback control of an uncertain linear parameter-varying mass-spring-dashpot system. We conduct a Monte-Carlo simulation study to evaluate the level of performance delivered by RAC-PF when compared with two other controller selection algorithms for multi-controller architectures. We compare RAC-PF with a method based on extended Kalman filtering (Hassani [2012]) and an ideal (nonrealistic) approach capable of perfect identification. The key result of this chapter is that, for the time scale and state dimension of the problem considered, RAC-PF is computationally tractable and can match the performance of the best available multi-controller methods in the literature. For mixed linear/nonlinear problems, we also introduce a marginalised particle filter formulation which can reduce the computational cost of the algorithm.

Chapter 5 returns to the problem of sodium nitroprusside administration discussed in Chapter 2 and applies the RAC-PF approach to it. The performance of the new approach is tested in an extensive Monte-Carlo simulation campaign, in which virtual patients are drawn from population distributions for the uncertain dose-response parameters and a variety of disturbance intensities and parameter

variation trends are used to challenge the feedback control system. The key result of this chapter is the ability of RAC-PF to deliver safe control of mean arterial pressure as demonstrated throughout the simulation campaign.

Chapter 6 summarises the work, lists the key findings of the previous chapters and discusses directions for future research.

Appendices A and B are also provided. These provide further details on the computational implementation of the RAC-PF method in the Matlab/Simulink environment for the interested reader and describe the additional digital resources attached to this thesis.

Chapter 2

Robust control design for automatic regulation of blood pressure

This chapter presents a solution to the problem of closed-loop administration of sodium nitroprusside (SNP) for the control of mean arterial pressure (MAP) based on Robust Multiple-Model Adaptive Control (RMMAC). In doing so, it describes the SNP dose-response model as well as a structured methodology for the design of multiple robust controllers, which will be drawn on in later chapters. The focus of this chapter is the development of a closed-loop system which can deliver satisfactory MAP control performance in the presence of broad parametric uncertainty in the dose-response. We introduce some adaptations to the original RMMAC architecture, in particular to cater for the existence of long, uncertain input time delays. We detail the operation of the RMMAC methodology and compare the results with those of two earlier approaches for the regulation of MAP. Our findings expose potential risk concerns arising from non-robust designs and highlight the value of RMMAC as a method which can deliver robust stability and performance, for all foreseeable parametric combinations, where the model of the controlled system can be deemed linear.

The content of this chapter closely follows the author's research paper *Robust control design for automatic regulation of blood pressure (Malagutti et al. [2013])*. Section 2.1 provides a brief summary of the SNP control literature and expands on some of the concepts introduced in Chapter 1; Section 2.2 provides an outline of the patient model and the control problem; Section 2.3 describes the proposed control architecture; Sections 2.4 and 2.5 describe and provide the results of the numerical simulations; Section 2.6 analyses the results and raises possible directions for further research.

2.1 Background

The cardiovascular system is essential to the life of the human body. It is a hydraulic system which utilises blood as its working fluid and, as such, can be characterised in terms of pressure and flow. Only a relatively narrow range of MAP and cardiac

output (CO) values are compatible with life and, under normal (physiological) conditions, the human body is equipped with internal control systems to maintain a suitable and steady operating point in the face of external stimuli. In patients whose autonomic regulation is impaired or insufficient, medical intervention is required to ensure that the system does not drift away from the physiological range for MAP and CO. This is generally achieved by intravenous infusion of suitable drugs.

This chapter focuses on the vasoactive drug sodium nitroprusside (SNP) and its use in the management of acute hypertension (a temporary state of dangerously elevated MAP) in peri-operative and intensive care settings (Varon and Marik [2008]). SNP is a vasodilator, i.e., a drug which causes the tension in the walls of arterioles to be reduced, thereby lowering blood pressure. It is fast-acting and is powerful enough to cause dangerous hypotension and/or cyanide toxicity if overdosed (He et al. [1986]). Significant variability (up to 30-fold, according to Slate et al. [1979]) in sensitivity to the drug exists among different patients and the sensitivity can even change for one patient over time. Close monitoring by nursing staff and regular "titration" (adjustment) of the dose depending on the patient's response are therefore required to achieve the clinical goals of lowering MAP and ensuring patient safety.

The repetitive, time-consuming nature of the MAP monitoring and SNP dose adjustment tasks is such that an automatic feedback control approach could bring benefits in terms of improved patient outcomes and lower clinical costs (Bailey and Haddad [2005]). The dose-response model for SNP, however, is characterised by time delays, modelling uncertainty, potentially time-varying parameters and output disturbances (Slate et al. [1979]), rendering the MAP regulation problem a challenging one from an engineering perspective. Clinically desirable control performance cannot be achieved with a single-controller feedback control approach and this has been recognised by several authors, leading to a variety of adaptive control strategies being proposed over the last three decades (a number of these have been cited in Chapter 1; we also recommend Yu [2006] and Isaka and Sebald [1993] for a comprehensive review). Closed-loop SNP administration is also the only closed-loop drug adminstration problem for which a fully automatic solution was ever commercialised: the IVAC Titrator device (IVAC Corporation, San Diego, CA, USA) was first marketed in 1987. Despite clinical trials with the Titrator showing its potential to deliver better outcomes than manual control (Cosgrove et al. [1989],Bednarski et al. [1990],Chitwood et al. [1992]), the device was withdrawn from the market shortly after its introduction. Bequette [2007] analyses the failure of this unique device and highlights cost and regulatory reasons as key to its demise. However, it is remarkable that, over two decades later, no alternative devices have been developed and operator-based control of drug infusion still remains the standard of care in the clinical setting.

We have considered whether there may be residual safety concerns associated with the models used, or particular features of the operation of proposed approaches, which would make clinical operators uncomfortable with reliance on automatic administration as it has been proposed thus far. In earlier work (Malagutti et al. [2011]), we analysed the approach of Martin et al. [1987] and advocated caution against possible instances of undesirable behaviour which we were able to simulate under par-

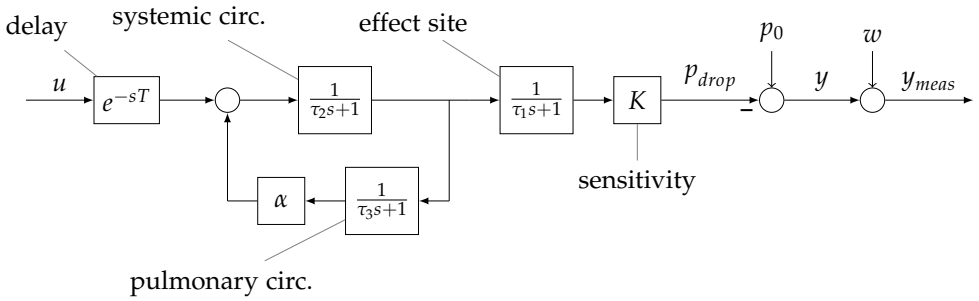

Figure 2.1: Block description of the patient model (open-loop plant). Notation: u input signal (drug infusion rate); T pure delay constant; τ_1, τ_2, τ_3 time constants; α recirculation fraction; K sensitivity (gain) parameter; p_{drop} MAP drop due to u; p_0 patient's natural MAP in the absence of pharmacological intervention; y output MAP; w measurement noise; y_{meas} actual measured MAP.

ticular operating conditions characterised by the presence of time-varying patient parameters and a range of disturbances including non-zero-mean signals.

This chapter considers the possibility of using RMMAC (Fekri et al. [2006]), a recent result in the area of adaptive control, to achieve safe feedback control of SNP infusion. RMMAC has been developed to conduct feedback control of linear time-invariant (LTI) systems. It features robust techniques for controller design (μ synthesis) and a Kalman filter-based approach for on-line model estimation. RMMAC can cater systematically and explicitly for modelling uncertainty (an inherent characteristic of all pharmacological models), as well as incorporate performance constraints on input and output signals. We deem these to be key advantages of this methodology in the context of drug delivery applications. We seek to investigate whether RMMAC can provide a general platform for the development of safer and thus more clinically viable automatic drug delivery technology.

2.2 Problem description

2.2.1 Patient response model

An experimentally validated model of a patient's response to SNP is given by the transfer function of equation (2.1) (Martin et al. [1987], modified from Slate et al. [1979]). A block diagram representation is shown in Figure 2.1.

$$\frac{P_{drop}(s)}{U(s)} = e^{-sT} \frac{K(\tau_3 s + 1)}{((\tau_3 s + 1)(\tau_2 s + 1) - \alpha)(\tau_1 s + 1)} \tag{2.1}$$

This third-order linear, open-loop stable, single-input single-output (SISO) model consists of three compartments modelled as first-order linear systems representing the systemic circulation, the pulmonary circulation and the drug effect site. An internal loop exists to account for recirculation of the drug within the cardiovascular system. A pure time delay effect is observed at the input. In accordance with Martin

et al. [1987], we assume the time constants to be known and time-invariant (τ_1=50s, τ_2=10s, τ_3=30s) and consider a large range of variability for the the patient's gain factor $K \in [0.25, 9.5]$mmHg·hr·ml^{-1} (this range sensitivity corresponds to a SNP concentration of 200μg/ml) and the time delay parameter $T \leq 50$s. In the interest of model generality, we also assume considerable variability in the recirculation constant $\alpha \in [0.25, 0.75]$.[1] We note that although the time constants are assumed fixed, changes in α can shift the position of the system poles. The extent of intrapatient variability is not well documented in the literature but, from clinical data published in Meijers et al. [1997], we extrapolated that up to a four-fold change in sensitivity over one hour could be expected in patients undergoing cardiac surgery. As we were unable to locate information on time-variability of the other two variable parameters, we assume here the maximum expected rate of change for T and α to correspond to variations spanning the full range of variability over one hour. To the authors' knowledge, the above combination of parametric uncertainty and time-variability results in the most general description ever adopted for the SNP response model.

2.2.2 Signals and sampling rate

The system receives a control signal u at the input, i.e., the drug administration rate in ml/hr, and exhibits a MAP drop p_{drop} at the output. This differs from the output of the system y, which is given by the affine transformation $y = p_0 - p_{drop}$, where the offset term p_0 represents the patient's "natural" value of MAP when no drug is administered. It is important to note that in many past adaptive control approaches p_0 has been deemed measurable (at time $t = 0$s) and constant or, at most, affected by broadband random noise. This is a convenient description for control design purposes, however, it is not realistic from a clinical perspective. Indeed, breathing and renin-angiotensin activation have been recognised as potential disturbances in Slate et al. [1979]. Perioperative events including surgical trauma and the concurrent administration of other drugs are also mentioned in Martin et al. [1992]. In this work, p_0 is modelled as an arbitrary signal with a mainly low-frequency spectrum (as detailed in Section 2.3.1).

The actual measured output signal y_{meas}, as shown in Figure 2.1, is given by the combination of signal y and noise w, which describes both beat-by-beat fluctuations in MAP and the errors associated with the acquisition and processing of the signal from the patient. Upon analysis (not shown here) of a number of MAP traces from real intensive care patients obtained from the MIMIC II database (Saeed et al. [2011]), we have deemed white Gaussian noise with a standard deviation of 2mmHg to be a suitable model for w. This choice is consistent with the assumptions of other authors (Martin et al. [1986], He et al. [1986], Pajunen et al. [1990]).

A final remark concerns the use of continuous-time models and methods when MAP is a quantity that cannot be measured continuously. A meaningful sampling rate must be determined for the operation of the proposed control system. In order to operate with a realistic signal, we treat y_{meas} as a discrete-time signal with a

[1] Notation: $x \in [a, b] \equiv a \leq x \leq b$.

sampling time of 2s. From a clinical implementation perspective this would mean obtaining MAP as a stepwise signal given by the average of arterial pressure (such as would be measured continuously by an intra-arterial catheter) over each heart beat, where a heart beat can be defined, for example, as the time between repeated features of an electrocardiogram recording or by another equivalent measure. Such a signal retains as much dynamic information about MAP as possible and is not monitoring equipment-specific. The time delay introduced by the required signal processing operations (1 beat) is also negligible when compared with the system's own large time delay. Since heart rate varies in patients, in order to work with a data stream with uniform step lengths we consider y_{meas} as a downsampled version of the previously described signal according to a sampling rate $f_s = 0.5$Hz (thus implying that no loss of MAP information would occur as long as a patient exhibits a heart rate $\geq$ 30bpm). The dynamics of the patient response for frequencies in excess of 10^{-1}Hz can be deemed negligible, therefore we consider f_s to be fast enough to allow us to adopt continuous-time methods for controller synthesis.

2.2.3 Control performance requirements

The following performance requirements apply (Malagutti et al. [2012b]):

- a settling time of preferably 10 minutes or less, but no more than 15 minutes;
- MAP should be contained within $\pm$5mmHg of the desired set-point value when in steady state operation, $\pm$10mmHg otherwise;
- temporary deviations from the above range may occur, but under no circumstances should the system display resonant (persistent oscillatory) or unstable behaviour or cause MAP to drop below a pre-determined danger threshold (set at 60mmHg for the purpose of this work);
- to ensure that SNP toxicity is prevented, the infusion rate should not exceed a pre-determined value. We consider an upper limit for the drug infusion rate of $3\text{ml}\cdot\text{kg}^{-1}\text{hr}^{-1}$ (He et al. [1986]);
- high-frequency dynamics in the control signal should be limited since drug delivery is generally provided through mechanically actuated infusion pumps, which are likely to suffer from actuator slew rate limitations.

2.3 Control architecture

In Figure 2.2, we show the block diagram of the Robust Multiple-Model Adaptive Control architecture for this drug delivery application. In a multiple-model adaptive control system, it is assumed that the behaviour of the controlled plant (response of patient MAP to SNP) can be matched at any time by that of one of a series of candidate models included in a model bank. A suitable controller designed for the

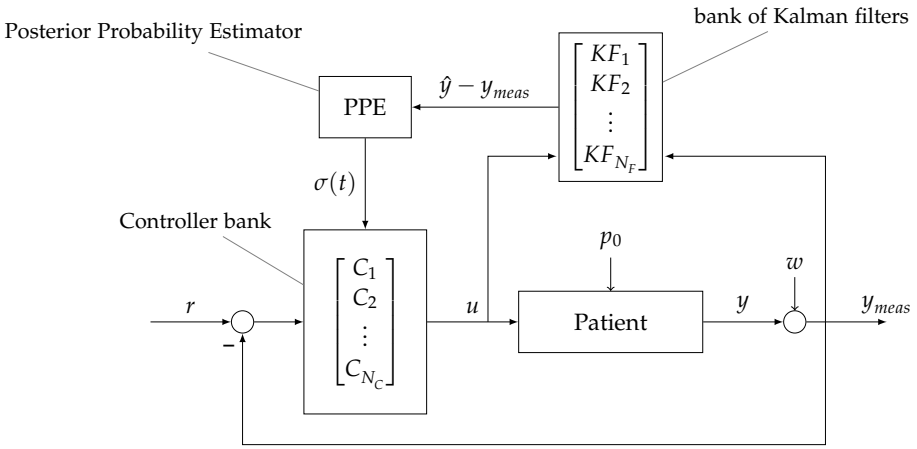

Figure 2.2: RMMAC architecture. Notation: r reference signal (desired MAP value); $C_{1,\ldots,N_C}$ candidate controllers; u control signal (drug infusion rate); p_0 patient's natural MAP; y output MAP; w measurement noise; y_{meas} measured MAP; $KF_{1,\ldots,N_F}$ Kalman filters; $\hat{y}$ KF estimate of MAP output; $\sigma(t)$ controller switching signal.

best-matching model is placed in the feedback loop, where it is expected to yield satisfactory performance. A common issue with multiple-model methods is the determination of the breadth of the uncertainty space which the models need to cater for and the number of models required to achieve this. An advantage of RMMAC is that the choice of the models to be included in the bank naturally follows from the controller design process. In RMMAC, controllers are designed for robust performance using μ synthesis; the operation of matching the real plant with the best candidate model involves the use Kalman filters and a probability estimator.

2.3.1 Controller design

Modelling for robust design

A comprehensive block diagram for the model is shown in Figure 2.3. It includes a description of parametric uncertainty for the gain and recirculation parameters:

$$\alpha = 0.5 + 0.25\delta_1, \quad K = K_{nom} + K_r\delta_2, \quad \delta_1, \delta_2 \in \mathbb{R},\ |\delta_1| \leq 1,\ |\delta_2| \leq 1,$$

following the assumptions that $\alpha = (0.5 \pm 0.25)$ and $K = (K_{nom} \pm K_r)$ where K_{nom} is the nominal sensitivity value and K_r is half the width of the uncertainty range.

Delay is treated as an unmodelled dynamic of the system. The worst-case delay is $T = 50$s and neglecting it would introduce a multiplicative modelling error of $e^{-sT} - 1$. This error can be bounded by the high-pass transfer function $W_{um}(j\omega)$ as shown in Figure 2.4. The block surrounded by the dotted box in Figure 2.3 has transfer function

$$1 + \Delta_{um} \cdot W_{um}, \quad \Delta_{um} \in \mathcal{H}_\infty, \quad \|\Delta_{um}\|_\infty \leq 1$$

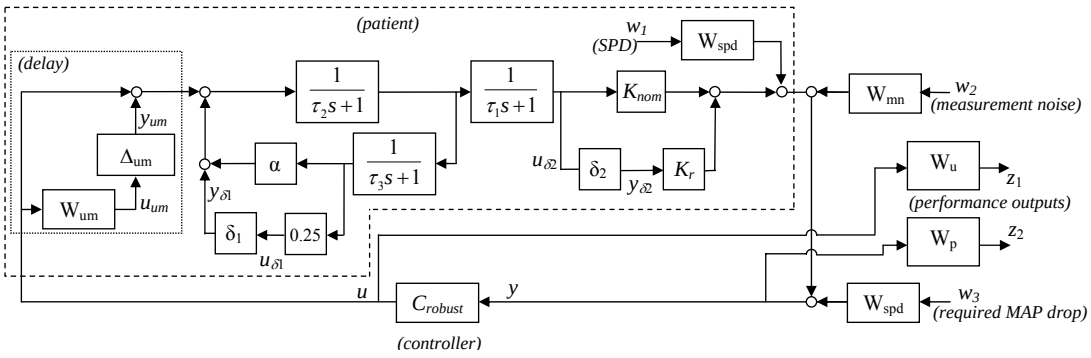

Figure 2.3: The system model used for the robust controller design.

and is an effective conservative representation of all possible patient delay dynamics for $T \leq 50$s.

The structure of Figure 2.3 represents the system description used for controller design. A signal called set-point disturbance (SPD) is added to the output of the plant and represents the possible variations in p_0 as discussed in Section 2.2. SPD is assumed to be a predominantly low-frequency signal and is generated using an arbitrary signal ($w_1 : \|w_1(j\omega)\|_\infty \leq 1$) filtered by a low-pass system with transfer function $W_{spd}(j\omega)$ (Table 2.1). This corresponds to admitting MAP fluctuations occurring at a maximum rate of approximately 10mmHg/min, which we deemed a suitably large rate of change in the interest of model generality. The same filter is also used as a command prefilter for the reference signal ($w_3 : \|w_3(j\omega)\|_\infty \leq 1$), which is set by the clinician (we presume this will be a step-wise signal) and specifies the required MAP drop. While a prefilter may not be strictly necessary for this application in which reference changes are likely to be few and infrequent, we must define a frequency-domain bound for exogenous signals for the purpose of using μ synthesis for controller design. The enforcement of such bound through a prefilter ensures that the design assumptions are not violated in practice. The transfer function $W_{spd}(j\omega)$ is a suitable bound/prefilter for the reference since it has a steady-state gain of 32dB and a range of $\pm$40mmHg from baseline can be deemed sufficient to cover all possible setpoint requirements. Its pole location also corresponds to a settling time of less than 10min, which complies with the performance requirements of Section 2.2.3 in terms of command following. We remark that there is no specific reason other than computational convenience behind our decision to use W_{spd} as both a disturbance colouring filter and a command prefilter. Measurement noise is modelled as a random gaussian signal w_2 filtered by the high-pass filter W_{mn} (Table 2.1).

Two weighting transfer functions are also included to reflect the performance requirements for the system. These are essential for controller synthesis as will be discussed in the next subsection. The weighting function W_p is the performance weight applied to the error signal ($W_p : \|W_p Y(j\omega)\|_\infty \leq 1$); it imposes a maximum error of 6dB ($\pm$2mmHg) at steady state and 22dB ($\pm$12.5mmHg) at higher

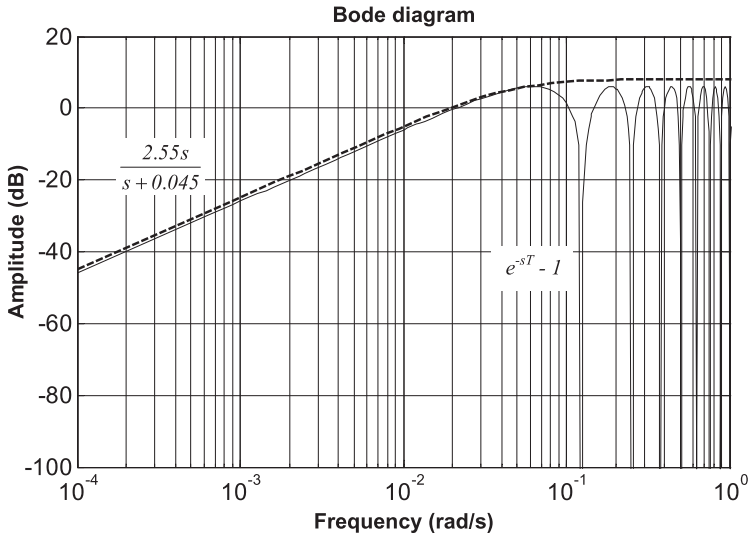

Figure 2.4: Magnitude bode plot of the upper bound W_{um} (dashed) for the multiplicative modelling error (solid) introduced by treating delay as an unmodelled dynamic.

frequencies. The weighting function W_u places constraints on the control signal ($W_u : \|W_u(j\omega)U(j\omega)\|_\infty \leq 1$) in terms of maximum amplitude at low frequency (200ml/hr, roughly equivalent to the toxicity threshold for a 65kg patient) and penalises high-frequency control dynamics.

Controller design via μ synthesis

The new controllers were obtained using the technique of mixed-μ synthesis. In the interest of brevity, we refer the reader to Zhou et al. [1995] for a detailed description of μ synthesis. For the scope of this exposition, it will be sufficient to explain that the *structured singular value* μ—a commonly used tool in $\mathcal{H}_\infty$ optimal control—is defined as

$$\mu(\mathcal{M}(j\omega)) = \sup_{\omega\in\mathbb{R}^+} \frac{1}{\inf\limits_{\Delta(j\omega)} \{\overline{\sigma}(\Delta) : \det(I - \mathcal{M}\Delta) = 0\}}, \tag{2.2}$$

where $\overline{\sigma}$ indicates the maximum singular value and the $\mathcal{M}$–Δ structure is a particular form of the interconnected system as shown in Figure 2.5. In our particular setting

$$\Delta = \begin{pmatrix} \delta_1 & 0 & 0 & 0 \\ 0 & \delta_2 & 0 & 0 \\ 0 & 0 & \Delta_{um} & 0 \\ 0 & 0 & 0 & \Delta_p \end{pmatrix}, \text{ where } \begin{cases} \Delta_p \in \mathbb{C}^{3\times 2} \\ \|\Delta_p\|_\infty \leq 1 \end{cases}.$$

In plain language, μ represents the inverse of the minimum increase in plant uncertainty which would result in the system being unable to meet the required specifications with a particular controller C in the loop. A result derived from the

Table 2.1: Transfer function reference table

Block name	Transfer function	Purpose
W_{um}	$\frac{2.55s}{s+0.045}$	unmodelled dynamics bound
W_{spd}	$\frac{40}{(125s+1)^2}$	SPD and reference filtering
W_{mn}	$\frac{s}{0.25s+0.075}$	Measurement noise filter
W_p	$\frac{(700s+1)^2}{(2500s+1.4)^2}$	Weighting TF (output signal)
W_u	$\frac{20s+200}{80s+1}$	Weighting TF (control signal)

small gain theorem states that the system is capable of providing robust performance if $\mu \leq 1$ (Gu et al. [2005]).

The μ synthesis approach to controller design involves an iterative search, among the set of stabilising controllers C_s, to identify the controller which achieves the largest robustness margin, i.e., the smallest value of μ.

$$\inf_{C \in C_s} \sup_{\omega \in \mathbb{R}^+} \mu(\mathcal{M}(j\omega)) \tag{2.3}$$

Software tools for μ synthesis are available as part of the Matlab Robust Control Toolbox.[2] *Mixed-*μ synthesis, which we use, is an extension of the μ synthesis algorithm which can account for the fact that the uncertainty space of some of the parameters is real and not complex. This reduces, to some extent, the conservativeness of the resulting controller design.

Controller design results

The μ synthesis method can be used in an iterative fashion in order to establish how many robust controllers are actually required in order to meet the specifications of the control problem. Following the approach of Fekri et al. [2006], we programmed an iterative Matlab algorithm to determine the maximum achievable performance of the system as a function of the range of plant uncertainty considered. Achievable performance is rated according to a scalar parameter A_p which multiplies the performance weight, i.e., $W_p^* = A_p \cdot W_p$. The algorithm operates as follows:

1. set $A_p = 1$;
2. set up the interconnected system of Figure 2.3, include the required range of uncertainty and use W_p^* as the performance weight on the error signal;
3. run the mixed-μ synthesis tool on the system generated at step 2;
4. if the value of μ is just below unity ($0.985 \leq \mu \leq 1$), A_p is deemed to represent the maximum achievable performance and the controller synthesised at step 3 can ensure that performance level is met, otherwise, A_p is increased or decreased as required and another iteration (starting at step 2) takes place.

[2] Matlab®is a numerical computing environment developed by The Mathworks, Natick, MA, USA.

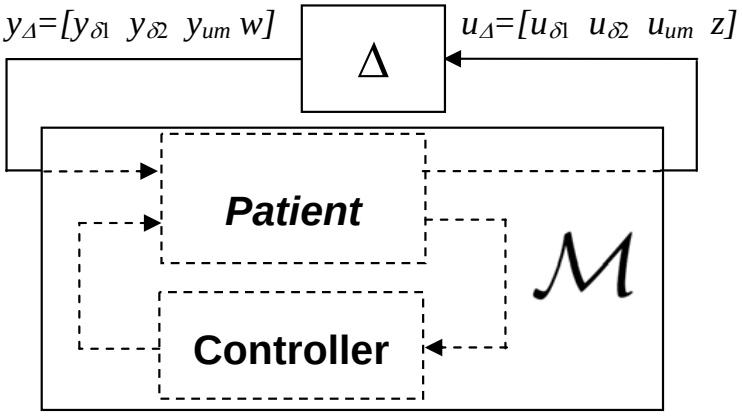

Figure 2.5: $\mathcal{M}$–Δ interconnected structure for μ synthesis. Note $w = [w_1\ w_2\ w_3]$, $z = [z_1\ z_2]$

As the performance weights W_p and W_u represent the required minimum performance for the system, a final value of $A_p \geq 1$ means that a controller exists such that the system can exceed the requirements, while $A_p < 1$ indicates that μ synthesis cannot produce a suitable controller to meet the required performance over the considered uncertainty set.

All runs of the algorithm included the full complex uncertainty introduced by delay and the full range of real parametric uncertainty associated with the recirculation constant α, while a variety of subsets of the uncertainty set of K were considered. This was done to obtain comparable results with multiple-model approaches in the literature such as He et al. [1986] and Martin et al. [1987], where K is considered to be the only varying parameter.

Figure 2.6 shows the three fundamental design cases which we used to evaluate a trade-off between the number of controllers and the maximum achievable A_p as a function of the breadth of the uncertainty subset of K considered:

- a global non-adaptive robust controller (GNARC), i.e., a controller able to provide robust performance over the full uncertainty range of K. The maximum A_p achieved was 0.026, indicating that a single-controller architecture would not meet the requirements of this problem;
- fixed non-adaptive robust controllers (FNARCs), i.e., multiple controllers (ideally, infinitely many), each designed to maximise performance for a point value of K (no uncertainty on K). The results of this design case are representative of the maximum achievable performance with a multiple-controller system. It is clear from the graph in Figure 2.6 that such an ideal system would be able to meet and even significantly exceed the required level of performance, more notably so in the high-K region of the uncertainty range;
- local non-adaptive robust controllers (LNARCs), i.e, controllers capable of providing satisfactory performance over non-infinitesimal subsets of the uncertainty space of K. This design case represents the "middle ground" between

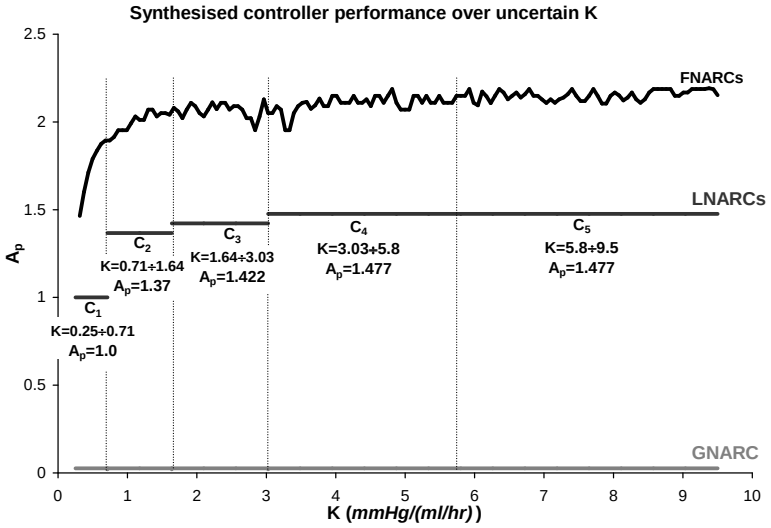

Figure 2.6: Results of GNARC, FNARC and LNARC controller design instances. The graph shows the maximum achievable performance A_p as a function of the uncertainty range of K considered.

the GNARC and the FNARCs. A controller design covering a larger uncertainty subset will result in a system with inferior performance. It is up to the designer, therefore, to strike a suitable compromise between controller bank complexity (number of controllers) and system performance (maximum A_p). In the results shown, we defined suitable performance as either $A_p = 1$ (the minimum required) or 60% of the minimum FNARC over the corresponding uncertainty subset, whichever the greatest. Five controllers were required to cover the whole uncertainty range of K.

2.3.2 Patient-model matching and controller selection

The actual behaviour of the system is matched to that of one of a number of candidate models using a bank of Kalman filters and a posterior probability estimator (Figure 2.2). Each Kalman filter uses information from the input signal $u(t)$ and measured output $y(t)$ to generate a one-step-ahead estimate of the state $\hat{x}_i(t+1)$ and corresponding output $\hat{y}_i(t+1)$ on the basis of the ith candidate model ($i \in \{1, 2, ..., N\}$) through a predict-update cycle as shown below:

predict cycle:

$$\begin{aligned} \hat{x}_i(t+1|t) &= A_i\hat{x}(t) + B_iu(t) \\ \hat{y}_i(t+1|t) &= C_i\hat{x}(t|t-1) \end{aligned} \tag{2.4}$$

update cycle:

$$\begin{aligned} r_i(t+1) &= y(t+1) - \hat{y}(t+1|t) \\ \hat{x}(t+1|t+1) &= \hat{x}_i(t+1|t) + Hr_i(t+1) \end{aligned} \tag{2.5}$$

where the notation $\hat{a}(t+1|t)$ indicates the estimate of signal a at time $t+1$ using

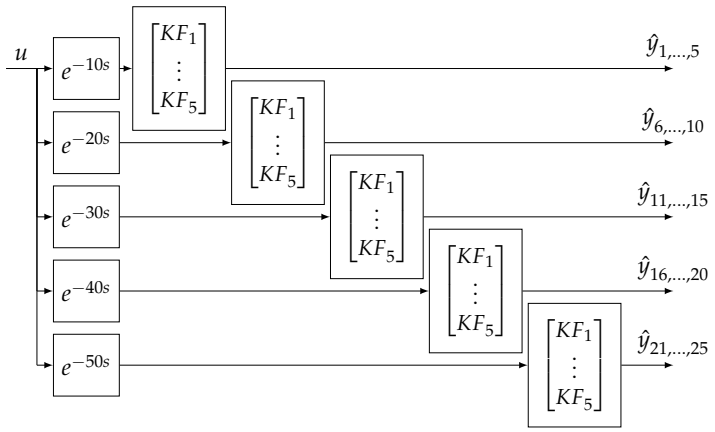

Figure 2.7: Redundant Kalman filter bank structure to cater for the uncertain delay term.

information available up until time t; r_i is the residual signal given by the difference between the estimate and the actual observed output; A_i, B_i and C_i are the state-space matrices describing the ith model; H is the Kalman filter innovation gain. In order to reproduce the approach of Fekri et al. [2006], a steady-state formulation for the Kalman filter was used for the purposes of the work described here. This means that H was determined *a priori* on the basis of knowledge of the variance of the Gaussian components of setpoint disturbance and measurement noise (w_1 and w_2, respectively, in Figure 2.3).

The Kalman filtering approach requires that the system be linear-gaussian. The description provided in Section 2.2 shows that this assumption is violated here. For now, we assume that non-gaussian signal components can be taken to be either zero-mean signals of lower magnitude than the gaussian components (which can, therefore, be dealt with reasonably by increasing the anticipated value for noise variance for the purpose of filter design) or non-zero-mean signals slower than the system's dynamics (which can, therefore, be dealt with through the Kalman filter's inherent adaptive capability). Simulations provided in Fekri [2005] show that RMMAC can deal with some degree of non-gaussianity under these conditions. Clearly, these assumptions could have implications in terms of the method's clinical applicability and will be discussed further in Section 2.6. A further issue lies with the presence of an unknown, yet potentially large delay term T, which Kalman filtering cannot take into account. A workaround for this problem was developed by adding redundancy to the estimation bank. The Kalman filter design was carried out on the basis of the linear part of the system alone to generate five filters (one for each robust controller range). The bank was then duplicated five times, with different amounts of delay (10s, 20s, 30s, 40s and 50s) being applied to the drug infusion signal u entering each of the duplicate banks (see Figure 2.7).

The 25 residual signals are then used in the following recursive posterior proba-

bility estimation:

$$P_i(t+1) = \left[\frac{\beta_i \left(e^{-\frac{1}{2} r_i'(t+1) S_i^{-1} r_i(t+1)} \right)}{\sum_{j=1}^{N_F} \beta_j \left(e^{-\frac{1}{2} r_j'(t+1) S_j^{-1} r_j(t+1)} \right) \cdot P_j(t)} \right] P_i(t), \tag{2.6}$$

where $N_F = 25$ is the total number of Kalman filters; $r_j(t); j = 1, \ldots, N_F$ is the difference (residual) between the measured output y and the j-th filter estimate $\hat{y}_j$; S_j is the steady state residual covariance matrix of $r_j(t)$; $\beta_j = \frac{1}{(2\pi)^m / 2 \sqrt{\det S_j}}$ is a constant scaling factor, and $P_j(t)$ is the probability that model j is the model which best represents the patient behaviour at time t. This formulation is the same as adopted in Fekri et al. [2006].

On the basis of P_i, a switching signal $\sigma(t)$ for controller selection is generated:

$$\sigma_k(t) = \sum_{h=0}^{N_T - 1} P_{k + N_C \cdot h}(t), \tag{2.7}$$

where $N_T = 5$ is the number of delay cases considered, N_C is the number of controllers and $k = 1, \ldots, N_C$.

Finally, the control signal $u(t)$ is given by

$$u(t) = \sum_{k=1}^{N_C} \sigma_k(t) u_k(t), \tag{2.8}$$

where $u_k(t)$ is the control signal generated by controller k in the controller bank.

2.4 Numerical simulations

We have implemented the RMMAC system described in Section 2.3 in Matlab and Simulink and tested it in a number of computational simulations. We present here two illustrative situations. The first case is one in which the pressure of a hypertensive but otherwise steady patient (fixed parameters and small-magnitude random fluctuations in p_0) is to be regulated over a period of several hours according to a step-wise reference signal. This is representative of a typical postoperative situation where successful automatic closed-loop administration of SNP has been achieved in the past. The second simulation represents a much more challenging case. The proposed system is set to follow the same step-wise regulation as in the first case in the presence of larger random baseline pressure variations combined with an upward DC change in p_0 (e.g., representing a very unstable patient with a worsening hypertensive state), and substantial changes in the delay and sensitivity parameters over time. While K and T are set to vary in a sinusoidal pattern in this example (for computational convenience), it should be clarified that the nature of the μ synthesis design is such that robust performance should be expected regardless of the shape

of parameter variation as long as the correct controller for the region being traversed by the changing parameter is placed in the loop. In this regard, the challenge to the system lies in whether the probability estimator of Section 2.3.2 can successfully track K—the key parameter for model selection—as it quadruples its value over 1 hour, thus achieving the maximum expected rate of change as mentioned in Section 2.2.1. For the time-varying case, we ease the performance specifications and require an acceptable MAP error range of $\pm$10mmHg instead of $\pm$5mmHg as the system can be deemed to be in a transient throughout the experiment. The simulation conditions for the two cases are summarised in Figure 2.8, together with the relevant results.

As well as RMMAC, two other control architectures taken from the literature were simulated under the same conditions. These were:

- a combined PD controller and self-tuning regulator which uses least-squares to estimate the response to SNP as an ARMAX model and implements a minimum variance control law (as in Meline et al. [1985]) with infusion constraints (as in Arnspanger et al. [1983]) and an additional on-line dead time detection method (as in Stern et al. [1985]) to cater for variable system delays. Although a detailed description of the IVAC Titrator device is not available in the literature, this architecture was deemed similar—notwithstanding any unpublished supervisory algorithms—to that used in the Titrator approach on the basis of available publications (Cosgrove et al. [1989], Petre et al. [1983]);
- the multiple model adaptive control (MMAC) architecture of Martin et al. [1987], which employs 7 candidate models selected with a prediction error method, 7 PI controllers, and a bank of Smith's predictors for delay compensation. This was chosen as an example of an earlier multiple-model method in the literature.

2.5 Results

The results of the first set of simulations (Figure 2.8–left) show that under steady conditions all three systems are capable of maintaining the patient stable and achieve the desired pressure drop while meeting the tracking performance requirements. These results are very similar to simulation results published by other authors (Arnspanger et al. [1983], He et al. [1986], Martin et al. [1987],) and indeed to the traces exhibited by postsurgical patients during *in vivo* experiments (Martin et al. [1992]).

However, a noticeable difference in performance between the systems can be seen in the second case (Figure 2.8–right), with the Titrator and MMAC approaches bursting into undesirable oscillations. The three bottom sets of graphs in Figure 2.8 provide more information on the reasons underpinning failure of the non-RMMAC comparison systems. In the case of the MMAC system, while in the steady experiment convergence to the correct model (model 4 in this case) is good, an increased level of noise does force some occasional unnecessary controller switchings. The main issue for this approach is that output predictions on the basis of which the candidate models (and controllers) are compared relies on the value of p_0 measured at

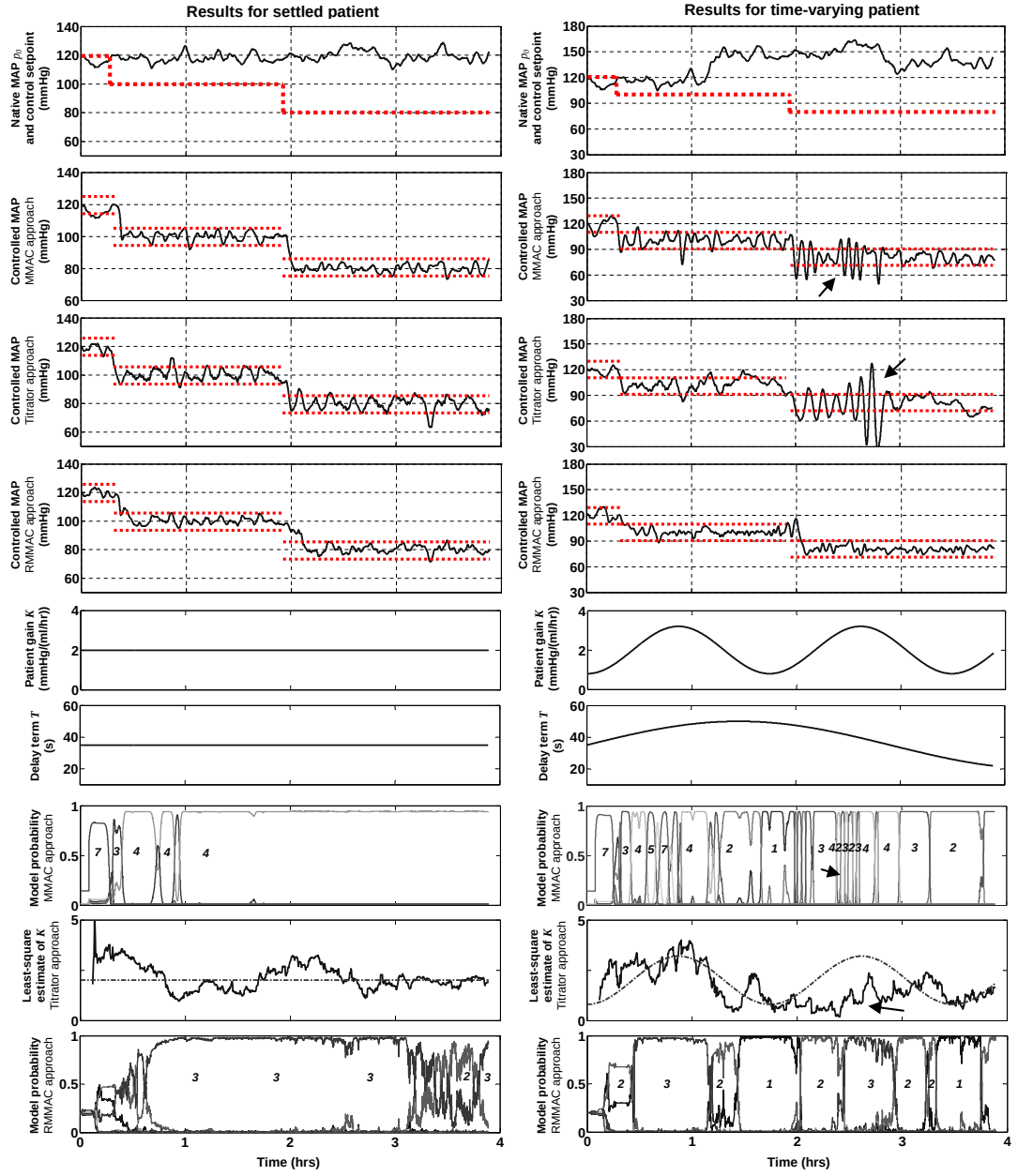

Figure 2.8: Results of simulations. From the top: baseline MAP p_0 and required setpoint; controlled MAP for the MMAC, Titrator and RMMAC approaches; parameters K and T over time; probability results for matching models in MMAC; estimate of patient gain vs real gain in the Titrator approach; probability results for matching models in RMMAC. The dotted lines in the controlled MAP traces indicate the allowed error range. The numbers in the model probability graphs indicate the model with the highest likelihood. *(left)* Settled patient, allowed tracking error $\pm$5mmHg. *(right)* Patient with time-varying parameters, allowed tracking error $\pm$10mmHg; the black arrows highlight instances of undesirable transient oscillations or issues with online estimation as discussed in the text.

time $t = 0$ and assumed fixed. As a result, when p_0 is raised further the apparent sensitivity of the patient becomes lower (increased infusion for an apparently unchanged required drop) and the accidental—albeit short-lived—switching of an incorrect, more aggressive controller (controller 2 in this case) is enough to cause undesirable hypotensive peaks. The self-tuning regulator faces a similar problem as can be seen by the result of the recursive parameter estimation (we extrapolated the DC gain for the estimated system, and show a comparison with the true value of K). While in the steady case the parameter estimate converges to the correct value, in the more disturbed experiment the sensitivity is underestimated, once again causing the system to burst into oscillations. Both non-RMMAC systems are able to resume effective control following these transient effects. However, the hypotensive peaks are a clear example of potentially dangerous dynamics which a safe system should ensure are avoided. In contrast, RMMAC remains within the prescribed $\pm$10mmHg error range, and the model probability graphs show that our approach retains the ability to correctly track the variations of K even under challenging circumstances.

2.6 Discussion

We have presented a detailed description of the control design methodology for a new, RMMAC-based architecture for automated control of SNP infusion in acute hypertensive patients, together with two sets of results illustrative of the potential of the new approach in overcoming the limitations of past adaptive control solutions.

Our analysis of past approaches suggests that they can be deemed reasonably safe in patients whose underlying MAP can be considered as almost stationary, such as may be expected in recovering postoperative patients. However, we advocate caution about undesirable behaviour which may occur under more challenging conditions as shown in our simulations. The presence of potentially non-zero-mean output disturbances is a particularly critical issue in this system. A control approach which (incorrectly) assumes the mean of p_0 to be constant may fail to distinguish between a change in patient sensitivity and a change in the DC component of p_0 and, as a result enact inappropriate control action thus rendering the closed-loop system unsafe. While it can be argued that the presence of transient oscillations would provide additional system excitation and facilitate the correct identification of the sensitivity parameter, due to the long dead times involved in this application transient instability may be dangerous. In light of these findings, we suggest that this lack of generality, although previously unreported in the literature, may have impacted on considerations about costs and perceived benefits of automated drug delivery technology and ultimately affected its uptake in the clinical setting to date.

The new RMMAC-based approach has delivered promising results which support the feasibility of automatic SNP administration even in time-varying, highly disturbed conditions (e.g., as may be encountered in an intraoperative setting). As well as achieving stability and performance in simulations, we have shown that the RMMAC methodology offers a systematic process to incorporate knowledge of the

model uncertainty into the design process. This a favourable characteristic in this field of application as pharmacological models are derived from population studies and are, therefore, inherently characterised by parametric uncertainty.

The use of an iterative μ-synthesis approach for controller design, in particular, has allowed us to mathematically demonstrate that the required performance could not be attained over the expected range of parametric uncertainty using a single linear controller, thus conclusively recognising the necessity to employ adaptive control. In a multi-controller architecture, we defined a trade-off between the number of controllers and maximum achievable performance and we were able to cater for a broader range of modelling uncertainty than considered by previous authors using a lower number of controllers (5 vs 7 used in Martin et al. [1987] and 8 used in He et al. [1986]).

With μ-synthesis giving mathematical certainty of robust stability (and performance) of the interconnected system between each possible set of patient parameters and its matching controller, we have clearly exposed that the overall stability (and therefore ultimate safety) of the closed-loop system rests on reliable system identification, i.e., in the ability of the system to track the patient's parameters so that the correct controller can be placed in the loop at all times. This is a general issue in adaptive control and we have shown a simulation example of how a combination of time-varying parameters and non-zero mean disturbances may lead to incorrect system identification and consequently to inappropriate control action. Without resorting to additional layers of supervisory algorithms, RMMAC has displayed good performance and avoided periods of transient instability. This is largely due to the use of the redundant bank of Kalman filters of Figure 2.7, which is able to deliver more accurate system estimation results than previous approaches. As we have already acknowledged, however, Kalman filtering is not the estimation tool of choice in the presence of uncertain time delays and non-gaussian signals. Indeed, convergence of (2.6) to the correct model can only be mathematically guaranteed in an ideal environment with fixed, known time delays and gaussian input signals (Fekri [2005]), which is clearly not the case here. Due to the violation of this assumption, the RMMAC system presented cannot be deemed "robust" in a strict control engineering sense. Improved performance and avoidance of transient instability over previous approaches can only be evaluated—and have been shown—heuristically through the results of simulations. While the main focus of this chapter has been to set out the methodology for this approach, further work should consider a comprehensive simulation campaign involving a wide variety of cases and parameter variations. As the linear-gaussian assumptions are likely to limit the broader applicability of RMMAC to drug delivery applications, we will also investigate whether a more general system estimation technique better suited to non-gaussian and possibly non-linear problems (such as particle filtering) may enhance the approach used thus far.

Since this work deals with the control of patient haemodynamics, a further point for discussion is that in standard mechanistic models of circulation (Guyton et al. [1972]) MAP is controlled by both CO and vascular resistance and that while SNP acts on vascular resistance, it does not directly affect CO. A key question, therefore,

concerns whether regulation of MAP alone is a sufficient condition to ensure patient safety. Indeed, joint control of MAP and CO has been proposed (see, e.g., Rao et al. [2003]). Further discussions with clinicians will be required to evaluate whether there are clinical risks associated with MAP-only control (also using a single vasoactive drug) and whether multivariable control may be preferable. It should be noted, however, that in current clinical practice continuous monitoring of cardiac output is characterised by calibration issues and low measurement accuracy (Alhashemi et al. [2011]). As a result, the haemodynamic stability of patients is first and foremost managed by targeting MAP (Varon and Marik [2008]), particularly in the case of hypertension. In light of this, our work has focussed on MAP alone. Nonetheless, provided that pharmacological models for drug action and drug interactions are available, the same approach presented here could be extended, with minor complications, to handle a multi-drug, multi-signal (multiple-input, multiple-output) case.

Chapter 3

Open-loop real-time estimation of a pharmacological system using particle filtering

This chapter investigates the usability of particle filtering in the context of a nonlinear pharmacological problem: the administration of propofol, a commonly used anaesthetic drug. The need for this investigation has arisen from our discussion (Chapter 2) of foreseeable limitations of Kalman filtering in relation to model estimation for closed-loop control of drug delivery in nonlinear and/or non-gaussian systems. We consider particle filtering as it is a numerical Bayesian inference method which can be used to conduct system estimation in a broader class of systems, including cases in which Kalman filter-based methods may not be applicable. The focus of this chapter is the design of a particle filter for the estimation of patients' individual pharmacokinetic-pharmacodynamic (PK-PD) characteristics. In the interest of clarity, the estimation problem is dealt with here in open-loop (i.e., in the absence of feedback control); the combination of particle filters and controllers will be examined in Chapters 4 and 5. We detail the typical formulation of a compartmental PK-PD model and develop a number of particle filters for the propofol case, based on different assumptions on available observation signals. We evaluate, through Monte-Carlo simulations, the ability of the method to conduct estimation in real-time and the quality of the model estimates under different observation scenarios. Our findings support the viability of particle filters for this application and highlight how incorporating inaccurate measurements through suitable measurement error models can improve the quality of the model estimates.

The content of this chapter closely follows the author's research paper *Open-loop real-time estimation of propofol pharmacokinetics-pharmacodynamics using particle filtering (Malagutti [a])*. Section 3.1 provides an overview of anaesthesia monitoring and controlled propofol administration; Section 3.2 presents the PK-PD model used, introduces the particle filtering approach and describes the computational simulations; Section 3.3 shows the results of the simulation experiments; Section 3.4 analyses the results, highlights the key findings and discusses potential extensions of the work.

3.1 Background

The drug propofol is a commonly used pharmacological agent which is administered intravenously to anaesthetise surgical patients. The anaesthetic effect manifests itself as a loss of consciousness and reactiveness to stimuli on the part of the patient. The degree of this effect is the subject of expert evaluation by the anaesthetist, who must ensure that Depth of Anaesthesia (DOA) remains adequate throughout the surgery: insufficient DOA may result in patients becoming (unpleasantly) aware of the procedures being performed, while excessive DOA may lead to extended recovery times and other complications, which range from mild to severe effects and even include death (Cobas and Varon [2006]).

The assessment of DOA does rely on a range of qualitative tests, such as the evaluation of movements or reflex responses (Heier and Steen [1996]). To facilitate the task of the anaesthetist in obtaining consistent anaesthetic outcomes on a range of patients, two main areas of research have developed over the years: mathematical dose pre-planning, with methods such target-controlled infusion (TCI), and quantitative measures of effect, most often brain activity-derived indices such as the Bispectral Index (BIS). TCI consists in the application of a pre-determined drug infusion pattern based on population-derived models of propofol distribution inside the human body (pharmacokinetic models), with the assumption that a particular concentration inside the body would lead to the desired effect. The BIS, on the other hand, as a quantitative measure of effect describes a relationship between brain activity and consciousness, allowing for feedback control systems targeting specific BIS level to be designed and implemented (e.g., the well-known Stanpump, see Struys et al. [1998]).

Clinical research and practice have demonstrated that these methods have the potential to bring improvements in the quality of anaesthesia. However, their ultimate ability to address differences in the pharmacological response of individual patients is still under question. The predictive ability of pharmacokinetic models is limited by parametric uncertainty arising from the substantial intra- and interpatient variability found in populations (Bienert et al. [2012]). Similarly, mathematical descriptions of the drug concentration-to-BIS effect relationship (pharmacodynamic models) may also vary across a population (Schnider et al. [1999]). As a result, TCI and BIS systems are used in clinical practice as a guide tool which must be integrated by the *soft knowledge* of an expert human operator.

We seek to investigate whether greater knowledge of a patient's individual pharmacokinetic and pharmacodynamic response could be gathered in real time from available measurements of BIS effect and plasma propofol concentrations. We do so by using particle filtering as our Bayesian inference tool of choice, applied to computer-generated data based on a population pharmacokinetic-pharmacodynamic (PK-PD) model. Bayesian inference (i.e., the process of determining the likelihood of a certain patient's response based on the available observations, or, in other words, the process of "locating" a patient's individual response amongst the different responses exhibited across a population) for the individualisation of pharmacological therapy is not a novel concept (Jelliffe et al. [1993]). However, to the author's

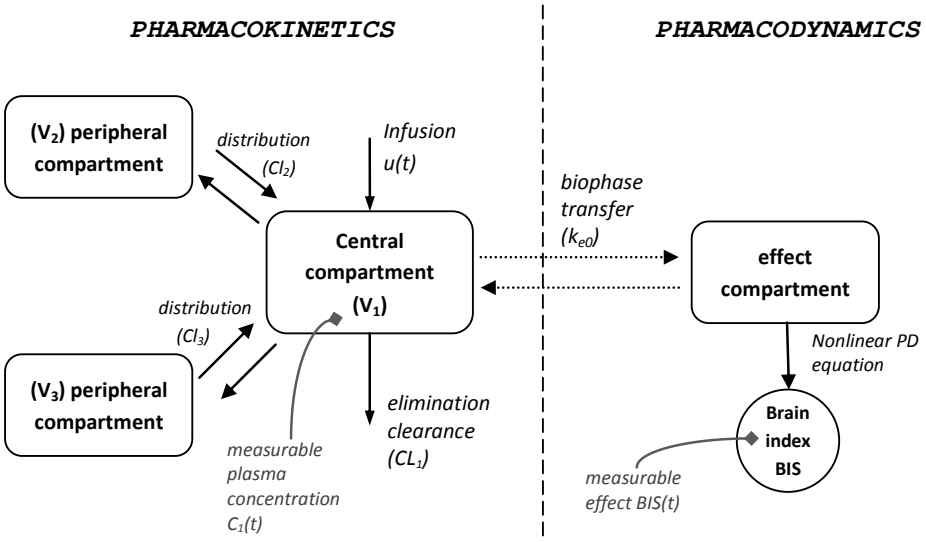

Figure 3.1: Schematic description of the compartmental pharmacokinetic-pharmacodynamic model for propofol.

knowledge, real-time inference using particle filtering has not been proposed before. Furthermore, we seek to evaluate whether recently developed techniques of breath propofol measurement (Takita et al. [2007]; Hornuss et al. [2012]), as a real-time yet less accurate (Kamysek et al. [2011]) way of measuring plasma propofol can provide adequately meaningful information for the inference process.

3.2 Methodology

3.2.1 Propofol response models

The model chosen to describe the dose-response characteristic of propofol is a joint PK-PD model which draws on the work of Schuttler and Ihmsen [2000] (multi-centre population study) for the pharmacokinetic part and on that of Wiczling et al. [2012] for the pharmacodynamics. The structure of the model is described in Figure 3.1.

Pharmacokinetics

The model is based on compartmental pharmacokinetics, that is, the distribution of the drug throughout the body is modelled as a combination of concentration-driven mass transfer processes which can be described as first-order differential equations. Three compartments are identified and referred to as the *central compartment*, *superficial peripheral compartment* and *deep peripheral compartment* (Schuttler and Ihmsen

[2000]). The transfer coefficients are named *elimination* (Cl_1) and *distribution (inter-compartmental)* (Cl_2, Cl_3) *clearances*. While the compartments do not have a direct physiological significance, three-compartment models are commonly used in the literature for propofol (see, e.g.,Bjornsson et al. [2010]; Wiczling et al. [2012] also discusses several available pharmacokinetic models). The model equations are shown below:

$$V_1 \frac{dC_1}{dt} = u(t) - Cl_1 C_1 + Cl_2 (C_2 - C_1) + Cl_3 (C_3 - C_1) \tag{3.1a}$$

$$V_2 \frac{dC_1}{dt} = Cl_2 (C_1 - C_2) \tag{3.1b}$$

$$V_3 \frac{dC_1}{dt} = Cl_3 (C_1 - C_3), \tag{3.1c}$$

where C_x is the concentration of propofol in compartment x and V_x is the volume of that compartment; $u(t)$ represents the dose administered intravenously (instantaneous mixing in the central compartment is implicitly assumed).

Pharmacodynamics

The pharmacodynamic model, linking the propofol concentration in the central compartment with the measurable BIS effect, is shown on the right hand side of Figure 3.1. A further, fictitious compartment is added to the model, representing diffusion into the body site where the drug determines its effect (named the *biophase*). In the propofol literature, this part of the model represents has been loosely linked to the distribution of the drug from the bloodstream to the brain (Bienert et al. [2012]). Diffusion is driven by the difference in concentration between the central compartment and the effect site, as per the equation:

$$\frac{dC_e}{dt} = k_{e0} (C_1 - C_e), \tag{3.2}$$

where k_{e0} is the distribution rate to the biophase and C_e is the concentration at the effect site. Finally, the effect concentration and the BIS value are described as having a non-linear sigmoidal relationship given by Hill's equation:

$$BIS(t) = BIS_0 \left(1 - \frac{E_{max} C_e^{\gamma}}{C_{50}^{\gamma} + C_e^{\gamma}}\right), \tag{3.3}$$

where BIS is the Bispectral Index score (0-100), the exponent γ is a parameter affecting the shape of the sigmoid, E_{max} is the maximum percentage drop in BIS achievable with propofol and C_{50} is the necessary concentration at the effect site to determine a 50% reduction in the BIS reading from the initial value BIS_0.

Population statistics and stochastic effects

Patient response is not deterministic and the values of the parameters are identified by fitting the model above to population data. Interindividual variability in the response exists and as such, parameters are best described in terms of probability distributions. Two types of parameter distributions are used in this work: normal distributions, i.e.

$$X \sim \mathcal{N}\left(\mu_X, \sigma_X^2\right),$$

with parameter X having mean μ and standard deviation σ, and log-normal distributions, i.e.,

$$X \sim \ln\mathcal{N}\left(\theta_X, \omega_X\right) \Rightarrow X = \theta_X e^{(\eta_X)}, \;\; \eta_X \sim \mathcal{N}\left(0, \omega_X^2\right),$$

where parameter X is characterised by a typical (median) value in the population θ_X and a random multiplicative effect, the logarithm of which is distributed normally.[1] These choices of distributions to describe parametric uncertainty are common in so-called pharmacological nonlinear mixed-effects modelling (Bonate [2011]).

For completeness and generality of the model, we also assume stochastic effects to affect the quality of the observations. These can be interpreted as describing measurement errors or residual errors in the fitted model, or a combination of both. For BIS measurements we follow the additive noise model used in Wiczling et al. [2012]:

$$BIS_{meas} = BIS + \epsilon_{BIS}, \tag{3.4}$$

where $\epsilon_{BIS} \sim \mathcal{N}(0, \sigma_{BIS}^2)$. For plasma concentration measurements, we consider a multiplicative error model, i.e.,

$$C_{1,meas} = C_1\left(1 + \epsilon_{C_1}\right). \tag{3.5}$$

For the term ϵ_{C_1}, we assume a normal distribution in the case of direct plasma concentration assays (also in accordance with Wiczling et al. [2012]), i.e., $\epsilon_{C_{1,p}} \sim \mathcal{N}(0, \sigma_{C_{1,p}}^2)$, and a custom distribution derived from "flattening" a normal distribution in the case of breath concentration measurements. Introducing the probability distribution function $\phi(X)$ for a normally distributed variable $X \sim \mathcal{N}\left(0, \sigma^2\right)$ as

$$\phi_{(0,\sigma^2)}(X) = \frac{1}{\sigma\sqrt{2\pi}} \exp\left\{-\frac{X^2}{2\sigma^2}\right\}, \tag{3.6}$$

[1] Alternative notation conventions in describing the log-normal distribution specify the median of the distribution $\ln\mathcal{N}\left(\xi, \omega_X\right)$ as e^{ξ} with $\xi \sim \mathcal{N}\left(0, \omega_X^2\right)$. In accordance with the notation used in Schuttler and Ihmsen [2000], we define here the median as θ_X, where $\theta_X = e^{\xi}$, instead. This choice, which implies the condition $\theta_X > 0$, appears to be customary in pharmacology as PK-PD parameters are most often positive and the value of the population median can be appreciated more readily with this notation.

Model parameter	Distribution	Distribution parameters
Pharmacokinetics (Schuttler and Ihmsen [2000])		
Cl_1	$\ln\mathcal{N}$	$\theta_{Cl_1} = 1.44$, $\omega_{Cl_1} = 0.362$
Cl_2	$\ln\mathcal{N}$	$\theta_{Cl_2} = 2.25$, $\omega_{Cl_2} = 0.488$
Cl_3	$\ln\mathcal{N}$	$\theta_{Cl_3} = 0.92$, $\omega_{Cl_3} = 0.480$
V_1	$\ln\mathcal{N}$	$\theta_{V_1} = 8.31$, $\omega_{V_1} = 0.385$
V_2	$\ln\mathcal{N}$	$\theta_{V_2} = 39.5$, $\omega_{V_2} = 0.505$
V_3	$\ln\mathcal{N}$	$\theta_{V_3} = 266.0$, $\omega_{V_3} = 0.446$
$\epsilon_{C_{1,p}}$	$\mathcal{N}$	$\mu_{\epsilon_{C_{1,p}}} = 0$, $\sigma_{\epsilon_{C_{1,p}}} = 0.013$
$\epsilon_{C_{1,b}}$	$\mathcal{N}$	$\mu_{\epsilon_{C_{1,b}}} = 0$, $\sigma_{\epsilon_{C_{1,b}}} = 0.25$
Pharmacodynamics (Wiczling et al. [2012])		
BIS_0	constant	$BIS_0 = 97$
k_{e0}	$\mathcal{N}$	$\mu_{k_{e0}} = 0$, $\sigma_{k_{e0}} = 0.088$
γ	constant	$\gamma = 1$
C_{50}	$\ln\mathcal{N}$	$\theta_{C_{50}} = 2.19$, $\omega_{C_{50}} = 0.417$
ϵ_{BIS}	$\mathcal{N}$	$\mu_{\epsilon_{BIS}} = 0$, $\sigma_{\epsilon_{BIS}} = 3.74$

Table 3.1: PK-PD parameters and distribution characteristics. The values represent patients with a body weight of 70kg, aged 40 years.

the probability distribution function for the error $\epsilon_{C_{1,b}}$ becomes

$$p\left(\epsilon_{C_{1,b}}\right) = \min\left\{\phi_{\left(0,\sigma^2_{C_{1,b}}\right)}\left(\sigma_{C_{1,b}}\right), \phi_{\left(0,\sigma^2_{C_{1,b}}\right)}\left(\epsilon_{C_{1,b}}\right)\right\} \tag{3.7}$$

A plot of the distribution is shown on the left hand side of Figure 3.2. The choice of such a distribution arises from a lack of detailed information in the literature about the measurement error characteristics of breath propofol concentration measurements. Studies have demonstrated that a correlation between plasma and breath concentrations exists (Takita et al. [2007]). However, animal experiments have indicated that the quality of this correlation may worsen with increases in cardiac output (Kamysek et al. [2011]). The right hand plot of Figure 3.2 shows the chosen distribution applied to the in-vivo data of Kamysek et al. [2011] as an attempt to cater, conservatively, for the potential error introduced by neglecting the effect of the haemodynamic state on the exchange of propofol between plasma and exhaled breath.

Table 3.1 summarises the parameters and the statistical distributions used in this study.

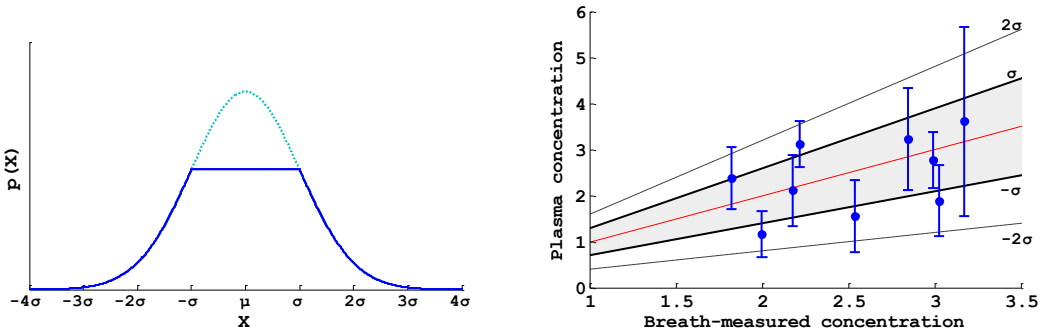

Figure 3.2: *Left:* Probability distribution used to model the error term in breath-derived propofol concentration measures (solid), compared with the corresponding normal distribution (dashed). *Right:* Experimental data on simultaneous breath and plasma propofol measurements (from Kamysek et al. [2011]) superimposed on regions representing the distribution of the multiplicative error term. The grey-shaded region covers the interval of ± 1 standard deviation from the line of identity (red).

3.2.2 Particle filtering

Bayesian filtering

We consider a dynamical system characterised by deterministic and stochastic dynamics, i.e.,

$$x(k) = f_1\left(x(k-1), u(k), v(k)\right) \tag{3.8}$$
$$z(k) = f_2\left(x(k), u(k), w(k)\right), \tag{3.9}$$

where $x(k)$ is the state vector, $z(k)$ is the observation vector, $u(k)$ is an input vector, k is the discrete-time index, f_1, f_2 are arbitrary functions and $v(k), w(k)$ are input and output noise processes. Bayesian filtering seeks to estimate the posterior probability distribution of the system's state at k, conditional on the available observations, i.e., the distribution $p(x(k)|z(1:k))$, where $p(\cdot)$ indicates probability and $1:k$ denotes the time interval between 1 and k. In other words, the result of a Bayesian filter gives the probability with which the system can be deemed to be in a particular state given the information provided by the history of available observations. On the basis of the posterior probability distributions, other estimates about the system can be made, i.e.,

$$E(g(x(k)) = \int g\left(x\left(k\right)\right) p\left(x(k)|z(1:k)\right) dx(k), \tag{3.10}$$

where $E(\cdot)$ denotes the expected value and $g(\cdot)$ is another arbitrary function. This process of making "informed guesses" about an observed system is termed *Bayesian inference*.

Analytical solutions for the filtering problem exist only for restricted categories

of problems, for example Kalman filtering, which can be applied to systems characterised by linear dynamics and normally distributed (Gaussian) disturbances. For more general problems (non-linear, non-Gaussian), a closed-form solution to compute the posterior probability is not available and methods based on approximations must be used. Extensions of the Kalman filter have been proposed to this end, such as Extended Kalman Filtering (EKF) and Unscented Kalman Filtering (UKF), which rely on functional approximations to allow for the Kalman result to be applied to nonideal cases (Chen [2003]). Particle filters take a radically different approach in that they are a Monte-Carlo method, i.e., they attempt to approximate the true distribution by using a large number of randomly sampled candidate instances of the stochastic process to be estimated; each instance is called a *particle*. Particle filter methods have the definite advantage of asymptotic convergence (for $N \to \infty$, where N is the number of particles) to the true distribution Doucet and Johansen [2009], although, depending on the system, the parallel computation of the dynamics of too many particles may come at an unaffordable computational cost.

Particle filtering for propofol PK-PD

The pharmacological dynamical system describing the propofol response includes a non-Gaussian measurement error model as described in (3.7). Nonlinearities are also present, due both to the the PD component of equation (3.3), and to the fact that the model parameters are uncertain and must also be estimated by the filter. By recasting the problem as a joint state and parameter estimation task, the system state is augmented with the uncertain parameters, i.e., $x = \begin{bmatrix} x^{PKPD} & x^{\theta} \end{bmatrix}^T$ where x^{PKPD} and x^{θ} are vectors representing the PK-PD dynamics (as per equation (3.8)) and the parameters to be estimated, respectively. This renders the dynamics of the system a more general, nonlinear function of the state. In light of the exposition in the previous section, a particle filter is a suitable tool to deal with such a general case.

The particle filtering algorithm comprises of a few fundamental steps:

- **Initial condition:** an appropriately large number of particles (N) are sampled from a known or presumed initial probability distribution $p(x(0))$. In the specific case of the pharmacological problem, the initial (k=0) distributions of the parameters (x^{θ}) are given by the population statistics as per Table 3.1. The x^{PKPD} states represent the concentrations in the model compartments and can be deemed to have a zero initial condition if the observations start at a time when no drug has yet been administered.

- **Propagation:** the next state value for each particle is calculated, as is standard for a discrete-time dynamical system. In our specific problem, we assume the x^{PKPD} states to propagate in a deterministic way at each time step, i.e.,

$$x_i^{PKPD}(k+1) = f_1\left(x_i^{PKPD}(k), x_i^{\theta}(k), u(k)\right), \tag{3.11}$$

  where the above equation is an adaptation of (3.8). The subscript i denotes the

ith particle with $1 \leq i \leq N$. The states representing the parameters either held constant or varied stochastically depending on whether resampling occurs at time k, i.e.,

$$x_i^\theta(k+1) = \begin{cases} x_i^\theta(k)\,(1+\chi(k)) & \text{if } k \text{ is a resampling time step} \\ x_i^\theta(k) & \text{otherwise} \end{cases}, \tag{3.12}$$

where $\chi(k)$ is a diagonal $n \times n$ matrix (n being the number of parameters to be estimated) with entries sampled from the distribution $\mathcal{N}\left(0, 0.02^2\right)$, corresponding to random changes with a standard deviation of 2% in the value of the parameters. Although in this experiment it is assumed that the parameters are fixed for any one patient, allowing for stochastic variations in the parameter values when resampling reduces the risk of sample impoverishment, i.e., that after many resampling steps all particles might end up with the same parameter values, thus reducing the filter's capability.

- **Weighting:** when a new observation becomes available, the estimated value of the system output (BIS value or propofol concentration) for each particle is compared with the value of the observation and a corresponding weight is generated based on the distribution describing the likelihood of observations, i.e., $p(z(k)|x(k))$. In the case of a BIS observation, for example:

$$w_i^*(k) = \phi_{(0,\sigma_{BIS}^2)}\left(BIS(k) - \hat{BIS}_i(k)\right), \tag{3.13}$$

where ϕ is defined as in equation (3.6), w_i^* is the weighting attributed to the ith particle and $\hat{BIS}_i(k)$ represents the ith BIS estimate at time kT_s (T_s is the sampling time for the discretisation of continuous-time signals, cf. equation (3.3)).

- **Weight normalisation:** following weighting, weight normalisation is performed, i.e.,

$$w_i(k) = \frac{w_i^*}{\sum_{j=1}^N w_j^*}. \tag{3.14}$$

- **Resampling:** N particles are sampled from the distribution approximated by the weighted particles. By resampling, particles which poorly reproduce the system's behaviour are eliminated and reintroduced as copies of better performing realisations. A variety of schemes exist in the literature for this purpose (Douc and Cappe [2005]). Here, we adopt multinomial resampling, by which random numbers q_i ($1 \leq i \leq N$) are drawn according to a uniform distribution $\mathcal{U}[0,1)$ and used to select which particles to sample according to a multinomial distribution:

$$x_i^R(k) = x_j(k), \quad j : q_i \in \left[\sum_{r=1}^{j-1} w_r \sum_{r=1}^{j} w_r\right) \tag{3.15}$$

where the superscript R indicates the resampled particle and equation (3.15) is a numerical inversion of the cumulative probability distribution determined by the normalised particle weights. Following resampling, all particles are assigned the same weight $\frac{1}{N}$.

Figure 3.3 shows a flow chart summarising the particle filter algorithm. Estimates can be derived at any time by performing a weighted sum. The inference equation (3.10) for the particle filter becomes, therefore,

$$E(g(x(k)) = \sum_{i=1}^{N} g\left(x\left(k\right)\right) w_i(k). \tag{3.16}$$

3.2.3 Monte-carlo numerical simulations

In order to investigate the ability of the approach as described to estimate the propofol response characteristic, and thus perform a proof-of-concept evaluation of real-time Bayesian inference in this application based on current models, we designed a computational simulation campaign in which 1000 patients were sampled at random from the population parameters of Table 3.1. For all cases, we simulated an input sequence corresponding to an initial infusion of 2mg/kg of propofol for the first minute, followed by a 200 minute infusion at 0.2(mg/kg)min^{-1}, after which infusion stops and the recovery of consciousness takes place (a further 200 minutes are considered). This choice of infusion profile was deemed consistent with examples observed in the PK-PD modelling literature such as in Wiczling et al. [2012]; Bjornsson et al. [2010].

The performance of the approach was assessed by using observations taken during the anaesthesia section of the simulation (first 200 minutes) and evaluating the ability of the inferred model to predict the BIS and concentration trends during the recovery phase (last 200 minutes). The following modelling options were tested against the simulation data:

i. predictions based on the nominal model (no observation information used);

ii. predictions based on BIS observations alone (1 BIS observation every minute);

iii. predictions based on BIS and breath concentrations (1 breath observation every 5 minutes, 1 BIS observation every minute);

iv. predictions based on BIS and plasma concentrations (1 plasma observation every 5 minutes, 1 BIS observation every minute);

v. predictions based on breath concentrations alone (1 breath observation every 5 minutes);

The intervals between subsequent BIS and breath observations were deemed reasonable in the context of the application and available technologies. While BIS monitoring can be deemed essentially continuous, it has been argued that due to the

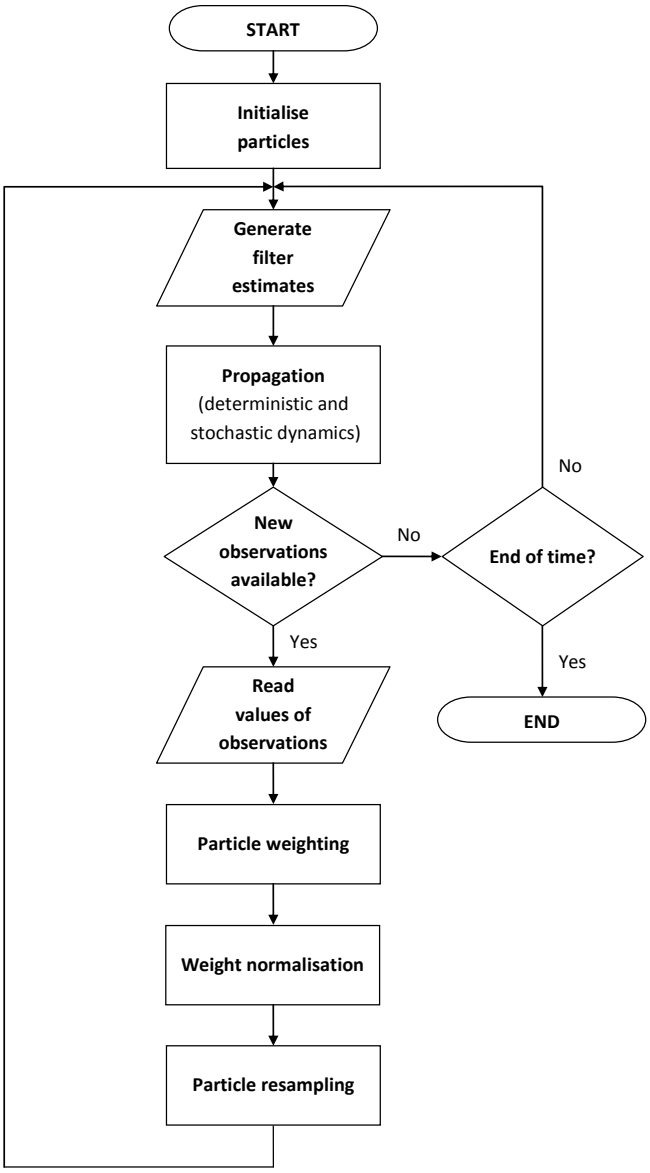

Figure 3.3: Flow chart describing the particle filtering algorithm.

low amounts of propofol exchanged between the blood and the breath, time is required for equalisation of airborne concentrations and therefore too frequent breath concentration measurements may not be informative (Takita et al. [2007]). Plasma concentration assays cannot be realistically conducted in real-time, but this case was contemplated and simulated in order to compare an ideal set of results against those of a filter relying on the less accurate breath measurements.

In assessing the prediction error we rely on weighted residuals (WR), i.e.,

$$WR(k) = \frac{z(k) - \hat{z}(k)}{z(k)}, \tag{3.17}$$

where z(k) is the observation (BIS or propofol concentration) and $\hat{z}(k)$ is the estimate. Weighted residuals (expressed as percentages) are a standard approach to express goodness-of-fit in pharmacological models (Bonate [2011]). The following measures are adopted:

- Mean Weighted Residual (MWR), defined as the mean of the WR values computed in the 200-400min window, to highlight bias in the estimate;
- Mean Absolute Weighted Residual (MAWR), defined as the average absolute value of WR in the 200-400min window, to evaluate accuracy in the estimate;
- Absolute Weighted Residual at the Endpoint (AEWR), to evaluate the error at the end of the prediction horizon (taken at 398min).

For all measures, we computed the mean value over the sampled population.

The simulations were programmed and run using Matlab and Simulink on a standard desktop computer (Intel® Core Duo™ CPU, 3.0GHz). In the simulations requiring a particle filter, 10,000 particles were used.

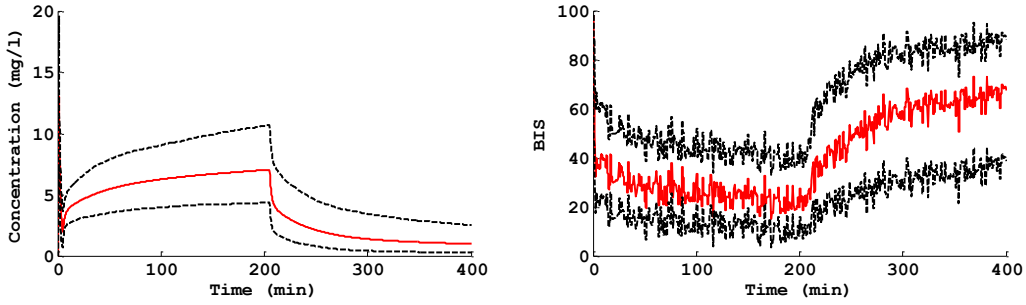

Figure 3.4: Simulated values of observable signals. The red line indicates the result for the nominal model (no parameter variations). The dashed black lines indicate the 5th and 95th percentile of the population responses. *Left:* Plasma concentration C_1. *Right:* BIS measurement (noisy).

3.3 Results

Figure 3.4 shows the concentrations and BIS responses across the population as per the model of Table 3.1. Although all sampled patients had the same values for the age and body weight covariates, the interindividual variability is considerable as displayed by the difference between the 5th and 95th response percentiles.

Table 3.2 summarises the results of the campaign. Most measures point to the model-based estimate (case `i`) as the worst overall performer. The case with BIS-only observations (`ii`) displays good predictive performance for BIS, but poor results in estimating the plasma concentrations. Conversely, a filter relying only on breath propofol concentrations (`v`) predicts plasma concentrations well but is inaccurate on BIS. Joint observation of C_1 and BIS (cases `iii` and `iv`) is associated with the best predictive results. As could be expected, the overall best performer is the case with the accurate plasma concentration measurements (case `iv`). However, it is notable that the predictive ability in the breath measurement case (`iii`) is very similar.

Figure 3.5 shows a typical result. We show the true and predicted $BIS(t)$ and $C_1(t)$ traces for patient number 863. The two plots show, at an individual patient level, the differences already highlighted by the population measures. BIS-only filters track plasma concentrations less accurately and vice-versa. Case `iv` yields the most accurate results. The estimate based on the nominal model provides the worst tracking.

A further result of interest is an insight into the accuracy of the estimation of individual model parameters. Figure 3.6 shows the particle filter distributions for the estimates of a pharmacokinetic and a pharmacodynamic parameter: V_2 and C_{50},

Measure	**Case**	C_1	BIS
MWR (%)	`i`	-29.8	-10.9
	`ii`	-58.0	4.02
	`iii`	-31.8	7.13
	`iv`	-26.6	1.83
	`v`	-20.3	-10.6
MAWR (%)	`i`	60.5	33.7
	`ii`	68.2	26.7
	`iii`	38.4	16.9
	`iv`	40.4	17.7
	`v`	40.6	29.9
AEWR (%)	`i`	76.8	23.8
	`ii`	93.6	18.5
	`iii`	57.4	14.6
	`iv`	57.4	13.6
	`v`	56.0	19.9

Table 3.2: Results of the simulation campaign

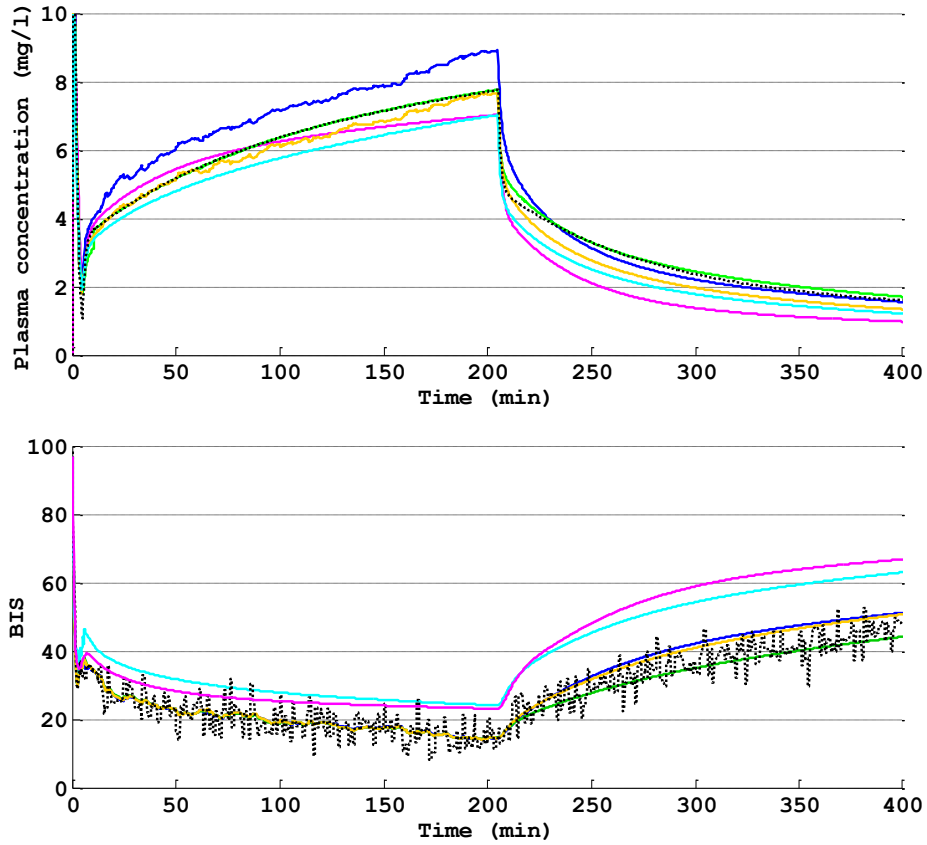

Figure 3.5: Observations and tracking by the five estimation approaches for simulated patient #863. The true observed values are shown by the dashed black trace. The solid coloured lines show the results of the five estimation methods: `i` (magenta), `ii` (blue), `iii` (gold), `iv` (green), `v` (cyan). *Top:* Plasma concentration C_1. *Bottom:* BIS measurement (noisy).

respectively. While the results on other parameters may be different, the comparison between the four methods is informative. The figures clearly show that the method relying on pharmacokinetic (concentration) information only does not estimate the pharmacodynamic parameters well, and vice-versa. The convergence of the estimate, as shown by the distance between the 5th and 95th percentile of the particle distribution, is greater when the more precise measures of plasma concentrations are available. It should also be noted that most of the convergence occurs in the first 50 minutes of observations, and that even with best estimation, the breadth of the confidence interval can be quite large. Taking Figure 3.6 as an example, the relative difference between the mean of the estimate and the 95th percentile for the best estimate case `iv` is a sizable 40% in the case of V_2 and 15% for C_{50}.

The simulation and particle filtering of each 400min patient case was carried out in approximately 120 seconds, i.e., about 20× faster than real-time.

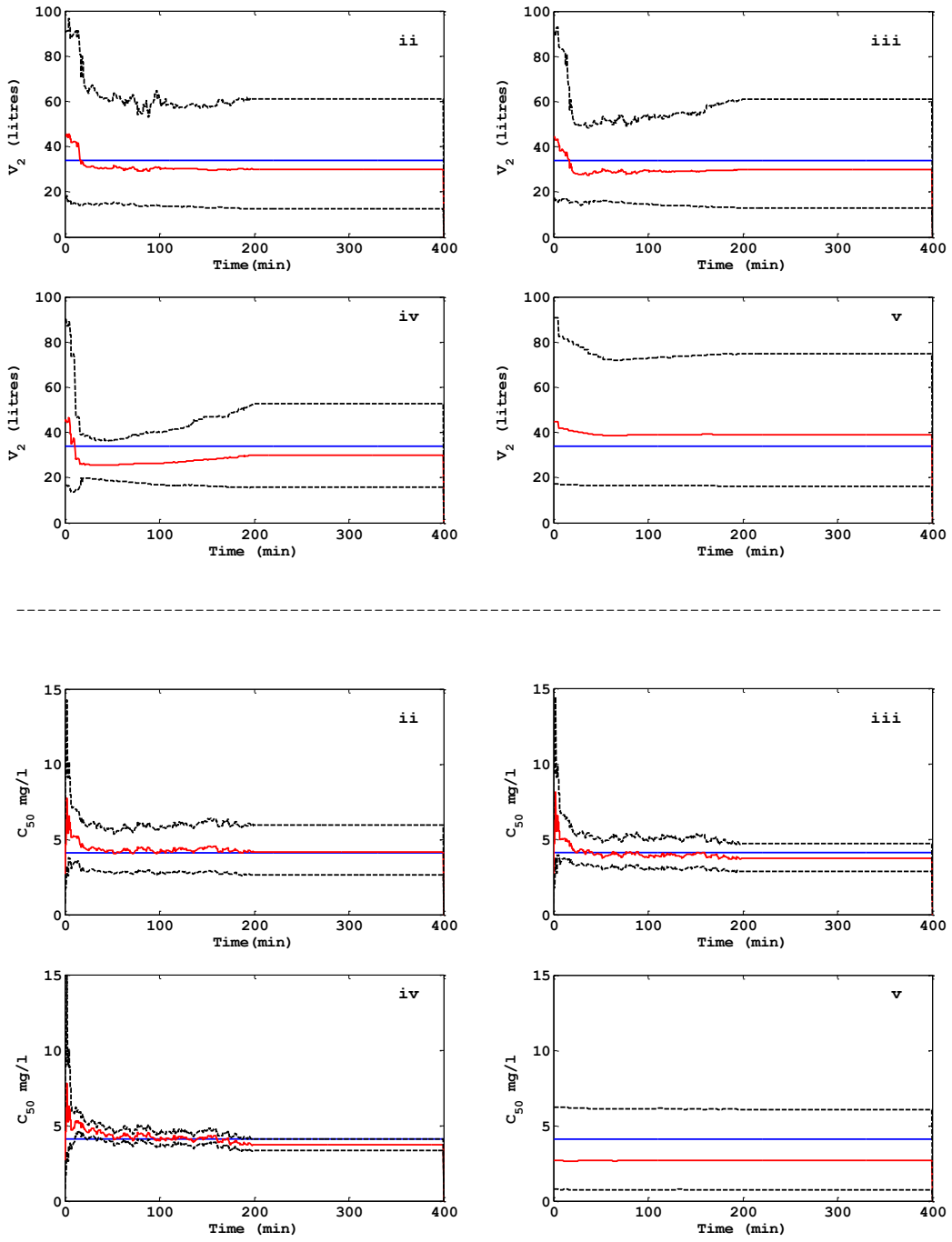

Figure 3.6: Convergence of parameter estimates for the four particle filter cases for patient #422. The case number is shown on the top right of each plot. All plots show the true value of the parameter (blue), the particle filter mean (red) and the 5th and 95th percentile of the particle distribution (black dashed). *Top section:* pharmacokinetic parameter V_2. *Bottom section:* pharmacodynamic parameter C_{50}.

3.4 Discussion

This chapter has introduced a method for real-time inference of a pharmacological dose-response system. The results raise interesting considerations both from a methodological and a clinical perspective.

From a methodological perspective, we have demonstrated that the particle filter approach as presented is able to deliver better predictive performance than a-priori predictions. Since there are no constraints on model linearity or on the distribution of stochastic processes, the proposed Bayesian inference method is general and, given any PK-PD model and a set of available observations, an appropriate particle filter formulation could be designed and implemented. As mentioned previously, a possible limitation of this approach lies in the computational burden of particle filters, which grows exponentially with the state dimension of the underlying model. Our simulation campaign has indicated that real-time computation of a large number of particles is possible in this case without requiring specialised hardware. Although we did not conduct a systematic analysis to select the number of particles, a comparison of selected simulations with varying numbers of particles ranging from 1,000 to 50,000 indicated 10,000 to be an adequate compromise between computational time and accuracy. Our positive finding in terms of the tractability of the real-time filtering problem can be attributed to the relatively slow dynamics of drug distribution and effect, when compared to the speed of computer processing.

The accuracy of parameter estimation warrants further discussion. The positive findings in terms of predictive capability are not matched by very precise parameter estimates. This can be partly attributed to measurement errors, particularly when large in magnitude and characterised by flat distributions such as (3.7), as they introduce significant uncertainty which the filter cannot resolve, thus resulting in a less focussed particle scatter in the parameter space. It is expected that improvements in the techniques and/or error models for breath propofol measurements would lead to more accurate estimation results. However, as already highlighted, the convergence of estimates is only marginally better when direct (and accurate) plasma measurements are made available to the filter. This raises further questions relating to underdetermination and adequate system excitation.

Underdetermination refers to the fact that there are fewer observable signals than unknown parameters and, as such, there may be multiple parameter combinations giving rise to similar observations. While the three-compartment formulation used here was deemed to be representative of the consensus in the literature, PK-PD models are not developed from first principles, and therefore the number of model parameters is the result of a trade-off choice between complexity and goodness-of-fit. Indeed, simpler (Wiczling et al. [2012]: two-compartment) and more complex (Bjornsson et al. [2010]: four-compartment) models do exist for propofol. Further work should evaluate whether a lower-order particle filter would be able to achieve similar levels of predictive ability with a better convergence of parameter estimates. In other words, whether the loss of higher-order dynamics associated with the use of a simpler model can be offset by an improvement in the focus of the particle scatter.

System excitation refers to the ability of the input provided to the system (drug infusion) to elicit input-out dynamics of sufficient intensity to allow for accurate parameter identification. From a systems engineering perspective, the mostly flat infusion profile presented by the literature as a "clinical standard" limits the amount of information available to the filter after the initial settling dynamics have been exhausted. This explains the lack of further convergence in the particle scatter, despite new observations being available, from approximately 50 min onwards (Figure 3.6). Indeed, pharmacokinetic studies of propofol have highlighted that close observation of plasma concentrations in the first few minutes after administration provides precious information on the response dynamics Masui et al. [2009]. Fast early-stage concentration measurements, however, are not possible with breath-based methods, due to the slow equalisation dynamics between breath and blood. We expect that a similar experiment conducted with greater variations in the infusion profile would result in further improvements in the inference results, although we acknowledge that alternative infusion profiles may be subject to clinical constraints which are beyond the expertise of this author. Ongoing excitation would become essential if the parameters were to be assumed as being time-varying, and not fixed as was done in this study. An evaluation of the scope to improve estimation results through alternative infusion profiles would be a valuable extension to this work.

From a clinical perspective, the results of this computational study have highlighted that even for an established PK-PD model, the breadth of possible responses owed to interindividual variability is substantial. In light of this it is clear that a TCI system relying solely on a-priori estimates based on measurable patient details (such as body weight and age) may grossly under- or overestimate plasma concentration and BIS trends, as confirmed by the large values in the error measures of case `i`. In terms of Bayesian inference, our findings show that particle filters are a viable tool to incorporate information from available observations and obtain a more accurate estimate of a patient's individual response in real time. Importantly, our work shows that inaccurate measurements can contribute to the inference process if incorporated through a suitable error model. In the case of propofol, this study supports the usefulness of information acquired through breath-based measurements of propofol concentration when used in conjunction with EEG-derived measures of effect such as BIS. The predictive capacity of methods `iii` and `iv`, in the standard conditions assumed for this simulation study, were found to be almost equivalent. Although the positive results shown here will need to be confirmed through in-vivo studies, our data suggest that more accurate real-time inference of individual patients' PK-PD response is possible with current technology. A better characterisation of individual response has the potential to improve clinical decision making and may also be used to support algorithms for automatic closed-loop drug administration.

Chapter 4

An adaptive multi-controller architecture with a particle filter-based supervisor

This chapter temporarily abandons the focus on medicinal drugs and presents work with a distinct control engineering focus. Having found (in Chapter 2) that the Kalman filter model estimation approach of Robust Multiple-Model Adaptive Control (RMMAC) may not be ideal to deal with systems which are not linear-Gaussian and time-invariant, and having explored (in Chapter 3) particle filtering as a more general model estimation approach, the main aim of this chapter is to investigate whether a combination of multiple robust controllers and real-time particle filtering can be used successfully as an adaptive feedback control architecture. We present here this novel approach, which we name Robust Adaptive Control with Particle Filtering (RAC-PF), and conduct Monte-Carlo simulations to compare its performance with that of another known extension for RMMAC: Robust Adaptive Control with Extended Kalman Filtering (RAC-EKF). The test-bench used for the comparison is a multivariable linear parameter-varying system. Our results show that when real-time computation of the particle filter can be achieved, RAC-PF can match the performance of RAC-EKF, indicating that there is no disadvantage in adopting the more general approach in problems where a more restrictive EKF-based methodology would be suitable.

The content of this chapter closely follows the author's research paper *An Adaptive Multi-Controller Architecture Using Particle Filtering (Malagutti et al. [2012c])*. Section 4.1 delivers some essential background information on multi-controller architectures; Section 4.2 provides details on the control architecture and its associated methods; Section 4.3 describes the benchmark case study; Section 4.4 presents the simulation results; Section 4.5 discusses the results and expands on directions for further work.

4.1 Background

Adaptive control is often required to control plants with large parametric uncertainty for which a single controller cannot yield adequate robust stability and performance. Many approaches to the problem of adaptive control have been considered in the literature (see Anderson and Dehghani [2008] and reference therein). Since this thesis considers a multi-controller approach, we direct the interested reader, in particular, to other multi-controller methods, which have received widespread attention. Examples of results can be found in the works of Schiller and Maybeck [1997]; Safonov and Tsao [1997]; Anderson et al. [2000]; Hespanha et al. [2001]; Fekri et al. [2006]; Al-Shyoukh and Shamma [2009]; Kuipers and Ioannou [2010]; Hassani et al. [2011]. Common to all these methods is the use of information gathered in real-time about the controlled plant to decide on appropriate control actions.

Architectures performing Multiple Model Adaptive Estimation and Control consist of a finite set of candidate controllers and an identification module. At least one of the candidate controllers is assumed to meet the desired closed-loop stability and performance requirements for the plant in the loop. The role of the identification module is to select, out of the candidate set of controllers, the controller which can deliver the "best" closed-loop performance. Except for unfalsified control (outlined in the work of Safonov and Tsao [1997]), which is not a model-based approach and utilises measured data to falsify—and assess the performance of—controllers in and out of the loop in real time based on a cost function, the other cited techniques use model-based approaches. Their identification modules compute a set of performance signals which are suitably defined indexes based on the output estimation errors with respect to a set of candidate reference models. Slightly different approaches are used in Al-Shyoukh and Shamma [2009], where the identification module explores award-based calibrated forecasts, and in Kuipers and Ioannou [2010], where multiple parameter estimators produce an explicit estimate of the unknown parameter which is then used for controller selection.

A common feature of the above multi-controller approaches is that they are designed to control systems which meet strict assumptions about the controlled plant, typically linear time-invariant (LTI) systems with gaussian disturbances. For example, Hassani et al. [2011] discuss a proof of asymptotic stability and model estimate convergence of RMMAC in the LTI case. Fekri [2005] outlines that acceptable robust performance can be obtained using RMMAC in cases of *mild violation* of the design assumptions (slowly time-varying systems and/or incorrect disturbance model). Kuipers and Ioannou [2010] show that a controller mixing approach can be used to improve estimation in the presence of perturbations in the disturbance power and bandwidth, but do not discuss variations of parameters. The applicability of multi-controller methods to a broader class of problems is the subject of ongoing investigation. Recently, Hassani [2012] experimented with a variation of RMMAC which conducts a joint estimation of the system state and uncertain parameters using an Extended Kalman Filter (EKF) and selects the controller accordingly. This architecture was named Robust Adaptive Control with Extended Kalman Filtering (RAC-EKF).

RAC-EKF delivered promising results in controlling time-varying plants, as the EKF estimates, and tracks the variation of, the parameter values over time.

In this chapter, we investigate the potential of using a particle filtering approach to inform controller selection in a multi-controller architecture. Particle filtering is a numerical, sequential Monte-Carlo method which computes an approximation of the probability distribution of the state of a partially observed dynamical system by iteratively refining an initial distribution as new observations become available (Cappe et al. [2007]). In recent years, particle filtering has attracted interest as a versatile stochastic filtering tool and has found many applications, including tracking (Schon et al. [2011]), signal processing and telecommunications (Djuric et al. [2003]), geophysics (Van Leeuwen [2009]), and biomedical engineering (Zenker et al. [2007]). As already mentioned in Chapter 3, particle filters are a very general tool, which can be used in non-linear, time-varying and non-gaussian problems. However, they are associated with a potentially burdensome computational cost. To the authors' knowledge, estimating the probability distribution of the uncertain plant parameters in order to mix the control actions of a bank of (robust) controllers in a multi-controller feedback architecture is a novel proposal, and worthy of investigation. Here, we develop a new approach, RAC-PF, and employ it to control a linear parameter-varying, two-input two-output (TITO) uncertain plant with gaussian disturbances. As this plant is a natural candidate for the RAC-EKF approach, we seek to compare the two, in order to evaluate whether there are any advantages or disadvantages in terms of closed-loop performance in adopting the more general tool RAC-PF.

4.2 Methodology

4.2.1 Problem description

We assume that the plant to be controlled is a linear system with uncertain, potentially time-varying parameters, as expressed by the equations

$$\dot{x}(t) = A(\theta(t))x(t) + Bu(t-\tau) + Gw(t) \tag{4.1a}$$

$$y = C(\theta(t))x(t) + v(t), \tag{4.1b}$$

where $x(t) \in \mathbb{R}^n$ is the state of the system, $u(t) \in \mathbb{R}^m$ is the control input, $y(t) \in \mathbb{R}^q$ is the measured output, $w(t) \in \mathbb{R}^r$ is a non-measurable input disturbance, and $v(t) \in \mathbb{R}^q$ is measurement noise. The control input is applied with actuation delay τ. Also, $\theta(t) \in \mathbb{R}^p$ represents the vector of uncertain parameters, which is assumed to belong to a known compact set: $\theta(t) \in \Omega, \forall t$. The set itself is taken to be "large", which means that the poles of the plant can change considerably as a results of the variations of the parameters. However, the plant is assumed to remain open-loop stable at all times, i.e., $\mathrm{Re}\{\lambda_i\} < 0, i = 1, \ldots, n, \forall \theta \in \Omega$, with λ_i being the eigenvalues of matrix A.

The general structure of the proposed closed-loop architecture is shown in Figure 4.1. The system is to act as a regulator, minimising the effect of the disturbances on

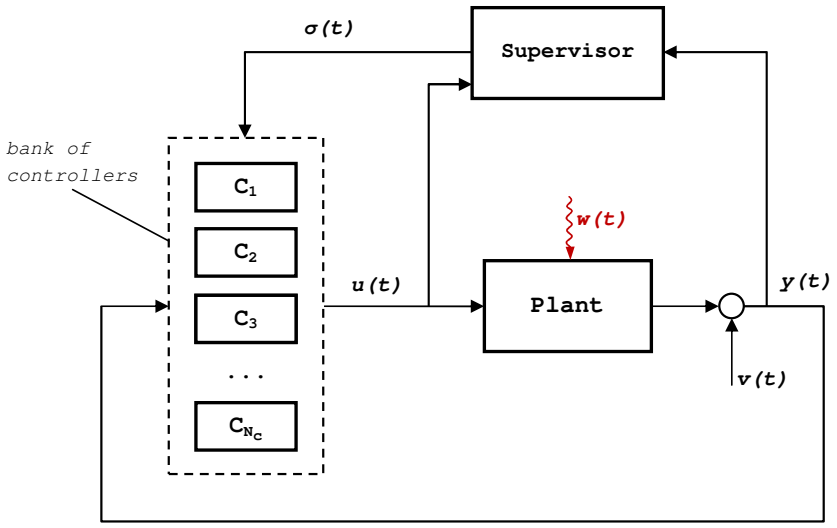

Figure 4.1: Multi-controller closed-loop architecture. Notation: $C_{1,\ldots,N_C}$ candidate controllers; $u(t)$ control signal; $w(t)$ plant noise; $v(t)$ measurement noise; $y(t)$ observed output; $\sigma(t)$ controller selection signal.

the output.

4.2.2 Controller design

The controller design methodology adopted here draws on $\mathcal{H}_\infty$ control theory and mixed-μ synthesis (Skogestad and Postlethwaite [2006]) much in a similar way as has been done in the RMMAC work of Fekri et al. [2006] and in Chapter 2 of this thesis. Such an approach is particularly suited to dealing with uncertain plants as it allows the designer to compute a linear controller which ensures that the feedback interconnection of the plant and the controller is stable for every allowed value of the uncertain parameters (robustness). Moreover, the method provides a systematic performance-based process for designing the bank of controllers. By using mixed-μ synthesis in an iterative algorithm, a single or multiple controllers (bank of controllers) can be computed, the number of which is the natural outcome of performance design specifications for the adaptive system. The required performance is defined as the maximum allowable percentage increase in the $\mathcal{H}_\infty$ norm of selected performance signals (for our regulator, higher performance corresponds to a lower RMS value for $C(\theta(t))x(t)$) when compared to the best performance achievable if the uncertain parameters were known exactly (in a hypothetical system capable of perfect identification).

There is, of course, a trade-off between the breadth of the allowable uncertainty space and maximum achievable performance. When the parametric uncertainty set Ω is large, a global robust controller (hereafter referred to as GNARC: Global Non-Adaptive Robust Controller) may lead to unsatisfactorily poor performance. A multi-

controller architecture features N_C robustly designed controllers, each catering for a subset of the uncertainty space $\omega_i \subseteq \Omega : \omega_1 \cup \cdots \cup \omega_{N_C} \equiv \Omega$ (LNARCs: Local Non-Adaptive Robust Controllers) and is therefore capable of delivering greater performance while ensuring robustness, provided that the correct plant-controller pair is used in the feedback loop at all times.[1] The breadth of subsets ω_i follows from the specification of a required performance improvement over the GNARC case. Although the methodology of Fekri et al. [2006] is well defined for single-input single-output plants, it can be extended quite readily to a multiple-input multiple-output case (see Hassani [2012] for details).

4.2.3 Parameter estimation and particle filtering

The key challenge of adaptive control in such a multi-controller architecture is, therefore, that of selection of the correct LNARC. Most approaches in the literature either estimate the uncertain parameters and select the controller based on the estimation result (as in Kuipers and Ioannou [2010]; Hassani [2012]), or they associate a performance signal to each model and controller (as in Schiller and Maybeck [1997]; Anderson et al. [2000]; Hespanha et al. [2001]; Fekri et al. [2006]; Hassani et al. [2012]). In Schiller and Maybeck [1997]; Fekri et al. [2006] a posterior probability for each controller is computed using dynamic hypothesis testing.

In the problem discussed here, arbitrary time-variability of the parameters over a large uncertainty set is assumed. In Chapter 3, we have highlighted that the joint estimation of the system's state and parameters constitutes a nonlinear filtering problem. Hassani [2012] proposes the use of an extended Kalman filter (EKF) as a suboptimal solution.

We consider an alternative approach based on particle filtering (PF). As introduced in Chapter 3, particle filtering is a sequential Monte-Carlo method which aims to compute the approximate posterior probability density of the (augmented) state, conditioned on the available observations of input and output until that time point, i.e. $p(x(k)|Z(0{:}k))$, where $Z(0{:}k) \equiv \{u(j)\ y(j)\}_{j=0}^{k}$ is the observation vector, with $k = \lfloor \frac{t}{T_s} \rfloor$, and T_s being sampling time, since PF is a numerical, therefore discrete-time method.

A thorough theoretical presentation of PF can be found in Doucet and Johansen [2009]. For the purpose of this chapter, it will suffice to recall that the posterior probability density is approximated by a finite number of samples (particles), which can be understood as candidate realisations of the system to be estimated. At time $k = 0$, N particles are initialised by sampling from a known or presumed prior probability density $p(x(0))$. Each particle carries a state estimate $\hat{x}_h(0)$, with $h = 1 \ldots N$. Throughout the subsequent time steps, particles undergo a state update, weighting and resampling process. We described this algorithm in Chapter 3. A visual illustration of the particle filtering steps is provided in Figure 4.2.

[1] The risk of instability induced by incorrect plant-controller pairing is not considered here; discussions on this topic can be found in the work of Dehghani et al. [2009]

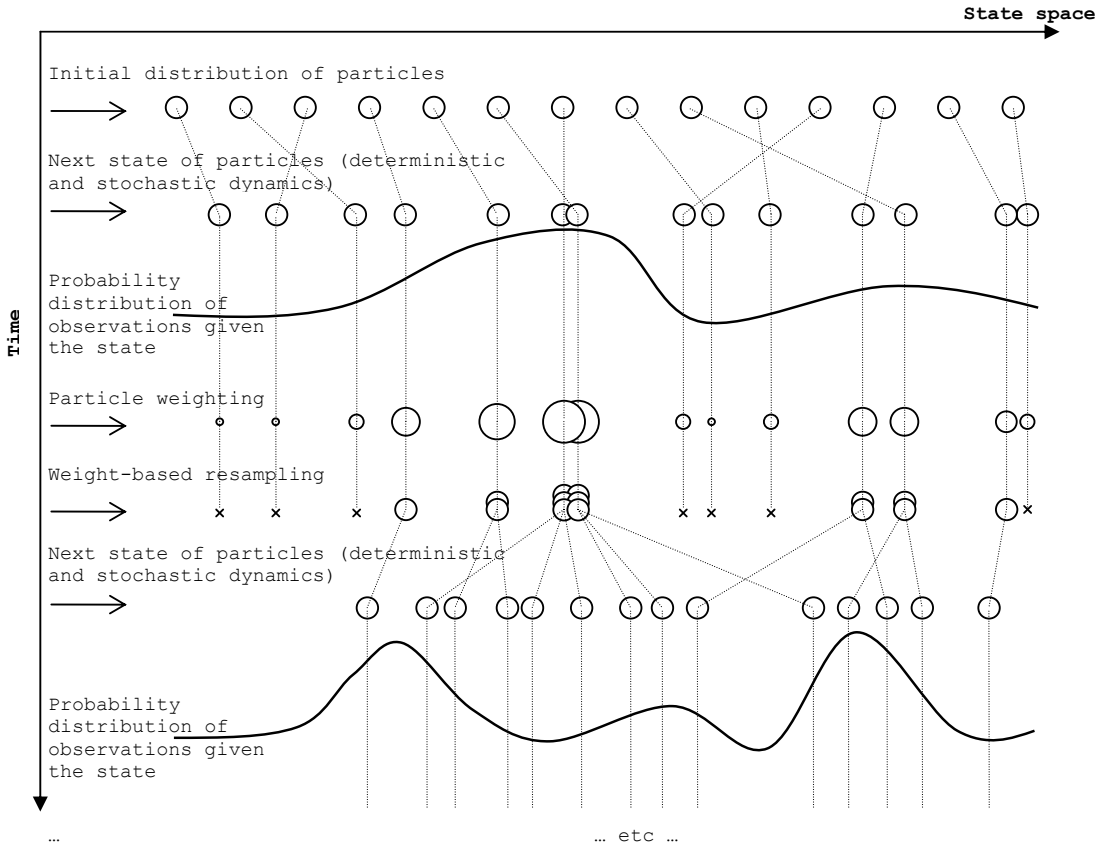

Figure 4.2: Illustration of the sampling-weighting-resampling process, which underpins particle filtering.

Over a number of iterations, the particles cluster in the state space in a way that approximates the posterior probability density of the state, i.e.,

$$\hat{p}(x(k) \in \eta | Z(0{:}k)) = \frac{n_\eta}{N}, \tag{4.2}$$

where $\eta \subseteq \Omega$ and n_η is the number of particles for which $\hat{x}_h(k) \in \eta$. As the number of particles increases, so does the accuracy of the approximation but also the computational cost. Also, models with a greater number of states require more particles to be approximated. Since this problem involves a system which can be described as linear conditionally on the time-varying parameters, a specialised form of the filter called marginalised PF (also known as Rao-Blackwellised PF; see Schon et al. [2005]) can be exploited. In a marginalised PF, the conditionally linear states are estimated using the optimal Kalman filter result (marginalisation), while the other (nonlinear) states are estimated by the standard PF algorithm. This helps reduce, to some extent, the computational burden of the algorithm.

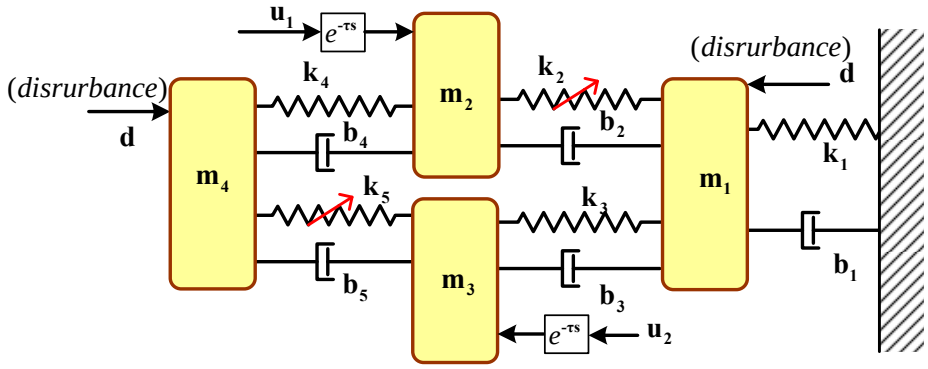

Figure 4.3: The MSD system. The spring coefficients k_2 and k_5 are uncertain.

4.2.4 Controller selection

Controller selection is obtained by integrating the approximate probability density function which results from the particle filter iterations. Specifically, the number of particles n_i associated with each uncertainty subset i, with $i = 1, \ldots, N_C$, determines the probability of model i being the correct one. The results shown in Section 4.4 are generated using a weighted approach to controller selection. The input signal u fed to the plant is a weighted sum of the control signals u_i generated by the individual controllers,

$$u = \sum_{i=1}^{N_C} \pi_i u_i, \quad \pi_i = \frac{n_i}{N}, \tag{4.3}$$

where π_i is the approximate probability of the true plant parameters belonging to subset i, and N is the total number of particles.

4.3 Control Example

4.3.1 Model description

In this section we apply the proposed methodology to control a *mass spring dashpot* (MSD) assembly. The MSD system, depicted in Figure 4.3, has a noncollocated control property and in that sense it is very similar to applications such as flexible robot arms (where the control action is applied to a point far from the arm tip) or flexible spacecraft structures where the controls (e.g., control-moment gyros) are away from the radar/telescope that must be pointed accurately. It also closely approximates the dynamics of an active suspension system.

The control action is exerted as forces acting on masses m_2 and m_3 (with actuation delay τ), while the control goal is to regulate the displacements of masses m_1 and m_4, the measurement of which is corrupted by independent random gaussian noise processes $v_1(t)$ and $v_2(t)$ with a power spectral density of 10^{-5}. Disturbance forces $d(t)$ act on masses m_2 and m_4, where $d(t)$ is generated by low-pass filtering of two

independent random gaussian noise processes, i.e.,

$$\begin{bmatrix} d_1 \\ d_2 \end{bmatrix} = \begin{bmatrix} \frac{0.1}{s+0.1} & 0 \\ 0 & \frac{0.1}{s+0.1} \end{bmatrix} \begin{bmatrix} w_1 \\ w_2 \end{bmatrix}, \tag{4.4}$$

with a power spectral density of 10 for $w_1(t), w_2(t)$.

A state-space description of the plant (augmented to include the noise model (4.4)) is given in (4.5).

$$A = \begin{bmatrix} 0 & 0 & 0 & 0 & 1 & 0 & 0 & 0 & 0 & 0 \\ 0 & 0 & 0 & 0 & 0 & 1 & 0 & 0 & 0 & 0 \\ 0 & 0 & 0 & 0 & 0 & 0 & 1 & 0 & 0 & 0 \\ 0 & 0 & 0 & 0 & 0 & 0 & 0 & 1 & 0 & 0 \\ -\frac{k_1+k_2+k_3}{m_1} & \frac{k_2}{m_1} & \frac{k_3}{m_1} & 0 & -\frac{b_1+b_2+b_3}{m_1} & \frac{b_2}{m_1} & \frac{b_3}{m_1} & 0 & \frac{1}{m_1} & 0 \\ \frac{k_2}{m_2} & -\frac{k_2+k_4}{m_2} & 0 & \frac{k_4}{m_2} & \frac{b_2}{m_2} & -\frac{b_2+b_4}{m_2} & 0 & \frac{b_4}{m_2} & 0 & 0 \\ \frac{k_3}{m_3} & 0 & -\frac{k_3+k_5}{m_3} & \frac{k_5}{m_3} & \frac{b_3}{m_3} & 0 & -\frac{b_3+b_5}{m_3} & \frac{b_5}{m_3} & 0 & 0 \\ 0 & \frac{k_4}{m_4} & \frac{k_5}{m_4} & -\frac{k_4+k_5}{m_4} & 0 & \frac{b_4}{m_4} & \frac{b_5}{m_4} & -\frac{b_4+b_5}{m_4} & 0 & \frac{1}{m_4} \\ 0 & 0 & 0 & 0 & 0 & 0 & 0 & 0 & -.1 & 0 \\ 0 & 0 & 0 & 0 & 0 & 0 & 0 & 0 & 0 & -.1 \end{bmatrix} \tag{4.5}$$

$$B = \begin{bmatrix} 0 & 0 \\ 0 & 0 \\ 0 & 0 \\ 0 & 0 \\ 0 & 0 \\ \frac{1}{m_2} & 0 \\ 0 & \frac{1}{m_3} \\ 0 & 0 \\ 0 & 0 \\ 0 & 0 \end{bmatrix} \quad G = \begin{bmatrix} 0 & 0 \\ 0 & 0 \\ 0 & 0 \\ 0 & 0 \\ 0 & 0 \\ 0 & 0 \\ 0 & 0 \\ 0 & 0 \\ .1 & 0 \\ 0 & .1 \end{bmatrix} \quad C^T = \begin{bmatrix} 1 & 0 \\ 0 & 0 \\ 0 & 0 \\ 0 & 1 \\ 0 & 0 \\ 0 & 0 \\ 0 & 0 \\ 0 & 0 \\ 0 & 0 \\ 0 & 0 \end{bmatrix}$$

The values of the model constants are $m_1 = m_2 = m_3 = m_4 = 1\text{kg}$, $k_1 = 0.15\text{N/m}$, $k_3 = k_4 = 0.1\text{N/m}$, $b_1 = b_2 = b_3 = b_4 = b_5 = 0.1\text{Ns/m}$, $\tau = 0.01\text{s}$. The spring coefficients k_2 and k_5 are uncertain parameters, with $k_2 \in [0.75, 2.5]\text{N/m}$ and $k_5 \in [0.9, 2.5]\text{N/m}$.

4.3.2 Controller bank design

As mentioned, in the proposed adaptive control approach the parametric uncertainty set is divided into smaller subsets and a robust controller is designed, using mixed-μ synthesis, for each subset. The complete procedure of subdivision of parametric uncertainty and local controller design is explained in Hassani [2012]. This process defines three subregions or uncertainty intervals as indicated in Table 4.1

Table 4.1: Summary of controller design

Controller	Uncertainty Interval k_2	Uncertainty Interval k_5
GNARC	[0.75 2.50]	[0.90 2.50]
LNARC # 1	[1.27 2.50]	[1.50 2.50]
LNARC # 2	[0.75 1.27]	[0.90 2.50]
LNARC # 3	[1.27 2.50]	[0.90 1.50]

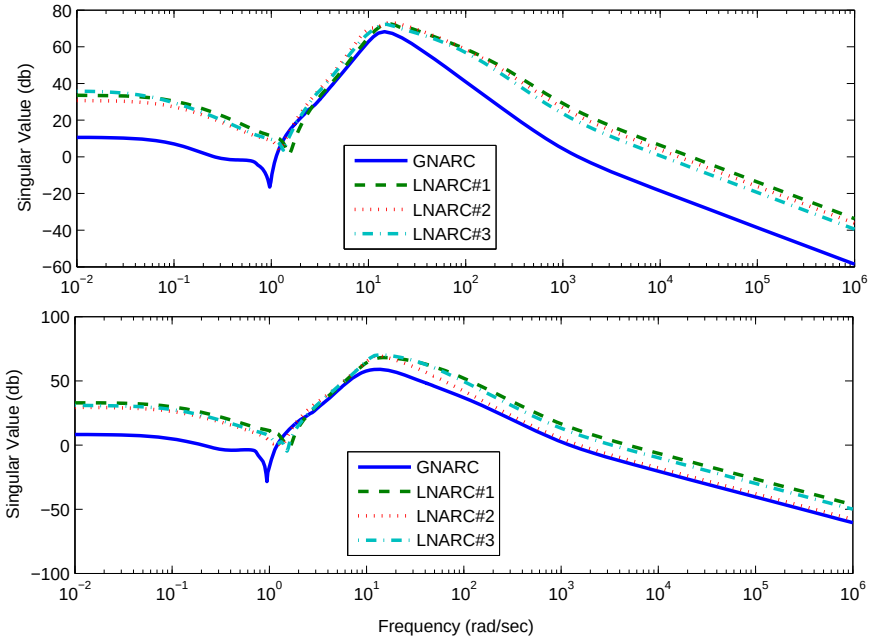

Figure 4.4: Maximum Singular Values of the Global and Local Controllers.

Note that all controllers are TITO LTI systems. Figure 4.4 compares the maximum singular value plots of the GNARC compensator and the three LNARCs. At low frequencies the local controllers generate a loop-gain about 25dB larger than the GNARC. This leads to greater disturbance rejection in closed-loop, especially in the frequency region where $d(t)$ has most of its power, i.e., $\omega \leq 0.1\text{rad/s}$. We emphasise that each individual local controller closed-loop design guarantees performance- and stability-robustness over its associated parameter subinterval (Table 4.1).

4.3.3 Particle filter

The problem of joint estimation of the state and uncertain parameters is recast as a discrete-time nonlinear filtering problem as follows:

$$\begin{aligned} x^l(k+1) &= A_d(x^n(k))x^l(k) + B_d u(k - \lfloor \tfrac{\tau}{T_s} \rfloor) + G_d w(k) \\ x^n(k+1) &= f(x^n(k)) \\ y(k) &= Cx^l(k) + v(k) \end{aligned} \tag{4.6}$$

where τ denotes input time delay. Notation x^l, x^n identifies the "linear" and "nonlinear" states, respectively ($x^n = [k_2\ k_5]^T$). Subscript d indicates zero-order hold discretisation of (4.5). The sampling time used is $T_s = 0.005\text{s}$.[2]

The fact that the sampling time is much faster than the plant dynamics is also relevant to PF design. We wish to avoid the risk that an overly rapid selection of the

[2]Controllers designed with mixed-μ synthesis can be of very high order; care must be taken to select an appropriate sampling time for discretisation.

particles may lead to an incorrect estimate. The implemented PF uses conducts the operations of particle weighting, resampling, and time update of the nonlinear states every $N_s = 100$ time steps; see (4.7a) and the algorithm below.

Given a rate of change bound for the uncertain parameters, e.g., here we assume $|\dot{k}_2|, |\dot{k}_5| < 0.175\text{Nm}^{-1}\text{s}^{-1}$, the most general update function for x^n is

$$x^n(k+1) = x^n(k) + \chi \quad (\forall k = l(N_s), l \in \mathbb{N}) \tag{4.7a}$$

$$\chi \sim \begin{bmatrix} U(-0.175N_sT_s, 0.175N_sT_s) \\ U(-0.175N_sT_s, 0.175N_sT_s) \end{bmatrix}. \tag{4.7b}$$

Uniform distributions (U) are used to capture the rate of change constraints while making no assumptions on the trend of parameter variations.

Marginalised Particle Filter algorithm

(a) *Initialisation*. Set state $x_h(0)$ for particles $h = 1, \ldots, N$ as

$$x^f(0) = 0 \quad x^n(0) \sim \begin{bmatrix} \mathcal{U}(0.75, 2.5) \\ \mathcal{U}(0.9, 2.5) \end{bmatrix},$$

also set time index $k = 0$ and weights $W_h(-1) = 0$.

(b) *Weighting*. For each particle h, compute the estimated output as $\hat{y}_h(k) = Cx_h^f(k)$. Then, evaluate the particles' normalised weights $\tilde{W}_h(k)$ as

$$W_h(k) = W_h(k-1) + p(y(k)|x_h(k)), \quad \tilde{W}_h(k) = \frac{W_h(k)}{\sum_{ii=1}^{N} W_{ii}(k)},$$

where, for this problem (bivariate normal distribution),

$$p(y(k)|x_h(k)) = \frac{1}{2\pi S_{h,11} S_{h,22}\sqrt{1-\rho^2}} e^{-\frac{1}{2(1-\rho^2)}\Psi},$$
$$\Psi = \left[\frac{(x_{h,1}-y_1)^2}{S_{h,11}^2} + \frac{(x_{h,4}-y_2)^2}{S_{h,22}^2} + \frac{(2\rho(x_{h,1}-y_1)(x_{h,4}-y_2))^2}{S_{h,11}S_{h,22}} \right],$$

with $S = \begin{bmatrix} S_{11} & \rho S_{11}S_{22} \\ \rho S_{11}S_{22} & S_{22} \end{bmatrix}$ being the Kalman innovation covariance matrix.[3]

(c) *Resampling*. If $k = l(N_s), l \in \mathbb{N}$, resample N particles on the basis of $\tilde{W}(k)$ using a residual resampling algorithm Hol et al. [2006] and reset $W_h(k) = 0$; otherwise, go to step (d).

(d) *Time update*. For each particle $h = 1, \ldots, N$,

(i) Kalman filter correction of the linear state estimate using the available observation $y(k)$

$$x_h^f(k|k) = x_h^f(k|k-1) + H_h(y(k) - Cx_h^f(k|k-1)),$$

where H is the Kalman innovation gain.[3]

(ii) If $k = l(N_s), l \in \mathbb{N}$, sample χ (4.7b) and update x_h^f (4.7a), then compute $A_{d,h}(x_h^n(k))$ and $B_{d,h}(x_h^n(k))$; otherwise, go to (iii).

(iii) Time update of the marginalised linear states $x_h^f(k+1|k)$ via (4.6).

(e) *Iteration*. Set $k \to k+1$ and repeat over from Step (b).

[3]The Kalman filter matrices can either be computed on-line (Schon et al. [2005]) or pre-computed as a function of x^n and accessed via look-up tables to reduce computational time.

4.3.4 Numerical simulations

We used the proposed architecture in two sets of numerical simulations. First, we considered a number of cases in which the unknown spring coefficients are assumed constant (simulated control horizon: 100s), in order to create a map of the magnitude of achieved output RMS as a function of k_2 and k_5. Then, we examined cases of sinusoidal variations of the time-varying parameters (simulated control horizon: 700s), in order to evaluate the system's ability to adequately track the plant as it evolves through time and implement a suitable control action. For each simulation, four different approaches to controller supervision were implemented:

- the proposed particle filter-based supervisor (identified as Robust Adaptive Control with Particle Filtering, RAC-PF);
- a supervisor based on Extended Kalman Filtering, analogous to that detailed in Hassani [2012] (identified as RAC-EKF);
- a supervisor based on exact knowledge (Perfect Identification) of the real parameter values, i.e., a system which is not realistically feasible but provides a reference in terms of maximum achievable performance by switching among the available controllers (identified as RAC-PI); and
- a system with no supervisor utilising only the GNARC controller, which gives an indication of the best achievable performance with robust non-adaptive control.

Due to the presence of stochastic processes (random plant noise and measurement noise), each case was simulated as a batch of 50 Monte-Carlo runs (each run used different initial seeds for the generation of the random processes). The simulations were performed in Matlab and Simulink. The RMS values of the output are deemed to be an indication of the performance of each approach and are computed from simulation time $t = 50$s onwards. This is intended to exclude from the computation any transients associated with initialisation bias. For each method we introduce measures of RMS performance improvement over the GNARC method and performance degradation over the RAC-PI method as:

$$\%Impr. = \frac{RMS_{GNARC} - RMS_{method}}{RMS_{method}} \tag{4.8a}$$

$$\%Degr. = \frac{RMS_{method} - RMS_{RAC-PI}}{RMS_{RAC-PI}} \tag{4.8b}$$

4.4 Results

Figure 4.5 shows a typical output result (specifically, for a constant parameter case). The different level of performance between the GNARC and the adaptive approaches is visually evident. It is also clear that the performance of RAC-PF, RAC-EKF and

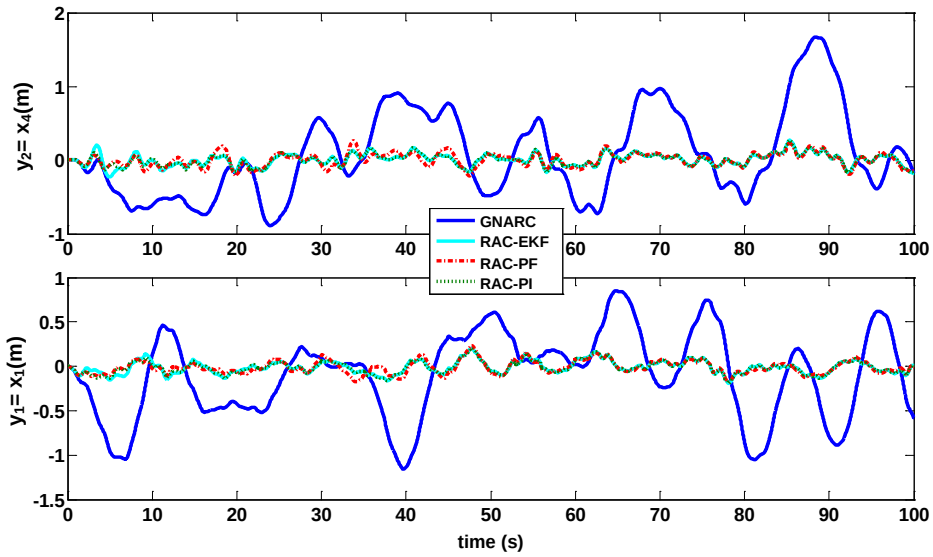

Figure 4.5: Output for the four different control methods in a constant-parameter simulation with $k_2 = 1.3\text{N/m}$ $k_5 = 2.1\text{N/m}$

RAC-PI is very close, to the extent that they are hardly distinguishable. This justifies the use of quantitative comparison measures of (as per equation (4.8)), which will be presented by means of figures and tables in the following subsections.

4.4.1 Constant parameters

In Figure 4.6, we show the RMS values of the system outputs when using RAC-PI. These are computed as the average result for the Monte-Carlo batch over a uniformly spaced grid of 210 points spanning the uncertainty region. Discontinuities in the surface plot can be seen at the edges of the LNARC design subregions (Table 4.1). Output RMS is shown to increase for lower values of k_2 and k_5.

Figure 4.7 presents the output RMS results for the RAC-PF approach. A key difference between these plots and those of Figure 4.6 is the absence of discontinuities: this is due to the fact that the weighted approach to controller selection ((4.3)) creates a smooth transition between adjacent controllers. This has the potential to avoid transients induced by switching operations and may improve performance at subset boundaries. The RMS values are only slightly higher than those of RAC-PI, as had been anticipated by inspection of Figure 4.5.

The percentage degradation of RAC-PF with respect to RAC-PI is shown in Figure 4.8. This shows some performance loss with peaks of up to 60% for x_1 and 40% for x_4; the plot for x_4 shows that on the boundary region between subsets the new approach can perform slightly better than the perfect identification method (negative degradation). It should be remarked that since the RMS values are very small in absolute terms, the two methods still achieve, in practice, very similar results.

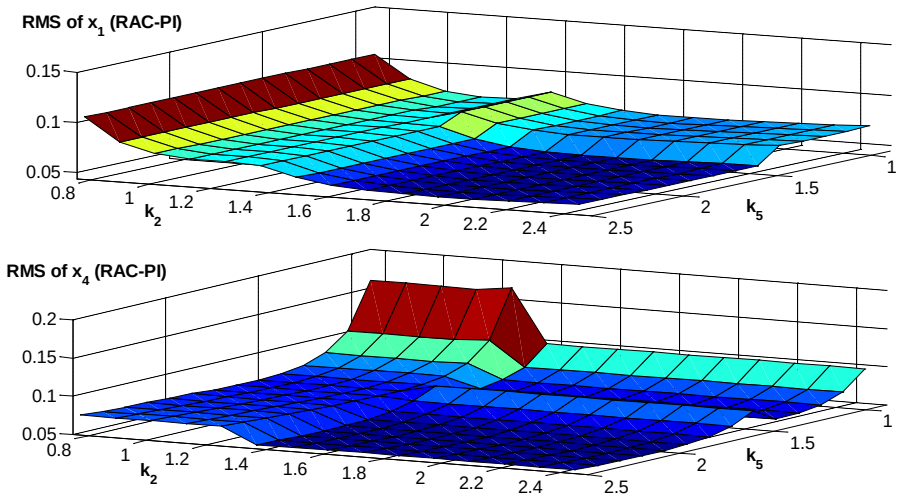

Figure 4.6: RMS of the output signals as a function of the uncertain parameter values k_2 and k_5 (RAC-PI).

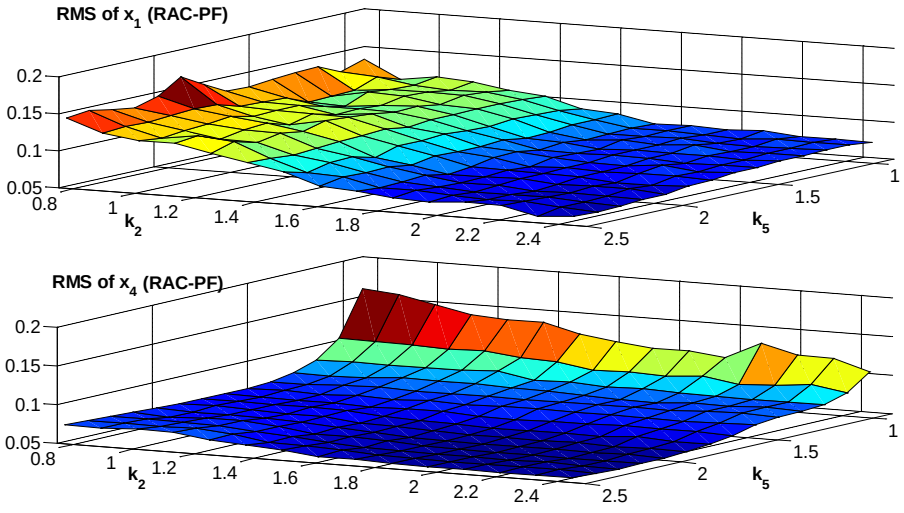

Figure 4.7: RMS of the output signals as a function of the uncertain parameter values k_2 and k_5 (RAC-PF).

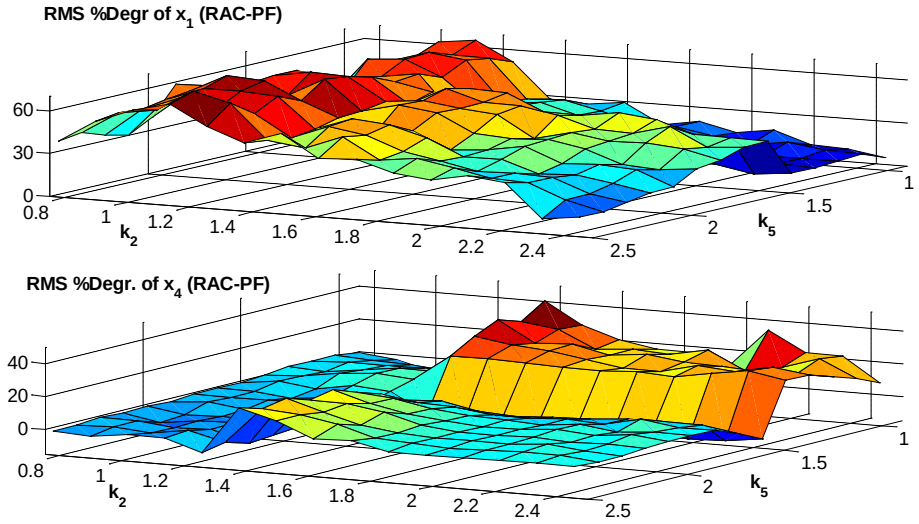

Figure 4.8: Performance degradation of RAC-PF over RAC-PI.

The plots of Figure 4.9 give a clear result in terms of improved performance over the GNARC, with 200 to 900% improvement for both x_1 and x_4. This reaffirms the superiority of adaptive control in the context of this example.

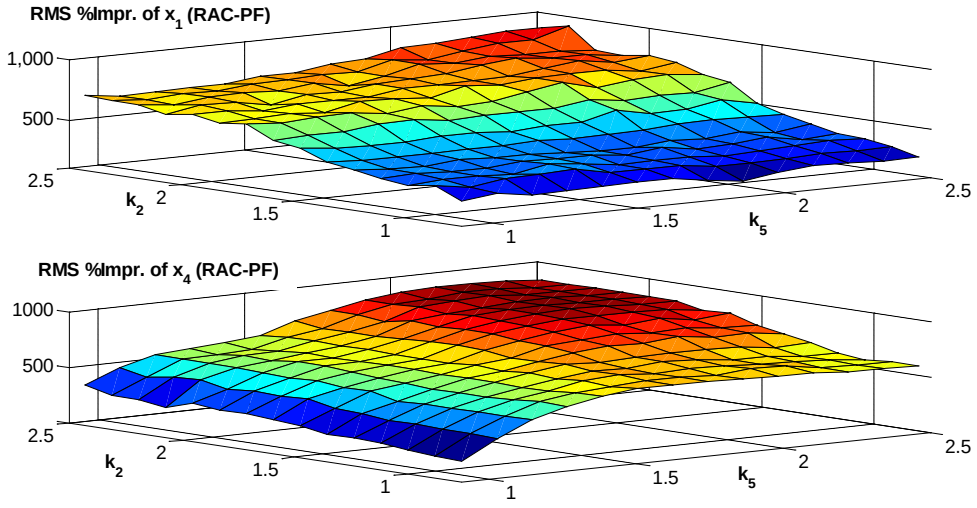

Figure 4.9: Performance improvement of RAC-PF over GNARC. Note the inversion of the k_2, k_5 axes to aid visualisation.

We compare the performance of the RAC-PF method also with the RAC-EKF method of Hassani [2012]. Figure 4.10 shows that RAC-PF produces a 5 to 45% higher RMS value for x_1 and 50% lower to 50% higher RMS value for x_4. RAC-EKF is therefore slightly better performing than RAC-PF for the constant parameter case.

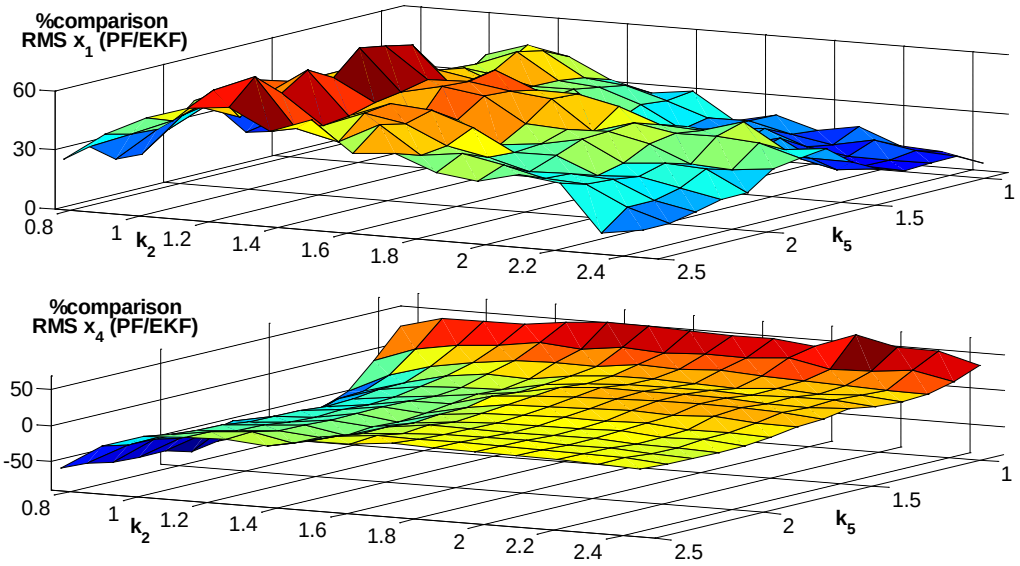

Figure 4.10: Percentage RMS increase using RAC-PF over RAC-EKF.

Finally, Figure 4.11 shows the distribution and evolution through time of the particles for one of the constant parameter simulations. As expected, the density map shows greater particle concentration in the proximity of the true value of the unknown parameters. The estimation results for the RAC-EKF method are also shown for comparison.

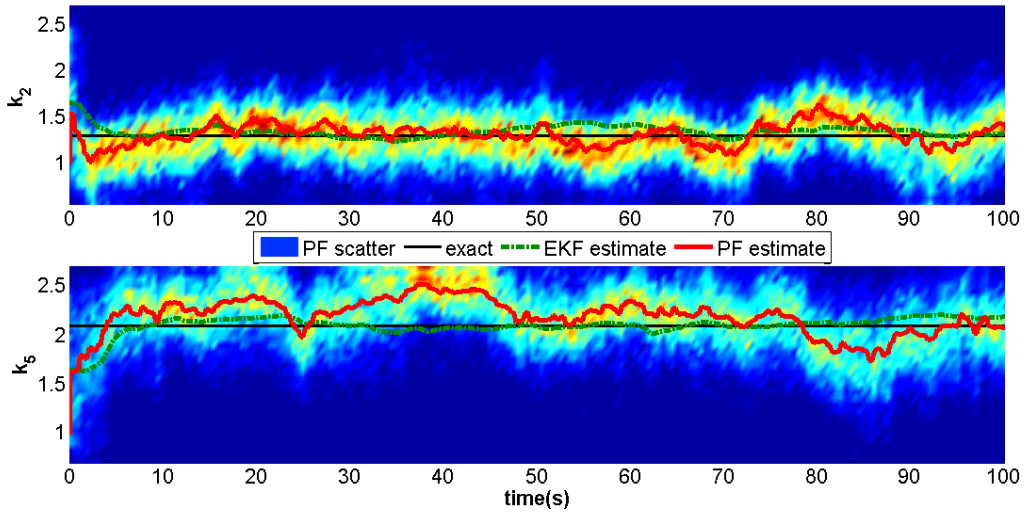

Figure 4.11: Comparing parameter estimation between PF and EKF for the constant parameter case. Particle scatter is described as a density map with warmer colour indicating greater particle density. The PF estimate is given by the mean of the particle distribution (4.2).

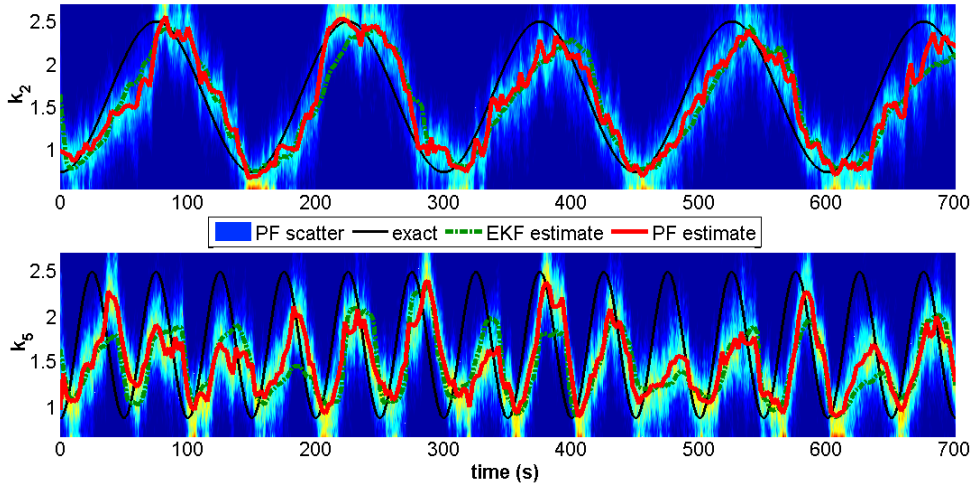

Figure 4.12: Comparing parameter estimation between PF and EKF for the parameter-varying case.

4.4.2 Time-varying parameters

For the time-varying case, sinusoidal variations are imposed on both uncertain parameters, at a frequency of $6.67 \cdot 10^{-3}$rad/s for k_2 and 0.02rad/s for k_5. The variations span the whole uncertainty range. The rate of the change is comparable with the dynamics of the other plant states: this represents a challenging task for adaptation.

Figure 4.12 shows the tracking of the parameters by the particle filter. The particle scatter and mean PF estimate show that the approach is able to track the uncertain parameters as they evolve through time. Tracking accuracy is lower for k_5, which varies at the very maximum allowed rate of change, still, this is sufficient to achieve stable control. The PF parameter estimate in fast-varying conditions is as accurate as—and in some cases even superior to—the one generated by the EKF.

The control performance is compared in Table 4.2. The comparison confirms that the adaptive architectures can deliver a dramatic improvement in performance over a global non-adaptive approach and shows that both RAC-PF and RAC-EKF can achieve very close performance to that of an ideal system capable of perfect identification, with RAC-PF delivering the best performance out of the two methods.

4.5 Discussion

We have proposed the use of the general numerical nonlinear filtering tool of particle filtering as a method to enact appropriate controller selection in a multi-controller architecture, particularly when used to control time-varying plants. In the case of the TITO time-varying plant presented here, the RAC-PF architecture has shown the ability to track the uncertain parameters well and deliver a level of performance very similar to that of the ideal RAC-PI system, even when rapid parameter variations

Table 4.2: Performance comparisons for the time-varying case

Controller	output	RMS	%Impr.	%Degr.
GNARC	x_1	0.59	0	91
	x_4	0.55	0	84
RAC-PI	x_1	0.090	556	0
	x_4	0.090	511	0
RAC-EKF	x_1	0.093	534	3.2
	x_4	0.110	400	18.1
RAC-PF	x_1	0.092	541	2.1
	x_4	0.097	467	7.2

were imposed.

The comparison with the results of the RAC-EKF approach is noteworthy, since the characteristics of the problem considered (linearity, zero-mean gaussian disturbances) are particularly suited to the use of Kalman filter-derived approaches. Indeed, an estimation approach based on the Extended Kalman Filter is a natural choice for this problem, as demonstrated by the minimal performance degradation exhibited by RAC-EKF when compared to the ideal system. The RAC-PF approach, however, has a much broader potential scope of application than RAC-EKF, since it can be readily extended to suit other estimation problems in which the tuning of Kalman-based methods would be complex, if at all possible (e.g., predominantly nonlinear systems, presence of variable/unknown time delays, arbitrarily distributed stochastic signals and/or parameter variations,...). The differences in performance between RAC-EKF and RAC-PF are very small, indicating that, from a control perspective, there would only be minor performance disadvantages in adopting RAC-PF as a one-stop design solution without having to evaluate a-priori the applicability of EKF. In fact, the performance of RAC-PF even exceeds that of RAC-EKF in selected regions of uncertainty for parameter x_4, particularly at the boundary of the uncertainty subintervals. This can be attributed to the "mixing" approach to controller selection adopted by RAC-PF, which is not possible under RAC-EKF (the result of the EKF is a parameter estimate, so only one controller can be switched into the loop at a time, in a so-called "switching" approach). Kuipers and Ioannou [2010] have also reported that mixing controller action in multi-controller approaches have the potential to deliver greater performance than switching approaches.

The additional breadth of scope of RAC-PF comes at the cost of increased computation. Simulations on a standard desktop computer (Intel®Core™2 Quad CPU 3.00GHz, 4GB RAM) ran just under real-time (88s computation time for a 100s simulation) using N =150 particles. This, however, included simulation of both the controlled plant and the feedback control approach. Faster computations could be expected from a dedicated system. Still, when compared to the computational cost of RAC-EKF (10s computation time for a 100s simulation), it is evident that the applicability of RAC-PF is dependent on the availability of adequate computational

resources. We have highlighted that in mixed linear-nonlinear problems, marginalisation of the particle filter may assist with a reduction of the computational burden. Further work on the optimisation of the particle filtering software code and its implementation on platforms other than Matlab are likely to further reduce the computational demands of the approach.

Chapter 5

Robust adaptive control with particle filtering for sodium nitroprusside administration

This chapter applies the robust adaptive control architecture with particle filtering (RAC-PF) described in Chapter 4 to the sodium nitroprusside (SNP) administration problem for the control of mean arterial pressure (MAP) already discussed in Chapter 2. We design and carry out a Monte-Carlo simulation campaign with the aim to evaluate the viability and effectiveness of the RAC-PF approach as a feedback control methodology to regulate MAP in patients experiencing acute hypertension. The simulation is designed to be broad and takes into account uncertainty in the patient response model, as well as potential non-zero-mean disturbances in the baseline arterial pressure and a variety of possible time trends in the variation of the response parameters. The results show that the proposed system can achieve adequate and safe feedback control of mean arterial pressure. Our findings also highlight the fundamental—and possibly clinically overlooked—role of system excitation in ensuring that successful simultaneous identification and control of time-varying drug administration systems can be achieved.

The content of this chapter closely follows the author's research paper *Particle filter-based robust adaptive control for closed-loop administration of sodium nitroprusside (Malagutti [b])*. Section 5.1 briefly reviews the scope of the work; Section 5.2 details the SNP dose-response model, the proposed RAC-PF control architecture, and the characteristics of the computational simulations; Section 5.3 reports on the outcomes of the simulation campaign; finally, Section 5.4 comments on the results and the potential of the proposed approach, and outlines further research directions.

5.1 Background

Earlier in this thesis (see Chapter 2), we introduced the reader to the proposed control task of regulating MAP in acute hypertensive patients through closed-loop infusion of SNP. We identified significant intra- and interpatient variability in the dose re-

sponse parameters, non-zero-mean disturbances in the baseline MAP and uncertain time delays as challenges to the design of a control methodology capable of delivering robust performance in this application. Although we reported on positive results by adapting the Robust Multiple-Model Adaptive Control (RMMAC) architecture of Fekri [2005] to this control problem (also detailed in Malagutti et al. [2013]), we acknowledged that the use of Kalman filter-based estimators was not ideal for an application where the basic assumptions for Kalman filtering (linear time-invariant systems with gaussian disturbances) were violated, albeit *sufficiently mildly* to allow for RMMAC to deliver acceptable performance (as discussed in Chapter 4, Section 4.1). Furthermore, in Chapter 2 we only showed selected simulations to demonstrate the ability of the approach to avoid undesirable transient behaviour, but did not report on a broader simulation campaign.

The work in this chapter presents a novel approach to the control of automatic infusion of SNP with a strong focus on robustness. Whilst retaining the same robust controllers designed for RMMAC in Chapter 2, the new methodology uses particle filtering to generate an estimate of the dose-response characteristic in real-time (as in Chapter 3) and exploits the estimation result to inform appropriate feedback control. We have named the new method Robust Adaptive Control with Particle Filtering (RAC-PF) and we have reported on a non-clinical case study featuring this architecture in Chapter 4. We deem particle filters—a much more general tool than Kalman filters—to be better suited to the estimation of systems characterised by time-varying parameters, non-Gaussian disturbances and even nonlinearities, such as may be present in pharmacokinetic-pharmacodynamic systems (Bonate [2011]). This chapter provides an overview of the RAC-PF design for the SNP administration problem and reports on an extensive computational simulation campaign designed to assess the viability of the new methodology and its effectiveness in delivering safe automatic feedback control of SNP infusion for a broad range of response characteristics and disturbances.

5.2 Methodology

5.2.1 Dose-response model

We have already shown the structure of the dose-response model for a patient receiving SNP, according to Martin et al. [1987], in figure 2.1. Three interconnected first-order linear systems represent the systemic and pulmonary circulation compartments and the drug effect site. In transfer function form, the dynamic behaviour of the system is given by:

$$\frac{P_{drop}(s)}{U(s)} = e^{-sT}\frac{K(\tau_3 s+1)}{((\tau_3 s+1)(\tau_2 s+1)-\alpha)(\tau_1 s+1)} \tag{5.1}$$

and the output is given by the affine transformation

$$y_{meas}(t) = p_0(t) - p_{drop}(t) + w(t). \tag{5.2}$$

Three system parameters are deemed uncertain and a priori unknown: K, T and α. These represent the sensitivity in the patient's response, the recirculation fraction and the input time delay, respectively. The allowed ranges for the values and the rates of change are summarised below (cf. Section 2.2.1).

$$\begin{array}{ccc} 0.25 < K(t) < 9.5, & \left[\frac{mmHg}{ml/hr}\right] & \left|\frac{dK}{dt}\right| < 3K(t)hr^{-1} \\ 10 < T(t) < 50, & [s] & \left|\frac{dT}{dt}\right| < 40hr^{-1} \\ 0.25 < \alpha(t) < 0.75, & & \left|\frac{d\alpha}{dt}\right| < 0.5hr^{-1} \end{array} \tag{5.3}$$

The offset term $p_0(t)$ is also treated as potentially time-varying in the interest of generality. As $p_0(t)$ represents a patient's underlying MAP, it is modelled here as a mainly low-frequency signal, given by the combination of its measurable value at $t = 0$ and an arbitrarily shaped but frequency-domain-bounded component, which we will refer to as *baseline disturbance* $p_{dist}(t)$:

$$\begin{array}{c} p_0(t) = p_0(t=0) + p_{dist}(t) \\ p_{dist}(t) : P_{dist}(s) \leq \frac{0.4}{s+0.01} \end{array} . \tag{5.4}$$

Thus, $p_0(t = 0)$ can be regarded as a known fixed offset at the output, while the disturbance component can be treated as part of the state as shown in the following state space description of the patient response model:

$$\begin{array}{rcl} \dot{x} & = & Ax(t) + Bu(t - T(t)) + Lv(t) + Mp_{dist}(t) \\ y_{meas} & = & p_0(t=0) - Cx(t) + w(t) \end{array} , \tag{5.5}$$

with

$$A = \begin{bmatrix} -\left(\frac{1}{\tau_1} + \frac{1}{\tau_2} + \frac{1}{\tau_3}\right) & -\left(\frac{1}{\tau_1\tau_2} + \frac{1-\alpha(t)}{\tau_2\tau_3} + \frac{1}{\tau_1\tau_3}\right) & \frac{\alpha(t)-1}{\tau_1\tau_2\tau_3} & 0 \\ 1 & 0 & 0 & 0 \\ 0 & 1 & 0 & 0 \\ 0 & 1 & 0 & -0.01 \end{bmatrix} \tag{5.6a}$$

$$B = \begin{bmatrix} 1 \\ 0 \\ 0 \\ 0 \end{bmatrix} \quad L = \begin{bmatrix} 0.0625 \\ 0 \\ 0 \\ 0 \end{bmatrix} \quad M = \begin{bmatrix} 0 \\ 0 \\ 0 \\ 0.4 \end{bmatrix} \quad C = \begin{bmatrix} 0 & \frac{K(t)}{\tau_1\tau_2} & \frac{K(t)}{\tau_1\tau_2\tau_3} & 1 \end{bmatrix} , \tag{5.6b}$$

where $v(t) \sim N(0,1)$, $w(t) \sim N(0,2)$ are normally distributed random noise signals at the input (actuation noise) and the output (measurement noise), respectively. The signal $y_{meas}(t)$ represents the measurable MAP value.

5.2.2 Control performance requirements

We refer the reader to Section 2.2.3 for the already discussed performance requirements for this application.

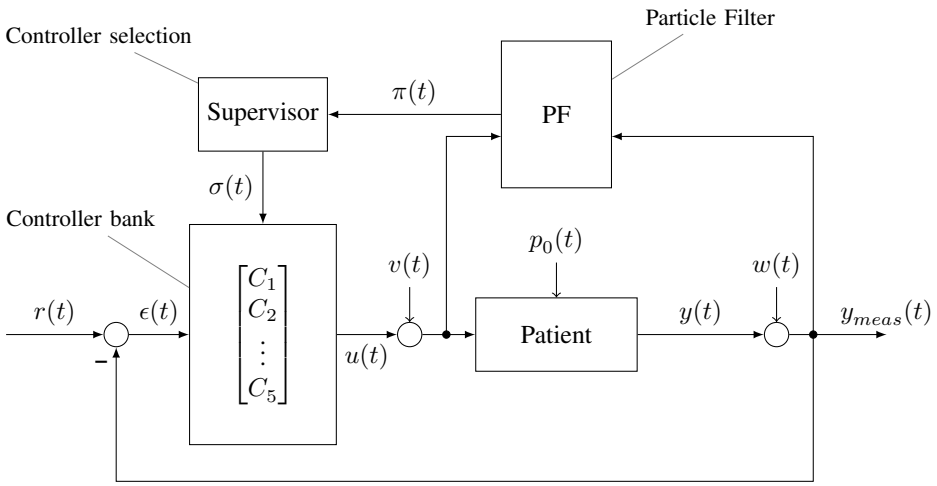

Figure 5.1: RAC-PF control architecture. Notation: $r(t)$ reference signal (desired MAP value); $C_{1,\ldots,5}$ candidate controllers; $\epsilon(t) = r(t) - y_{meas}(t)$ MAP tracking error; $u(t)$ control signal (drug infusion rate); $p_0(t)$ patient's underlying MAP; $y(t)$ output MAP; $w(t)$ measurement noise; $y_{meas}(t)$ measured MAP; $\pi(t) = \{\pi_i\}_{i=1,\ldots,5}$ probability of the estimated model parameters belonging to the uncertainty subset for which robust controller C_i has been designed; $\sigma(t)$ controller selection signal.

5.2.3 The control approach

The RAC-PF architecture is shown in Figure 5.1. In the proposed approach, multiple controllers are required in order to ensure that a controller-plant pair capable of maintaining closed-loop stability and delivering the required level of performance exists for all possible values of the patient parameters. A particle filter tracks the parameters in real-time and informs the controller selection algorithm with a probability result, which is in turn used to determine the most appropriate control signal for the closed-loop system.

Controller design

The controllers are designed using μ synthesis. Controller design and μ synthesis have been discussed previously and we refer the reader to Malagutti et al. [2012a, 2013] and Section 2.3.1 for a detailed description of the controller design methods and results as applied to the SNP dose-response model of (5.1).

For the purpose of the presentation hereof, it suffices to report that the performance specifications were imposed as frequency-domain bounds on signals $\epsilon(t)$ and $u(t)$ as shown in Figure 5.2. These constraints translate into requirements for a small reference tracking error at low frequencies (to ensure proper target following at steady state) and a mainly low-frequency infusion rate signal (to cater for the slew-rate limitations of the actuator, likely a motorised infusion pump). Our μ synthesis computations have shown that a single linear feedback controller could not deliver

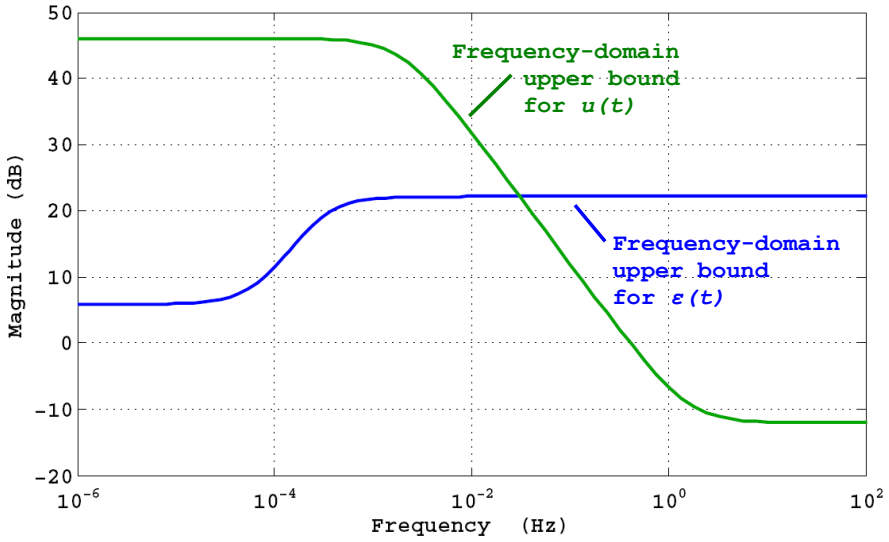

Figure 5.2: Performance bounds. Frequency-domain upper bound constraints for performance and control signals adopted for controller design using the μ synthesis technique.

the required level of performance due to the large ranges of parametric uncertainty (in particular the sensitivity parameter K). However, satisfactory performance could be achieved by subdividing the uncertainty range of K into multiple subsets and designing a robust controller for each subset. Figure 5.3 and Table 5.1 describe the 5 controllers resulting from our synthesis and the corresponding uncertainty subsets. Note that all controllers cater for the full uncertainty range of parameters α and T, while, with respect to K, each controller is associated with a region of *best performance* and a region of *acceptable performance* based on a minimum required normalised performance index $A_p = 1$ (cf. Section 2.3.1).

Controller number i	To suit K (best performance) (mmHg/(ml/hr))	To suit K (acceptable performance) (mmHg/(ml/hr))	To suit α	To suit delay T (s)
1	0.25 – 0.57	0.25 – 0.78	0.25 – 0.75	0 – 50
2	0.57 – 1.25	0.37 – 1.77	0.25 – 0.75	0 – 50
3	1.25 – 2.30	0.75 – 3.45	0.25 – 0.75	0 – 50
4	2.30 – 4.32	1.33 – 6.50	0.25 – 0.75	0 – 50
5	4.32 – 9.50	2.45 – 9.50	0.25 – 0.75	0 – 50

Table 5.1: Characteristics of the robust controllers.

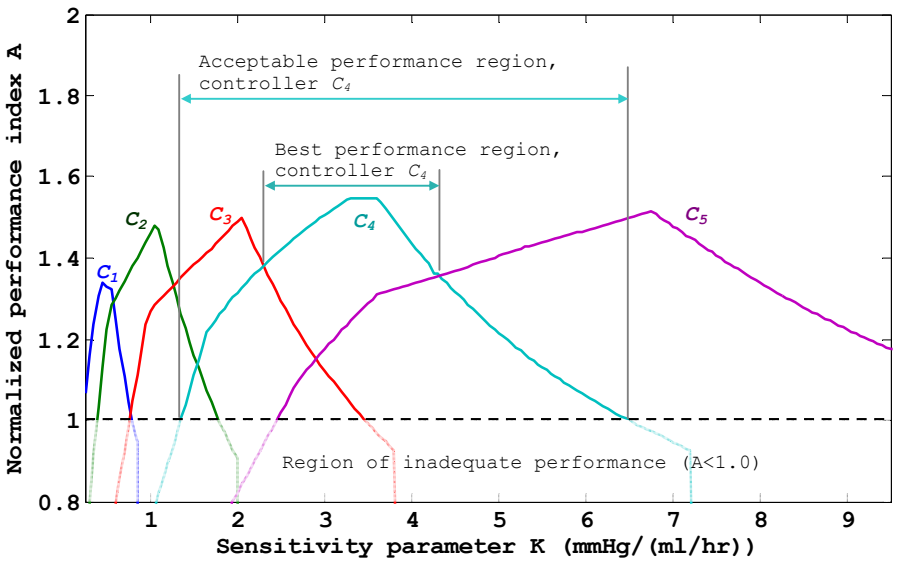

Figure 5.3: Controller performance results. Normalised performance of the uncertain dose-response model when paired with the designed controllers as a function of sensitivity parameter K. The required level of robust performance in the feedback interconnection can be achieved for $A_p \geq 1$.

Particle filtering

Particle filtering is used to jointly estimate the state and the uncertain parameters of the patient response (particularly patient sensitivity K) so that the correct controller can be used in the feedback loop. To this end, the estimation problem is recast as a nonlinear tracking problem to include the uncertain parameters in the state, as shown in (5.7) below. We refer to the original system states as "linear" states x^l, as opposed to the "nonlinear" states x^n representing the parameters. Such a mixed linear/nonlinear formulation makes it possible to use marginalised particle filtering as we have done in Chapter 4.

Since particle filtering is a discrete-time approach, a suitable sampling time must be chosen. Due to the nature of clinical MAP observations (require averaging over at least 1 cardiac cycle), we consider a sampling time $T_s = 2$s. The discrete-time description of the system used in the particle filter is given by

$$\begin{aligned} x^l(k+1) &= A_d(x^n(k))x^l(k) + B_d u(k - \lfloor \frac{T(x^n(k))}{T_s} \rfloor) + L_d v(k) + M_d p_{dist}(k) \\ x^n(k+1) &= f(x^n(k)) \\ y_{meas}(k) &= p_0(0) - C_d(x^n(k))x^l(k) + w(k), \end{aligned} \tag{5.7}$$

where $k = \lfloor \frac{t}{T_s} \rfloor$ ($\lfloor \cdot \rfloor$ is the *floor* operator). The subscript d indicates zero-order hold discretisation of continuous-time model (5.5).

The expression $f(x^n)$ indicates a function of x^n and describes the time update of the nonlinear states. It is given by:

$$x^n(k+1) = \begin{bmatrix} K(k+1) \\ T(k+1) \\ \alpha(k+1) \end{bmatrix} = x^n(k) + \chi(k), \tag{5.8}$$

where $\chi(k)$ is sampled from an array of probability distributions which are intended to reflect the likely trajectory of the parameters. Uniform distributions (U) are used to capture the constraints on the rate of change of parameters expressed in (5.3) while making no assumptions on possible shapes of variation (tracking by *random walk*), as shown below.

$$\chi(k) \sim \begin{bmatrix} U(-0.017K(k), 0.017K(k)) \\ U(-0.028, 0.028) \\ U(-0.00028, 0.00028) \end{bmatrix} \tag{5.9}$$

The particle filter algorithm follows the exact sampling, updating, weighting and resampling steps already described in Section 4.3.3 (also illustrated in Figure 4.2). Due to the fast sampling time with respect to the plant time constants, particle weights are accumulated over 120s between subsequent resampling events (cf. Chapter 4) to avoid impoverishment of the distribution which could arise from overly frequent resampling.

Controller selection

Controller selection is carried out by integrating the approximate probability distribution which results from particle filtering. The number of particles n_j associated with each of the *best performance* subsets listed in Table 5.1 is proportional to the probability of controller j being the correct one for insertion in the loop. Using the same weighted approach to controller selection as in Chapter 4, the drug infusion rate u can be computed as a weighted sum of the control signals u_j generated by each controller.

$$u = \sum_{j=1}^{5} \pi_j u_j, \quad \pi_j = \frac{n_j}{N}, \tag{5.10}$$

where π_j is the probability of the true parameters belonging to subset j and N is the total number of particles.

This is of course only one of the possible methods for controller selection. Alternative criteria could also be proposed, based on other properties of the probability distribution (e.g., mean, median, a specific percentile, presence of multimodality, etc.). This added flexibility is an advantageous aspect of the proposed architecture: some further tuning of the closed-loop system is possible without redesigning the controllers.

5.2.4 Numerical simulations

A broad computational simulation campaign was conducted in order to evaluate the ability of the proposed adaptive control approach to control MAP through SNP administration in a wide variety of conditions. To reflect the unpredictable nature of blood pressure disturbances and patient parameter variations, a large number of cases were randomly generated and simulated. All simulations involved a control horizon of 10,000 seconds (approximately 2 hours and 45 minutes), with a target MAP of 100mmHg for the time period 0s-4,000s and 80mmHg for 4,000-10,000s.

Two categories, or *simulation streams*, of hypertensive patients were simulated:

(a) relatively "settled" patients, i.e. displaying elevated MAP ($p_0 = 120$mmHg at $t = 0$) with $p_{dist}(t)$ modelled as a random, zero-mean, low-intensity additive disturbance (in the range $\pm$6mmHg);

(b) more "unsettled" patients, i.e. displaying the same initial MAP as (a) but greater intensity of random fluctuations (in the range $\pm$15mmHg), as well as two step increases in $p_{dist}(t)$ (+20mmHg) at 2,000s and 5,500s, modelling a worsening hypertensive condition.

Scenarios of controlled MAP reduction of 20-80mmHg were deemed quite general whilst clinically plausible.

The $p_{dist}(t)$ signal used in the simulations was generated by filtering the superposition of a gaussian white noise process and step signals (the latter only for stream b) with a suitable low-pass filter to meet the frequency domain bound assumption of (5.4). The seeds for the generation of all random processes were also randomised and changed for every simulation: no two simulations in the campaign, therefore, would exhibit the same $p_0(t)$, $w(t)$ and $v(t)$ traces.

For each simulation stream, the following simulation batches were computed:

(i) 40 simulations in which mid-range parameter values were chosen, i.e., K=4mmHg/(ml/hr), α=0.5 and T=30s, and held fixed throughout the control horizon;

(ii) 80 simulations in which the three model parameters K, α, and T were randomly selected from the allowed ranges as per (5.3) and held *constant* throughout the control horizon;

(iii) 80 simulations in which the initial values of the parameters were randomly selected as in (ii) with *piece-wise linear variations* throughout the control horizon. A random number of slope changes between 2 and 5 was selected for each run. The slope of the ramp was also selected at random each time ensuring it would not exceed the constraints of (5.3);

(iv) 80 simulations in which the initial values of the parameters were randomly selected as in (ii) with *piece-wise exponential variations* throughout the control horizon. Between 2 and 5 changes were again randomly selected for each run.

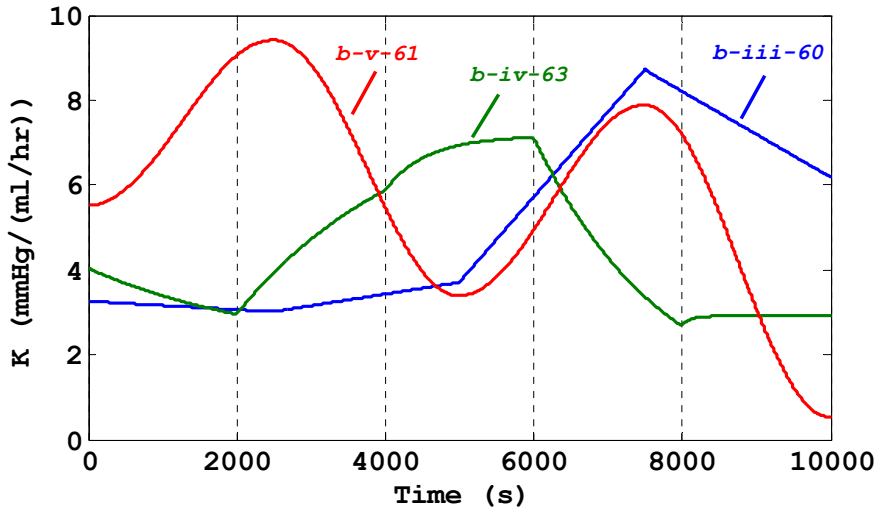

Figure 5.4: Examples of ramp, exponential and sinusoidal shapes for simulated parameter variations. The corresponding simulation runs are specified.

The exponent was also randomly selected in such a way that the slope of the resulting curve would not exceed the constraints of (5.3);

(v) 80 simulations in which the initial values of the parameters were randomly selected as in (ii) with *piece-wise quarter-sinusoidal variations* throughout the control horizon. Between 2 and 5 changes were again randomly selected for each run. The target value for each change was randomly selected in such a way that the slope of the resulting curve would not exceed the constraints of (5.3);

The main purpose of batch `i` was to help verify the ability of the approach to deliver repeatable results. Batches `ii` to `v` were intended to test the ability of the control approach to respond to a wide range of parameter variations (for examples of variation trends see Figure 5.4). The total number of simulations was 720, corresponding to 2,000 *in-silico* patient hours.

Due to the large amount of available data, aggregate measures for the control and identification performance were adopted. For each simulation run, the following measures were computed:

Measures concerning control performance

- t_{c_1}, t_{c_2} – the convergence time (10% to 90% of transition) as the two MAP setpoint changes are imposed;
- $t_{\pm 5}, t_{\pm 10}, t_{\pm 15}$ – the time (out of 10,000s) y_{meas} remained within $\pm$5mmHg, $\pm$10mmHg and $\pm$15mmHg of the setpoint $r(t)$, respectively;
- $\epsilon_{max}, \epsilon_{min}, \epsilon_{avg}$ – the peak positive and negative, and average setpoint tracking error recorded over the control horizon;

- t_{pp}, t_{npp} – the time the RAC-PF controller and the true patient system form a *provably performant (pp)* or *non-provably performant (npp)* pair as evaluated through μ analysis (Skogestad and Postlethwaite [2006]), i.e., a pp closed-loop pair would achieve a performance index $A_p \geq 1$ in Figure 5.3 (*Note*: Due to the inherent conservativeness of μ analysis, a npp pair does not necessarily indicate an unstable or underperforming closed-loop condition, but only that there is no mathematical proof of robust performance. At npp times, loop performance should be evaluated from other indices.);

- t_{sat} – the time the infusion rate signal remained at the maximum allowed value (controller saturation).

Measures concerning estimation of the response characteristic:

- t_0 – time (out of 10,000s) for which the K subinterval deemed the most likely by the particle filter, i.e. with the greatest π_i (intervals as per *best performance* in Table 1) contains the true simulated value of K;

- t_1 – time for which the K subinterval deemed the most likely by the particle filter is a neighbouring interval to that containing the true value of K;

- t_2 – time for which the K subinterval deemed the most likely by the particle filter is 2 intervals away from that containing the true value of K;

- $K_{rel}, T_{rel}, \alpha_{rel}$ – the mean relative estimation error for parameters K, T and α, respectively (the mean of the particles is used to determine the estimate).

The simulation environment was programmed using Matlab and Simulink and run on a standard desktop computer (Intel Core 2 Quad CPU, 3.0GHz).

5.3 Results

Figure 5.5 shows the results of simulation `b-v-54`: a case featuring large variations in the SNP response parameters over time and significant fluctuations in baseline MAP. From the graphs, it can be readily appreciated that the proposed control approach tracks the simulated time-varying response characteristics and meets the required performance specifications.

For completeness, and to provide context in the interpretation of the aggregate results for groups of simulations, Table 5.2 lists the overall results for simulation `b-v-54`.

The aggregate results for all of the simulations are shown in Table 5.3. For each measure, the mean value and standard deviation over the corresponding batch are displayed.

The results for batches `a-i` and `b-i` confirm the repeatability of results using the proposed method. The standard deviation values are much lower than for other batches, indicating that the system was able to deliver consistent outcomes, as required, when applied multiple times to the same case. The fact that the standard

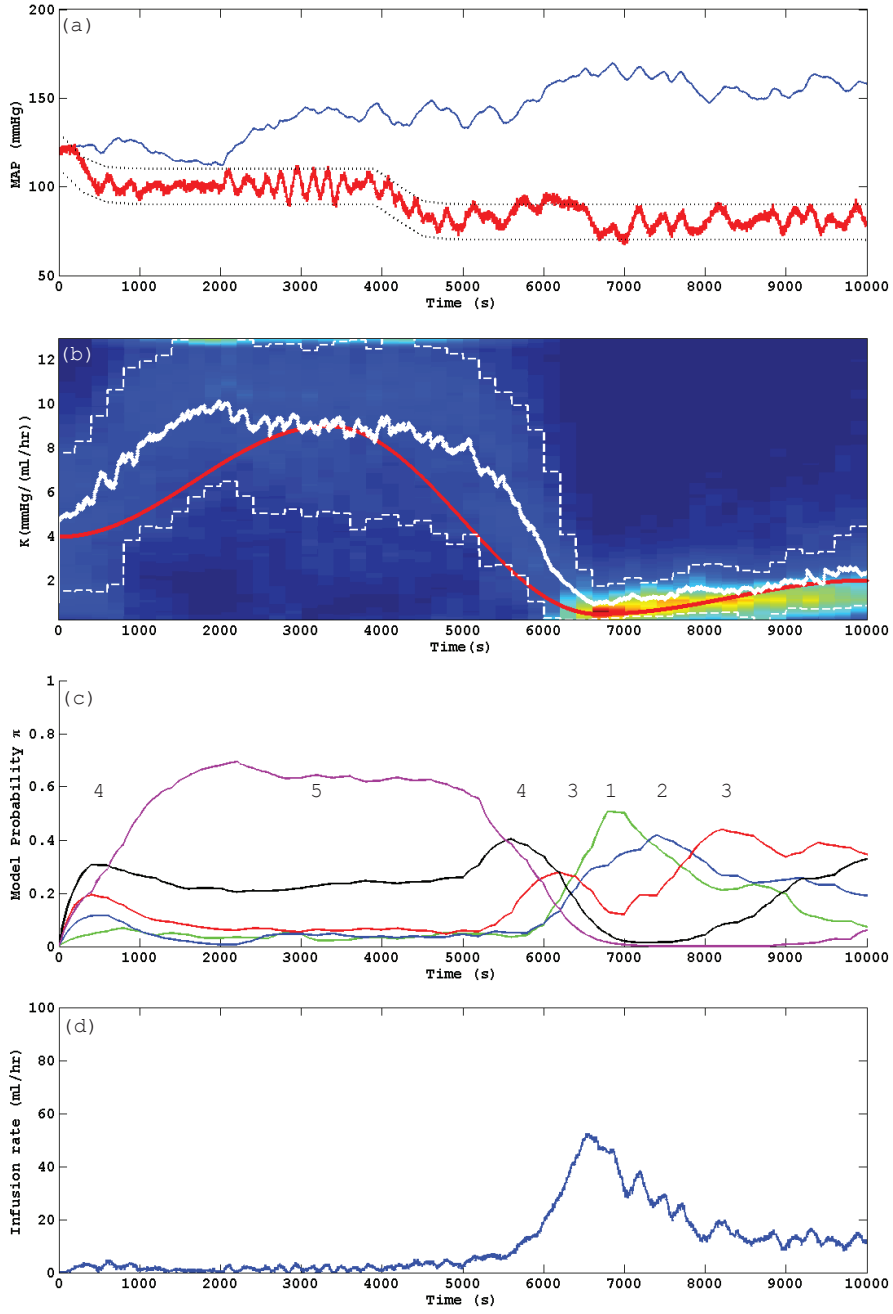

Figure 5.5: Results of simulation `v-b-54`. *(a):* $p_0(t)$ (blue) and controlled MAP output $y_{meas}(t)$ (red), the dotted lines indicate the $\pm$10mmHg allowed error range. *(b):* Real value of $K(t)$ (red) and mean particle estimate (solid white) superimposed on particle density map; the dashed white lines indicate the 15th and 85th percentile of the particle distribution. *(c):* Subinterval probability results, the superimposed numbers indicate the controller with the greatest probability. *(d):* Infusion rate signal $u(t)$.

t_0 (s)	t_1 (s)	t_2 (s)	t_{pp} (s)	t_{npp} (s)	K_{rel} (%)	α_{rel} (%)	T_{rel} (%)	
5924	3442	634	9716	284	81	-25	-22	

t_{c_1} (s)	t_{c_2} (s)	t_{sat} (s)	$t_{\pm5}$ (s)	$t_{\pm10}$ (s)	$t_{\pm15}$ (s)	ϵ_{max} (mmHg)	ϵ_{min} (mmHg)	ϵ_{avg} (mmHg)
186	332	0	6558	9368	9980	16.7	-14.07	1.08

Table 5.2: Aggregate results for simulation `b-v-54`.

deviation values are not zero can be explained in terms of the stochastic features present in both the patient model and the particle filter. As no two simulations are identical, some variability in the results exists even with parameters K, α and T being exactly the same.

When considering the other batches (`a/b-ii` to `v`), the results show that control of MAP was successfully achieved in all cases, with no instability or dangerous pressure drops observed in any of the computed simulations. The controlled MAP trace was maintained within $\pm$10mmHg of the desired setpoint for over 94% of the time in any given batch of simulations (considering $M_{t_{\pm10}} - 2\sigma$, i.e., 9404.74s for the worst-performing batch `b-v`). Similarly, the occurrence of temporary deviations $> \pm$15mmHg from the setpoint was prevented for over 98% of the time and peak tracking errors ($\epsilon_{max}, \epsilon_{min}$) had a magnitude of less than 20mmHg at all times. Tracking of the setpoint was achieved with negligible bias as shown by the very low value of ϵ_{avg} for all batches. It should be clarified that the above statistics refer to the whole simulation (including the initial condition and the two setpoint changes), thus suggesting that control performance remained entirely adequate throughout the simulation campaign. Furthermore, performance was consistent across simulation batches, indicating that the system can deal with time-varying parameters regardless of the shape of the variations, as long as the assumptions of (5.3) are met. Transition times $t_{c_{1,2}}$ also met the specifications and were contained below 10 minutes in almost all cases, with the longest observed transition taking approximately 13 minutes to settle. As could be expected, due to the simpler nature of the control task (lower disturbance), the performance results for stream `a` were better than those for stream `b`, although only marginally.

The results associated with the identification of patient parameters by the particle filter show that the system is tracked as it evolves through time (with t_0 and t_1 combined representing about 90% of the total simulation time on average). However, the system slightly but consistently overestimates K, and delivers estimation errors K_{rel} of about 50-70% on average. The large standard deviation values for α_{rel} and T_{rel}, on the other hand, suggest that the latter two parameters are not dependably identified (there is poor convergence of the particle scatter with respect to α and T). Although the estimation errors may seem significant, the precision in identification is adequate in the context of the required performance, since each controller can cater for variations of two to four fold in the value of K, and for all possible values of α

and T (Table 1). The t_{pp} result confirms this, by showing that the system pairs the patient with a suitable controller at most times, with closer inspection of simulation data showing that t_{npp} is accrued mostly in the initial stages when the particle filter has not yet converged. Notably—and perhaps counterintuitively at a first glance—identification of the patient response is more accurate for the more challenging cases of stream `b` than for stream `a` as indicated by higher values of t_0.

Each simulation took approximately 8 minutes to execute (corresponding to a simulation time-to-real time ratio of 1:20) using 1000 particles. This number of particles was found to deliver a reasonable compromise between accuracy in the results and computation time. A number of test simulations conducted ahead of the campaign did not show noticeable improvements in the estimation results when run using 5000 particles.

5.4 Discussion

We have tailored RAC-PF, a novel approach for the control of uncertain, time-varying systems, to the case study of automatic closed-loop SNP administration for the management of acute hypertension. Having adopted an underlying response model which is, to our knowledge, the most general ever adopted in the literature (with regard to the ranges of variablity of parameters, the allowed rates of change and shapes of variations, and the presence of both random and non-zero-mean changes in $p_0(t)$), the system delivered the required performance with no evidence of unsafe behaviour throughout the extensive simulation campaign presented herein. We therefore propose that RAC-PF may represent a viable solution to assist with automated control of hypertension not only in the traditionally considered post-operative setting, but also in the more challenging intraoperative context, where rapid changes in a patient's response characteristic may occur (Meijers et al. [1997]). The results provide a strong motivation for the approach to be tested further in in-vivo models (e.g., animal testing).

Only a limited number of authors have considered automatic control of MAP during surgery (although not specifically with SNP). The challenge of on-line adaptation to variations in the patient response has generally been addressed through ad-hoc rules (Furutani et al. [2004]) which mimic physicians' clinical decision process (Hoeksel et al. [1999]). The RAC-PF method is fundamentally different. By adopting a dose-response model which incorporates uncertainty, μ-synthesis allows the designer to conclusively determine a priori the minimum number of controllers required to achieve the desired level of robust performance, while particle filtering tracks the patient's response as it evolves through time to inform correct controller selection. In addressing the argument that methods for automatic drug administration may have been dismissed on grounds of perceived safety in the past, we deem the transparent nature of RAC-PF, where an explicit relationship is retained between the estimated posterior probability distribution of the patient response and the chosen control action, to be well suited to clinical applications. A further advantage of

Table 5.3: Summary of the results of the full simulation campaign.

Results	t_0 (s)	t_1 (s)	t_2 (s)	t_{pp} (s)	t_{npp} (s)	K_{rel} (%)	α_{rel} (%)	T_{rel} (%)	t_{c_1} (s)	t_{c_2} (s)	t_{sat} (s)	$t_{\pm 5}$ (s)	$t_{\pm 10}$ (s)	$t_{\pm 15}$ (s)	ϵ_{max} (mmHg)	ϵ_{min} (mmHg)	ϵ_{avg} (mmHg)
Constant mid-range case, settled (batch `i-a`): 40 simulations																	
mean M	604	9396	0	10000	0	69	11	-24	396	360	0	9442	9995	10000	8.43	-8.33	0.16
standard dev σ	128	130	0	0	0	5.0	3.0	5.0	46	59	0	104	14	0	0.72	0.95	0.05
Constant mid-range case, unsettled (batch `i-b`): 40 simulations																	
mean M	5986	4014	0	9640	360	40	-4.0	-20	397	332	0	8752	9968	9999	11.00	-10.28	0.43
standard dev σ	788	788	0	512	512	5.0	3.0	3.0	74	72	0	212	147	0.6	1.46	1.18	0.06
Constant randomised case, settled (batch `ii-a`): 80 simulations																	
mean M	4926	3790	1280	9826	167	63	3	25	390	375	0	9356	9944	9994	8.56	-8.43	0.21
standard dev σ	4338	3821	2414	252	252	79	24	54	126	101	0	612	146	34	1.98	1.98	0.22
Constant randomised case, unsettled (batch `ii-b`): 80 simulations																	
mean M	4804	4443	716	9478	522	42	2	27	392	359	0	8856	9907	9990	11.06	-9.85	0.43
standard dev σ	3038	2682	1324	576	576	54	22	57	101	75	0	868	87	40	3.24	2.98	0.25
Linear variations case, settled (batch `iii-a`): 80 simulations																	
mean M	2971	5358	1617	9898	102	85	14	10	421	385	0	9289	9941	9992	9.32	-8.97	0.24
standard dev σ	2297	2166	1911	204	204	73	19	26	120	110	0	435	114	42	2.10	2.72	0.23
Linear variations case, unsettled (batch `iii-b`): 80 simulations																	
mean M	4710	4460	731	9396	604	49	2.0	10	428	380	0	8710	9898	9991	12.03	-10.94	0.60
standard dev σ	1938	1772	882	694	694	39	15	24	124	104	0	612	151	41	2.44	2.90	0.35
Exponential variations case, settled (batch `iv-a`): 80 simulations																	
mean M	2152	5802	1938	9860	140	77	12	9	408	384	0	9405	9974	10000	8.78	-8.51	0.21
standard dev σ	2096	1945	2135	207	207	59	21	25	89	96	0	398	88	15	1.86	1.72	0.15
Exponential variations case, unsettled (batch `iv-b`): 80 simulations																	
mean M	4701	4474	729	9349	651	45	3.0	11	408	366	0	8860	9936	9995	11.44	-10.15	0.50
standard dev σ	1730	1744	970	796	796	38	17	25	94	101	0	471	90	31	2.15	1.95	0.21
Sinusoidal variations case, settled (batch `v-a`): 80 simulations																	
mean M	2834	5350	1689	9898	102	94	13	12	419	404	0	9164	9930	9994	9.95	-8.95	0.37
standard dev σ	2159	2030	1344	205	205	62	18	25	110	97	0	117	116	26	2.30	1.71	0.36
Sinusoidal variations case, unsettled (batch `v-b`): 80 simulations																	
mean M	4529	4568	848	9298	702	48	0.0	14	390	405	0	8450	9846	9976	13.15	-11.76	0.68
standard dev σ	1663	1534	882	871	871	31	15	26	107	124	0	674	220	80	3.64	3.84	0.47

RAC-PF over ad-hoc approaches is that the framework is not specific to SNP and the same methodology could be used to design controllers and estimators, given a reference dose-response model, for a different drug delivery problem.

The results also supports the viability of particle filtering in a real-time pharmacological application. The fact that simulations ran much faster than real-time without requiring particular hardware or software optimisation is a notable positive finding. Particle filter methods have been proposed to assist with the estimation of physiological systems and draw inference from patient data in order to support clinical decision-making processes (see, e.g., Zenker et al. [2007]). To our knowledge, however, such methods have been generally devised for off-line computations. Our work highlights the potential of particle filter as a viable tool for real-time closed-loop system identification. As pharmacokinetic/pharmacodynamic models commonly combine linear and nonlinear dynamics (Bonate [2011]), we anticipate that marginalisation would be applicable to a broad class of problems in this area. Further work should consider other case studies, including nonlinear and multiple-input-multiple-output systems, in order to identify any limitations to the practical use of particle filtering in estimating more complex systems.

On the point of identifiability of the system, a number of relevant comments can be made. Perhaps counterintuitively, the results show good control performance, but the identification statistics point to somewhat imprecise parameter estimates. As well as being a result of the underdetermined nature of the estimation problem (multiple uncertain parameters and a single output), this outcome stems from a well-known trade-off between control and identification in feedback systems (Forssell et al. [1997]). The very purpose of a feedback controller is to suppress some of the dynamics from the controlled system, thus the stronger the control action (performance), the lesser input-output information is available to estimate the response characteristic. An extreme situation would be that of a controller capable of forcing a perfect, flat-line MAP output at all times: in such a situation no knowledge of the patient characteristic could be gathered (arguably, adaptive control would not be required, either). The necessary imposition of performance constraints in our design, therefore, affects the precision of system identification. The fact that the controllers were designed to cater for all values of α and T and, as a result, the identification of these parameters was inaccurate, is a clear example of this trade-off. Furthermore, accuracy in identification depends on the level of *excitation* of the system, i.e. the amount of energy delivered by exogenous inputs (in this case, $r(t)$ and $p_0(t)$), which elicits observable dynamics at the output. Since $r(t)$ is mostly a constant signal, excitation is provided mainly by the changes in $p_0(t)$. This explains why identification is more accurate (greater t_0) for the more disturbed simulations of stream `b`. It should be remarked that the trade-off between identifiability and excitation is an inescapable one and affects both traditional clinician-based methods and computer-based solutions equally. A notable question arising in light of these considerations is whether the commonly stated clinical goal of maintaining a patient "settled" is a desirable one, or whether this is actually counterproductive when changes in a patient's response must be timely identified and acted upon. Our analysis suggests that impos-

ing a clinically acceptable, time-varying MAP target would result in greater system excitation and thus improve ongoing system identification.

Chapter 6

Conclusions

In this thesis, we have proposed a new feedback control architecture to address identified robustness and verifiability shortcomings in existing systems for the automatic feedback administration of medicinal drugs. The new adaptive control approach, named Robust Adaptive Control with Particle Filtering (RAC-PF), combines modern methods in robust control and stochastic filtering. We have demonstrated, through our simulation work, the potential ability of RAC-PF to deliver safe control in the case study of control of acute hypertension with the vasodepressor drug sodium nitroprusside.

The RAC-PF methodology inherits from the Robust Multiple-Model Adaptive Control (RMMAC) approach of Fekri [2005] a systematic, performance-based approach to the design of multiple robust controllers involving μ synthesis, which can be applied to a broad class of uncertain systems and provides a mathematical guarantee of local robust performance. We have combined the designed bank of controllers with a novel supervisory algorithm for controller selection based on particle filtering. The use of particle filters as a tool for real-time joint state and parameter estimation of the individual patient response model expands the applicability of this adaptive control architecture to a broad class of systems, including time-varying and non-linear systems, and systems featuring non-Gaussian stochastic processes (where the Kalman filter-based identification approach of RMMAC may be limiting, as discussed in Chapter 2). The Bayesian inference result from the particle filter is used to guide controller selection, while it also provides information on the dependability of the estimate. The transparency of the inference process allows for on-line verification of the operation of the automatic algorithm (e.g., by a clinical expert).

Throughout the dissertation, we have investigated the potential and limitations of RMMAC in relation to drug delivery (Chapter 2) and the viability of particle filter methods in estimating pharmacological response (Chapter 3), formulated the RAC-PF approach, and successfully tested it in Monte-Carlo simulation studies (Chapters 4 and 5). In this chapter, section 6.1 summarises the contributions of the work, while section 6.2 discusses a number of outstanding challenges and outlines recommended directions for future research.

6.1 Summary of contributions

Sodium nitroprusside administration requires multiple controllers. The approach adopted for the design of the multi-controller bank (common to RMMAC and RAC-PF) enables the designer to explore systematically the trade-off between the number of controllers and the maximum achievable level of robust performance. In relation to the closed-loop administration of sodium nitroprusside, we have conclusively demonstrated that the desired performance would not be achieved with a single (global) robust controller. This establishes the requirement for adaptive control in this application with unprecedented clarity.

Robust controllers can deliver improved safety. The results shown in Chapter 2 demonstrate a potential risk of undesirable closed-loop behaviour during the administration of sodium nitroprusside for two earlier non-robust methods. While the identified critical combination of high patient sensitivity, long transport delays and baseline arterial pressure increase may be unlikely to occur in practice, the results highlight a situation of unacceptable clinical risk. We show that robust controllers can prevent, by design, such risk of instability.

Particle filters are tractable when applied to a standard PK-PD response model. In Chapter 3 we have shown that it is possible to design a particle filter to conduct real-time Bayesian inference for the estimation of patient-specific response parameters. Such an algorithm is very general as it can cater for nonlinear and non-Gaussian effects. Despite concerns about the computational demands of particle filters, implementation on a three-compartment PK-PD model was found to be tractable without requiring particular software optimisation or special hardware.

Improved individualised anaesthesia is possible with current technology. Our results from Chapter 3 highlight that target-controlled infusion (TCI) methods for anaesthesia based on average population response models may considerably under- or over-predict patient response following intravenous propofol infusion. We show that it would be possible to improve the predictive performance of current models by incorporating already available real-time measurements such as Bispectral Index measurements, and that this can be achieved through a particle filter.

Inaccurate breath propofol concentrations can provide useful information. In the context of propofol delivery and patient-specific model estimation, we have demonstrated that techniques for real-time breath propofol concentration measurements, despite reported issues with accuracy, can provide useful additional information and may be incorporated in the particle filter approach, with a suitable error model, to yield more accurate estimates.

Development of a new closed-loop architecture. We have introduced a novel feedback control methodology which combines a bank of robustly designed controllers with a controller selection method based on the result of a particle filtering algorithm. We have named this new architecture Robust Adaptive Control with Particle Filtering (RAC-PF).

RAC-PF can be used for the control of linear parameter-varying systems. RAC-PF can be successfully employed in the control of linear parameter-varying systems. The results of the comparison with RAC-EKF conducted in Chapter 4 demonstrate very similar closed-loop performance between the two systems. While RAC-PF does have a greater computational cost than a Kalman filter-based approach, we have shown that where real-time operation can be achieved (i.e., sufficient computational resources are available and/or the system dynamics are not too fast), there is no disadvantage in tackling control design using the more general RAC-PF tool. We have also highlighted that in the case of linear parameter-varying or mixed linear-nonlinear problems, the RAC-PF algorithm can be made less burdensome through marginalisation of the particle filter.

RAC-PF can deliver safe control of sodium nitroprusside infusion. An extensive Monte-Carlo simulation of hypertension control based on the broadest dose-response model ever adopted in the literature is reported on in Chapter 5. The results allow us to conclude that, on the basis of the models available, RAC-PF can be deemed a safe solution for closed-loop drug delivery in relation to this application.

6.2 Final considerations and recommendations for future work

Translation to other drug delivery applications

The RAC-PF approach as presented here is a viable method for the control of sodium nitroprusside infusion. It is also a general feedback control architecture. Indeed, as shown in Chapter 4, where we used RAC-PF to successfully reduce vibrations in a mechanical system, the same design methodology may be adapted to suit other control problems.

In the field of closed-loop drug delivery, the application of RAC-PF in the established research areas of anaesthesia control (expanding on the identification work presented in Chapter 3) and diabetes management could be readily contemplated. The investigation of cardiovascular control would also be of particular interest both as a multi-variable case study and also one in which the particle filters could be used to cater for the inherent inaccuracy in blood flow measurements (the multi-drug cardiovascular response model of Woodruff et al. [1997] could be considered as a starting point). Adaptive control with robust methods in highly nonlinear applications is a further potential area where RAC-PF could be expected to provide an innovative edge. One such area is cancer chemotherapy, where threshold effects and stochastic effects, such as mutations, exist yet much simplified models are used for

feedback control design (see Parker and Doyle [2001] for a discussion of challenges in cancer modelling and Algoul et al. [2011] for a recent control proposal).

Investigation of alternative controller selection methods

In Chapter 5 we introduced a controller selection strategy which involves a probability-weighted sum of the control actions of the controllers in the bank (as per Equation (5.10)) and indicated that this is just one possible approach to controller selection. As the particle filter inference result is conceptually affine to performing a real-time quantitative assessment of a patient's response, we have discussed that the posterior probability distribution may serve both as the basis for controller selection and as an informative tool for clinicians. As such, there may be other clinical applications for which alternative controller selection methods, based on features of the distribution other than the mean, may be more clinically appropriate. Some examples where alternative methods may be informative include:

- where a mandatory level of confidence in the estimate is dictated by clinical risk considerations, a conservative selection may be informed by the location of a specific distribution percentile;
- where multimodal probability distributions can be expected (e.g., Zenker et al. [2007], in applying particle filtering to cardiovascular estimation, discuss that multimodal distributions may arise naturally in physiological systems), algorithms may be required to detect, and discern amongst, multiple probability peaks.

Alternative controller selection strategies, as well as their impact on performance and robustness of the system, represent a topic of definite interest for further research.

In-vivo testing

Methods which have been validated through extensive in-silico testing should progress to being investigated in-vivo. In light of the results of Chapter 5, RAC-PF may be considered for in-vivo evaluation as a closed-loop mean arterial pressure controller. In considering in-vivo translation of adaptive control approaches, additional challenges must be contended with; most critically, the issue of integrity of the observed signals. This is particularly true if the technology is expected to be deployed in an environment where unpredictable disturbances are likely to arise, e.g., in the operating room. This a well known issue. As an example, an early work on sodium nitroprusside administration by Martin et al. [1992] describes the need for an ad-hoc supervisory algorithm to reject artifacts in arterial pressure observations caused by events such as arterial catheter flushing and accidental sensor disconnections. Artifact rejection was deemed necessary in order to prevent erroneous signals from disrupting closed-loop control.

In RAC-PF, the accuracy of the Bayesian inference results—and, consequently, that of control—is directly affected by the quality of the disturbance model associated with the observations. Where measurement inaccuracies can be expected, these should be reflected in the model, as we sought to do by developing an alternative probability distribution for breath propofol observations in Chapter 3. Analysis of whether unexpected disturbances can be incorporated in a stochastic model of measurement error or require the development of a further supervisory layer needs to be conducted on a problem-by-problem basis. Tools developed in the area of sensor fault detection (see, e.g., Bequette [2010] for work developed in the context of glucose sensing in diabetes monitoring) may be considered in order to tackle this challenge. For problems which relate to intensive care patient observations, in-vivo data from the MIMIC II clinical database (Saeed et al. [2011]) represent a valuable resource for analysis. In Chapter 2, we introduced the assumption of normally-distributed measured errors for mean arterial pressure, which was based on the analysis of selected MIMIC II traces free of operational artifacts. This assumption will need to be reviewed ahead of in-vivo implementation.

Investigating sufficiency of excitation

As highlighted in the discussion sections of Chapters 3 and 5, the performance of the particle filter depends on the level of excitation provided to the system. This is not unique to particle filters but applies to system identification in general. A key consequence is that, in the absence of sufficient excitation, adaptive control may fail to track changes in the controlled system and thus fail to adequately adapt, resulting in undesirable closed loop performance or even transient instability. This is a general problem with model-based adaptive control and extends beyond the drug delivery applications considered in this thesis. In Chapter 4 we have cited the asymptotic convergence result for RMMAC under assumptions of persistency of excitation. As the particle filter inference also converges to the true posterior probability distribution for a sufficiently large number of particles (as mentioned in Chapter 3), a similar argument for convergence to the correct model estimate could be mounted for RAC-PF in relation to time-invariant systems.

In reflecting on drug administration problems, even if it is assumed that exogenous excitation is present, it is evident that the notion of asymptotic convergence is inadequate for this class of applications. In order for feedback control to be clinically useful, a correct model estimate must be achieved within a meaningful (bounded) time horizon. Furthermore, if underlying time-variations in model parameters are to be expected, robust operation requires that the model estimator converge to the correct parametric subset in a lower amount of time than it would take for the model to drift to an underperforming/unstable controller-plant pair. Timely convergence of the particle filter distribution depends on the nature of the reference input and disturbance signals, and the number and range of parameter subintervals to be discriminated between.

It is of course possible, as we have done for the sodium nitroprusside adminis-

tration case study in this thesis, to conduct a *post-hoc* verification of the robustness of a RAC-PF design through a Monte-Carlo simulation campaign which must include low-excitation scenarios (cf. "settled patients" in Chapter 5). If the results show evidence of undesirable transient behaviour, the problem may need to be reformulated by changing the performance target, redesigning the controllers and running a new simulation campaign. Depending on the complexity of the system to be controlled, this iterative design process may be lengthy.

In light of the above, a very relevant item for further work is a study of the inverse problem, i.e. computing an additional excitation signal to be provided at the reference input(s) which would ensure an adequate likelihood of discrimination between candidate parametric subintervals over a bounded time horizon. In our view, guaranteed sufficiency of excitation represents, at this time, the single most needed enhancement of RAC-PF as it would allow the designer to establish a-priori robustness not only on the controllers side but also in the convergence of the identification algorithm.

Investigating applications in other categories of systems

RAC-PF extends the reach of the RMMAC approach to a broader class of systems. The robust controller design approach makes it possible to design multiple linear controllers for closed-loop control of nonlinear, non-gaussian systems (plant nonlinearities can be dealt with through piece-wise linearisation and/or treated as unmodelled dynamics; non-gaussian signals do not pose a challenge to $\mathcal{H}_\infty$ methods, as long they are bounded in the frequency-domain), while particle filtering can deliver more general model-based estimation than Kalman filter methods.

Unfortunately, due to the numerical nature of particle filters, it is not possible to provide a theoretical proof of robustness for the RAC-PF approach. This means that RAC-PF might contribute to, but does not end, the ongoing search for the *Holy Grail* of adaptive control. Still, we are convinced that the promising results observed in our research call for further investigation of the method from an applications perspective, beyond the biomedical domain which we have focussed on in this thesis. Selected areas for which we have conducted some preliminary research and deem of particular interest are listed below:

- Control of linear parameter-varying plants for which estimation conducted through Extended Kalman Filtering may fail to converge, i.e., linear cases in which RAC-EKF would deliver a much inferior performance to RAC-PF (see Krener [2003] for a mathematical discussion of EKF convergence issues);
- Control of plants characterised by an open-loop-unstable characteristic, for which it is possible to consider a particle-filter formulation based on the Youla-Kucera parametrisation (Anderson [1998]).

Appendix A

Matlab/Simulink implementation of RAC-PF

This Appendix details the implementation of RAC-PF for the problem of controlled administration of sodium nitroprusside as described in Chapter 5. It is intended as a guide to the interested reader, to assist them in interpreting or reproducing the approach, and/or adapting it to a different type of control problem. All of the following details refer to the Simulink file `\AppendixA\AutoSNP_thesis.mdl`, which is provided as part of the digital resources attached to this thesis (see Appendix B). In the same folder (`\AppendixA`) are all the necessary function files and scripts to run a complete sample simulation and view the results.

This Appendix assumes a working knowledge of the Matlab and Simulink environments. Readers who are unfamiliar with these platforms may wish to refer to some introductory material such as Beucher and Weeks [2008].

The top-level Simulink implementation is shown in Figure A.1. In the schematic, we identify the three key areas of *simulation settings*, *closed-loop system* and *results output*. Each is detailed in a dedicated section below. The final Section A.4 describes how to run the provided sample simulation.

A.1 Simulation settings

This part of the model deals with setting the information required for a simulation run. The values of the model parameters and the seeds for the white noise randomiser are provided as Matlab workspace variables and must therefore be assigned ahead of launching the simulation, either manually or by running a script made for the purpose. Since all the simulated runs in Chapter 5 have the same characteristics in terms of baseline mean arterial pressure $p_0(0) = 120$mmHg and target controlled pressure (reference), these two signals are generated as part of the model. The intensity of the random disturbance process $p_0(t)$ and the magnitude of step increases in the offset pressure are determined as workspace variables (cf. 'settled' vs. 'unsettled' simulation streams in Section 5.2.4). Note that the target pressure drop is provided as a fraction with a denominator of 40. This is due to the presence of the low-pass shaping filter W_{spd}, which has been assumed to have a DC gain of 32dB as discussed

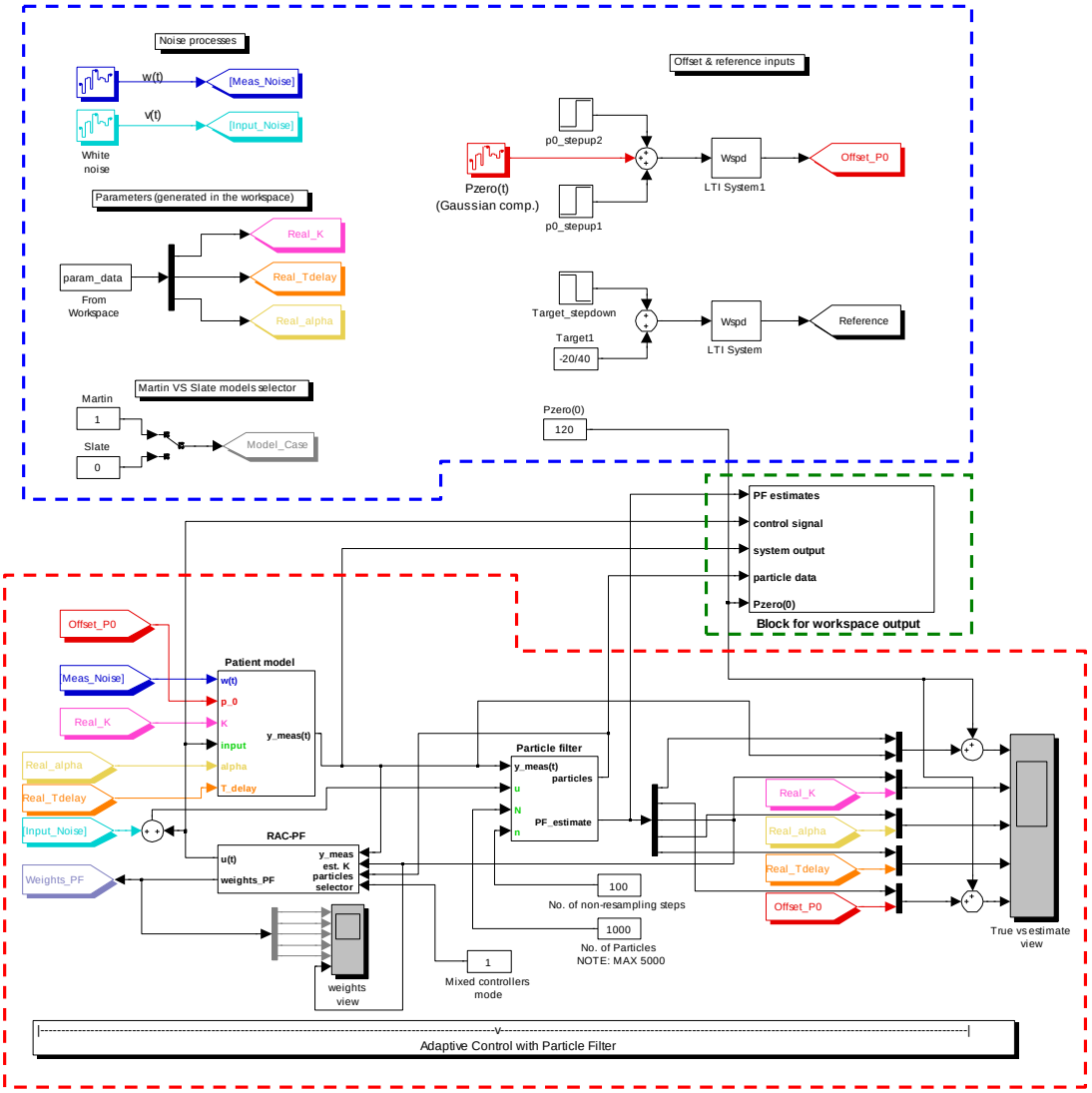

Figure A.1: Overall structure of the Simulink implementation of the sodium nitroprusside administration problem. Dashed boxes enclose the three key areas of *simulation settings* (blue), *closed-loop system*(red) and *results output* (green).

in Chapter 2.

The attached version of the implementation also includes a switch selector which can be actioned by the user to select between two models for sodium nitroprusside response. In this thesis we have considered the model used by Martin et al. [1987], but there is the option of testing the designed feedback solution also for the slightly different response model of Slate et al. [1979].[1]

Several other constant data used in the implementation are also drawn from the workspace. These are not shown explicitly in the diagram of Figure A.1 and must be initialised before any simulations can be run:

- The state-space objects representing the μ-synthesised controllers;
- The sampling time T_s;
- The W_{spd} filter;
- The look-up table which contains the matrix entries for the discrete-time formulation (cf. matrices A_d and B_d in equation (5.7)) of the response model and the Kalman innovation gain values for Kalman filtering (used for the marginalised KF).[2]

A script has been designed for this purpose (`initialise.m`).

A.2 Closed-loop system

This section represents the true "heart" of the approach. It takes care of simulating the response of the dynamical system, running the particle filter and conducting controller selection.

The following sub-sections detail the operation of the key functional blocks.

Patient model

Inside this block is a selector between two Simulink models of patient response behaviour. Figure A.2 shows the selection structure and the detail of the implementation of the model by Martin et al. [1987]. The latter effectively replicates the block diagram of Figure 2.1.

[1] Note that even though both models have the same uncertain parameters K, α and T, like values do not translate into a like response, so care must be taken if designing a comparative simulation campaign.

[2] The use of a look-up table is not strictly required as it is possible to calculate the system matrices and Kalman gains on the run. Using a look-up table does, however, render the algorithm much quicker. For information about the look up tables refer to the comments in the file `createLUT.m` provided in the digital materials.

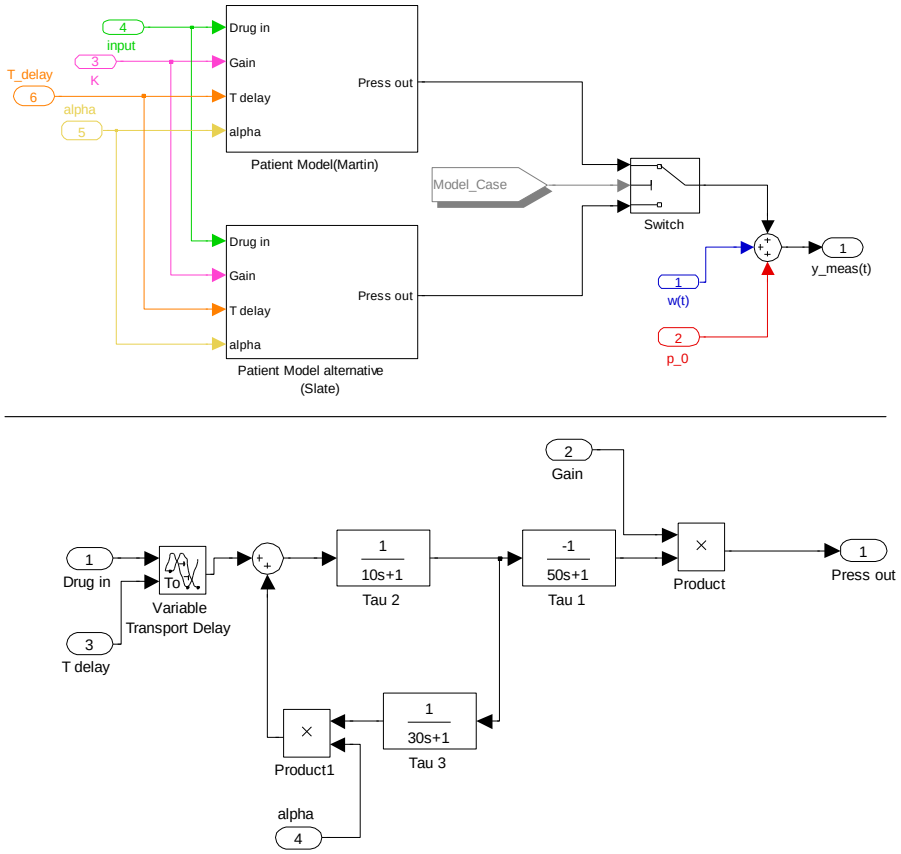

Figure A.2: *Top:* patient model selector. *Bottom:* block diagram of sodium nitroprusside response model according to Martin et al. [1987].

Particle filter

This block implements the particle filter estimator which takes the input u and output y_{meas} observations as input data, and proves particle estimates (mean of the distribution) and particle data at the output. The structure of the block is given in figure A.3.

The particle filter itself is mainly implemented through the *Particle Filter Function* block, which calls on the Matlab function `fcnPF.m`. This function, which is executed by the simulator at every time step, implements the marginalised particle filter algorithm as described in Section 4.3.3. The following operations are performed by the code `fcnPF.m`. We refer the reader to the code file and the comments therein for detailed line-by-line descriptions.

- acquiring particle data from the previous time instant;
- computing the update of the linear system states including a state correction through a Kalman filter gain;

- weighting the output of the system against the current observations;

- resampling at selected time instants and introducing stochastic variations to the parameters according to uniform probability distributions.

The *initialise or pass through* block calls upon the external function `fcnPF2.m`. It has the sole role of initialising the particle data at the beginning of the simulation (i.e. introducing the initial parameter distributions across the particle population, cf. equation (5.3)). At all other times it does not affect the signals.

We also remark the presence of the *delay subsystem*, which has the role of retaining a working memory (in the form of an array) of inputs over the previous 30 time samples (corresponding to 60 seconds as T_s =2s). The delayed inputs array is used in the particle filter, where it is indexed differently by different particles depending on their associated value for the uncertain input time delay.

Finally, we point out the presence in the block diagram of inputs for data from the real system. These inputs can be used, by making suitable changes to the particle filter code, to assign the particles the true values of the system parameters. This unrealistic mode of operation has been developed for code testing purposes only. During normal operation of the approach, these additional data inputs are effectively disconnected from the particle filter.

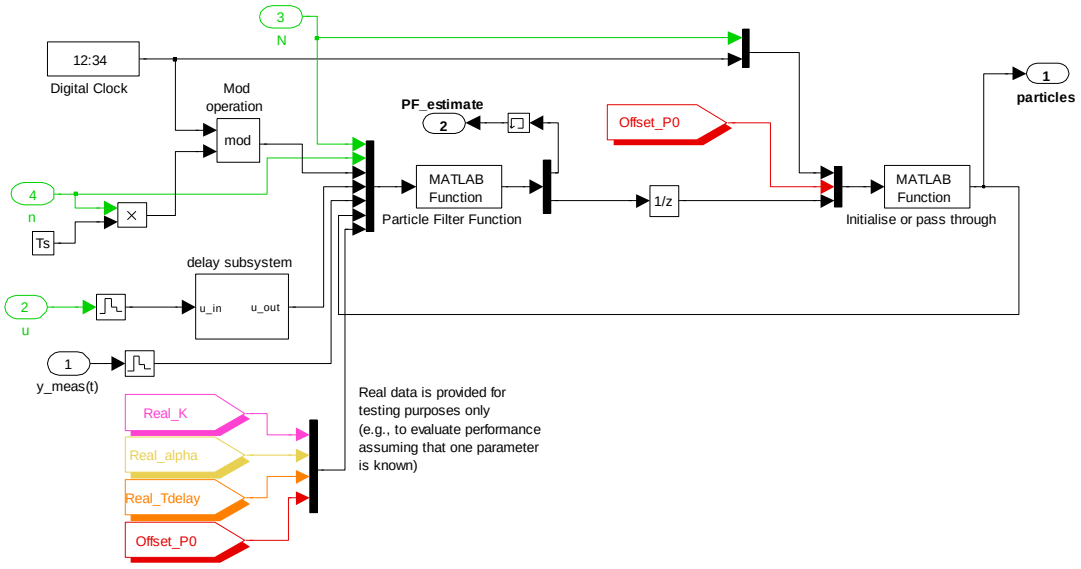

Figure A.3: Inner workings of the particle filter implementation block

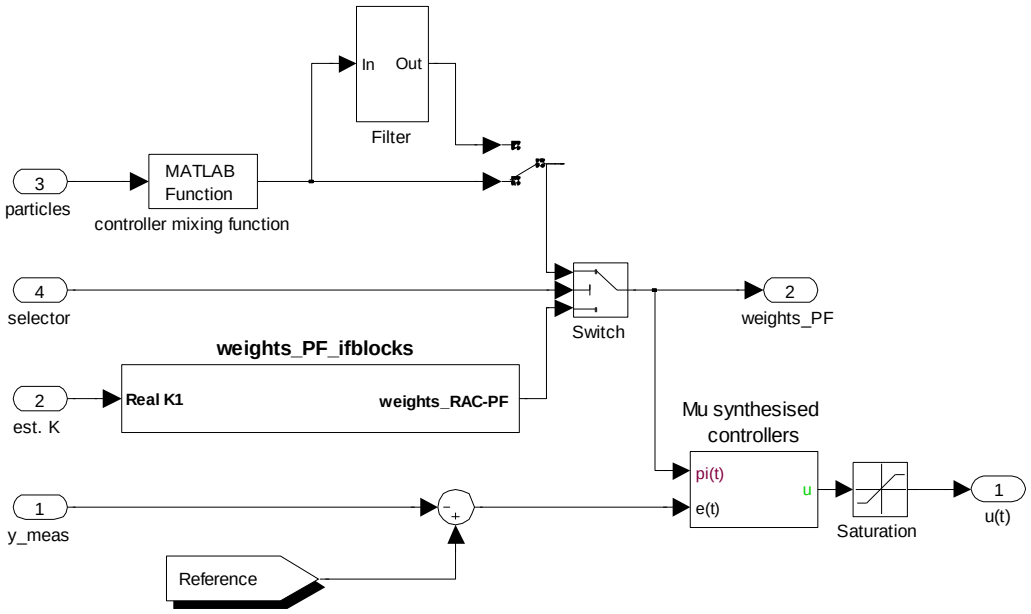

Figure A.4: Controller selection structure.

RAC-PF

This block, depicted in detail in Figure A.4, is responsible for controller selection.

Particle data is fed to the *controller mixing function* block, which calls upon the external function `fcnPF3.m`. This function computes the number of particles present in each subinterval for sensitivity parameter K, as per Table 5.1 and generates weights for controller mixing. A user-controlled options to experiment with pre-filtering (*Filter* block) of the controller weights prior to enacting controller selection is present, although it has not been not used at this time. The *selector* input allows the user to select a different controller selection mode based on all-or-none controller switching (i.e., the controller corresponding to the K subinterval with the greatest probability is assigned a weight of 1 and all others are assigned a weight of 0). This alternative controller mode based on switching is available for experimentation but was not the one used in this thesis. The weight signal is used to determine the controlled drug infusion rate through controller weighting as described in equation (5.10). The straight-forward weighted sum operation is conducted in the *mu-synthesised controllers* block. Also note that a saturation block is present: this implements the ceiling of administrable dose for toxicity reasons as discussed in Chapter 5.

A.3 Results output

The output section is a very simple block which takes care of writing all of the relevant simulation data to workspace variables. The inner workings of the block are shown in Figure A.5.

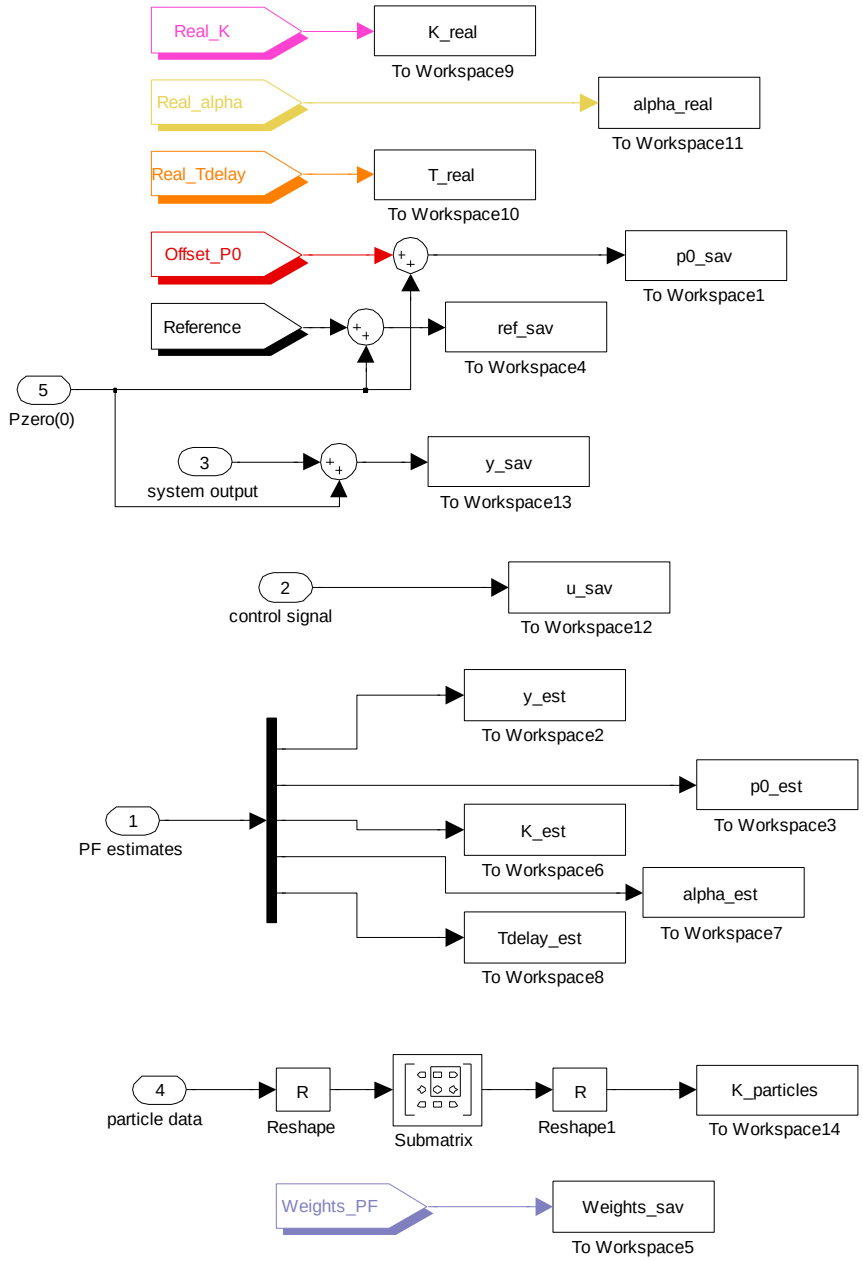

Figure A.5: Simulation output block. Signals of interest are saved in workspace variables.

The results data comprise of the simulated and estimated (mean of the particle filter) parameter values, the input u and output y signals, the model weights, as well as the values for the key uncertain parameter K for all particles (these are extracted as a subset of the particle information; the default number of particles for this operation is N =1000). The methods are set up for Simulink to deliver a mere 'dump' of simulation data. Any further processing of the results must be conducted in the workspace after the simulation is complete by running user-developed scripts. We have provided our code (see file `plotresults.m`) to generate plots such as those presented in Section 5.3.

A.4 Running a simulation

Running a simulation requires the following essential steps:

1. Initialise the simulation environment by running the function (`initialise.m`).
2. Set the desired characteristics for the simulation run. For the purpose, we have provided a file called (`createsim.m`), which sets high-intensity random fluctuations and two step changes in p_0, constant values for the parameters α and T, and some sinusoidal variations for K.
3. In the Simulink window, ensure that the user controls and constants representing the number of particles, number of non-resampling steps, controller blending mode, weight filtering and type of response model are set to the desired values.
4. Call on the Simulink environment to execute the simulation, either from the Matlab command line (using the command `sim`) or from the Simulink GUI ('play' button).
5. Once the simulation is complete, the results may be reviewed by running (`extractresults.m`) and/or plotting with `plotresults.m`.

When batches of simulations are required, as we did in Chapters 4 and 5, the operations listed above can be invoked automatically through a suitable looping script. Any data of interest must be computed and saved to file at the end of each run since running a simulation overwrites the workspace variables each time.

Appendix B

Attached digital materials

In the interest of reproducibility of the results presented in this thesis, a CD containing digital resources has been supplied as an attachment to this work. This Appendix is intended to assist the interested reader in the navigation of the additional content provided.

The content of the attached CD is shown in Figure B.1

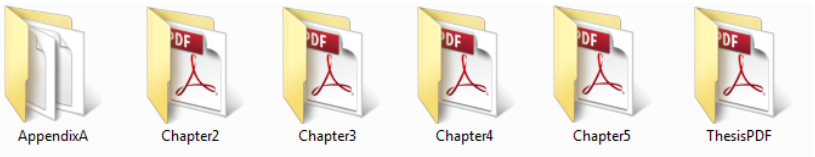

Figure B.1: Folder structure of the digital materials provided with the thesis

The materials are organised as follows:

- The folder `ThesisPDF` contains a digital copy of the thesis document;
- The folders `\Chapter2` to `\Chapter5` contain copies of the submitted/published research articles relating to each chapter.
- The folder `\AppendixA` contains sample code and Simulink models to conduct a sample simulation with RAC-PF as described in Appendix A.

For programming-specific information, refer to the comments embedded in the Matlab programming code. Additional materials and copies of the raw results discussed in the dissertation may be obtained by contacting the author.

A copyright note. The digital materials library attached to this thesis is released, and may be redistributed, *for academic research purposes only*, provided that the original source of the information is duly acknowledged. The materials are protected by copyright and all other uses—including but not limited to personal non-academic use, use in publications and uses of a commercial nature—are strictly prohibited without the prior written consent of the author.

Bibliography

Absalom, A. R.; Sutcliffe, N.; and Kenny, G. N., 2002. Closed-loop control of anesthesia using bispectral index. *Anesthesiology*, 96, 1 (Jan 2002), 67–73. (cited on page 5)

Al-Shyoukh, I. and Shamma, J., 2009. Switching supervisory control using calibrated forecasts. *IEEE Transactions on Automatic Control*, 54 (2009), 705–716. (cited on page 48)

Algoul, S.; Alam, M. S.; Hossain, M. A.; and Majumder, M., 2011. Multi-objective optimal chemotherapy control model for cancer treatment. *Medical & biological engineering & computing*, 49, 1 (2011), 51–65. (cited on page 84)

Alhashemi, J.; Cecconi, M.; and Hofer, C., 2011. Cardiac output monitoring: an integrative perspective. *Critical Care*, 15, 2 (2011), 214. (cited on page 28)

Anderson, B. D. O., 1998. From youla-kucera to identification, adaptive and nonlinear control. *Automatica*, 34 (1998), 1485 – 1506. (cited on page 86)

Anderson, B. D. O.; Brinsmead, T. S.; Bruyne, F. D.; Hespanha, J.; Liberzon, D.; and Morse, A. S., 2000. Multiple model adaptive control: Part I: Finite controller coverings. *International Journal of Robust and Nonlinear Control*, 10 (2000), 909–929. (cited on pages 48 and 51)

Anderson, B. D. O. and Dehghani, A., 2008. Challenges of adaptive control–past, permanent and future. *Annual Review Control*, 32, 2 (Dec 2008), 123–135. (cited on page 48)

Arnspanger, J. M.; McInnis, B. C.; Glover, J. R.; and Normann, N. A., 1983. Adaptive control of blood pressure. *IEEE Transactions on Biomedical Engineering*, 30, 3 (Mar 1983), 168–176. (cited on page 24)

Bailey, J. M. and Haddad, W. M., 2005. Drug dosing control in clinical pharmacology. *IEEE Control Systems Magazine*, 25, 2 (April 2005), 35–51. (cited on pages 3, 5, and 12)

Bednarski, P.; Siclari, F.; Voigt, A.; Demertzis, S.; and Lau, G., 1990. Use of a computerized closed-loop sodium nitroprusside titration system for antihypertensive treatment after open heart surgery. *Critical Care Medicine*, 18, 10 (Oct 1990), 1061–1065. (cited on page 12)

Bequette, B. W., 2007. Modeling and control of drug infusion in critical care. *Journal of Process Control*, 17, 7 (2007), 582–586. (cited on pages 4, 6, and 12)

Bequette, B. W., 2010. Continuous glucose monitoring: real-time algorithms for calibration, filtering, and alarms. *Journal of diabetes science and technology*, 4, 2 (2010), 404. (cited on page 85)

Beucher, O. and Weeks, M., 2008. *Introduction to MATLAB & SIMULINK (A Project Approach)*. Laxmi Publications, Ltd. (cited on page 87)

Bienert, A.; Wiczling, P.; Grzeskowiak, E.; Cywinski, J. B.; and Kusza, K., 2012. Potential pitfalls of propofol target controlled infusion delivery related to its pharmacokinetics and pharmacodynamics. *Pharmacological Reports*, 64, 4 (Jul 2012), 782–795. (cited on pages 30 and 32)

Bjornsson, M. A.; Norberg, A.; Kalman, S.; Karlsson, M. O.; and Simonsson, U. S., 2010. A two-compartment effect site model describes the bispectral index after different rates of propofol infusion. *Journal of Pharmacokinetics and Pharmacodynamics*, 37, 3 (Jun 2010), 243–255. (cited on pages 32, 38, and 44)

Bonate, P., 2011. *Pharmacokinetic-Pharmacodynamic Modeling and Simulation*. Springer. ISBN 9781441994844. (cited on pages 33, 40, 66, and 79)

Cappe, O.; Godsill, S. J.; and Moulines, E., 2007. An overview of existing methods and recent advances in sequential monte carlo. *Proceedings of the IEEE*, 95, 5 (2007), 899–924. (cited on page 49)

Chen, Z., 2003. Bayesian filtering: From kalman filters to particle filters, and beyond. *Statistics*, 182, 1 (2003), 1–69. (cited on page 36)

Chitwood, W. R.; Cosgrove, D. M.; and Lust, R. M., 1992. Multicenter trial of automated nitroprusside infusion for postoperative hypertension. *The Annals of Thoracic Surgery*, 54, 3 (1992), 517–522. (cited on page 12)

Clemens, A. H.; Hough, D. L.; and D'Orazio, P. A., 1982. Development of the biostator glucose clamping algorithm. *Clinical Chemistry*, 28, 9 (1982), 1899–904. (cited on page 5)

Cobas, M. A. and Varon, A. J., 2006. *Complications of Anesthesia*, chap. 1, 1–16. CRC Press. (cited on page 30)

Cosgrove, D. M.; Petre, J. H.; Waller, J. L.; Roth, J. V.; Shepherd, C.; and Cohn, L. H., 1989. Automated control of postoperative hypertension: a prospective, randomized multicenter study. *The Annals of Thoracic Surgery*, 47, 5 (May 1989), 678–683. (cited on pages 12 and 24)

Dehghani, A.; Lecchini-Visintini, A.; Lanzon, A.; and Anderson, B. D. O., 2009. Validating controllers for internal stability utilizing closed-loop data. *IEEE Transactions on Automatic Control*, 54, 11 (November 2009), 2719–2725. (cited on page 51)

Djuric, P. M.; Kotecha, J. H.; Zhang, J.; Yufei Huang abd Ghirmai, T.; Bugallo, M.; and Miguez, J., 2003. Particle filtering. *IEEE Signal Processing Magazine*, 20, 5 (2003), 19–38. (cited on page 49)

Douc, R. and Cappe, O., 2005. Comparison of resampling schemes for particle filtering. In *Proc. of the 4th Int. Symposium on Image and Signal Processing and Analysis*, 64–69. Zagreb, Croatia. (cited on page 37)

Doucet, A. and Johansen, A. M., 2009. *A tutorial on particle filtering and smoothing: Fifteen years later*, vol. 12, 656–704. Oxford, UK: Oxford University Press. (cited on pages 36 and 51)

Doyle, F.; Jovanovic, L.; Seborg, D.; Parker, R. S.; Bequette, B. W.; Jeffrey, A. M.; Xia, X.; Craig, I. K.; and McAvoy, T., 2007. A tutorial on biomedical process control. *Journal of Process Control*, 17, 7 (2007), 571 – 572. (cited on page 7)

Doyle, F. J.; Bequette, B. W.; Middleton, R.; Ogunnaike, B.; Paden, B.; Parker, R. S.; and Vidyasagar, M., 2011. Control in biological systems. In *The Impact of Control Technology* (Eds. T. Samad and A. M. Annaswamy). IEEE Control Systems Society. (cited on page 6)

Dumont, G. A.; Martinez, A.; and Ansermino, J. M., 2009. Robust control of depth of anesthesia. *International Journal of Adaptive Control and Signal Processing*, 23, 5 (2009), 435–454. (cited on page 6)

El-Jabali, A. K., 2005. Neural network modeling and control of type 1 diabetes mellitus. *Bioprocess and Biosystems Engineering*, 27, 2 (2005), 75–79. (cited on page 6)

El Youssef, J.; Castle, J.; and Ward, W. K., 2009. A review of closed-loop algorithms for glycemic control in the treatment of type 1 diabetes. *Algorithms*, 2, 1 (2009), 518–532. (cited on page 6)

Eren-Oruklu, M.; Cinar, A.; Quinn, L.; and Smith, D., 2009. Adaptive control strategy for regulation of blood glucose levels in patients with type 1 diabetes. *Journal of process control*, 19, 8 (2009), 1333–1346. (cited on page 6)

Fekri, S., 2005. *Robust Adaptive MIMO Control Using Multiple-Model Hypothesis Testing and Mixed-μ Synthesis*. Ph.D. thesis, Technical University of Lisbon. (cited on pages 3, 7, 22, 27, 48, 66, and 81)

Fekri, S.; Athans, M.; and Pascoal, A., 2006. Issues, progress and new results in robust adaptive control. *Int J Adapt Contr Signal Process*, 20, 10 (Dec 2006), 519–579. (cited on pages 13, 19, 22, 23, 48, 50, and 51)

Forssell, U.; Forssell, U.; Ljung, L.; and Ljung, L., 1997. Closed-loop identification revisited. *Automatica*, 35 (1997), 1215–1241. (cited on page 79)

Furutani, E.; Araki, M.; Kan, S.; Aung, T.; Onodera, H.; Imamura, M.; Shirakami, G.; and Maetani, S., 2004. An automatic control system of the blood pressure of patients under surgical operation. *International Journal of Control, Automation, and Systems*, 2, 1 (Mar 2004), 39–54. (cited on page 77)

Gentilini, A.; Rossoni-Gerosa, M.; Frei, C.; Wymann, R.; Morari, M.; Zbinden, A.; and Schnider, T., 2001. Modeling and closed-loop control of hypnosis by means of bispectral index (bis) with isoflurane. *Biomedical Engineering, IEEE Transactions on*, 48, 8 (2001), 874–889. (cited on page 5)

Girardin, C. M.; Huot, C.; Gonthier, M.; and Delvin, E., 2009. Continuous glucose monitoring: A review of biochemical perspectives and clinical use in type 1 diabetes. *Clinical Biochemistry*, 42, 3 (2009), 136 – 142. (cited on page 5)

Glass, P. S.; Bloom, M.; Kearse, L.; Rosow, C.; Sebel, P.; and Manberg, P., 1997. Bispectral analysis measures sedation and memory effects of propofol, midazolam, isoflurane, and alfentanil in healthy volunteers. *Anesthesiology*, 86, 4 (1997), 836–47. (cited on page 5)

Gu, D. W.; Petkov, P. H.; and Konstantinov, M. M., 2005. *Robust Control Design with Matlab*. Springer. (cited on page 19)

Guyton, A. C.; Coleman, T. G.; and Granger, H. J., 1972. Circulation: Overall regulation. *Annual Review of Physiology*, 34, 1 (1972), 13–44. (cited on page 27)

Hassani, V., 2012. *Multiple Model Robust Adaptive Estimation and Control*. Ph.D. thesis, Universidade Técnica de Lisboa, Instituto Superior Técnico, Lisbon, Portugal. (cited on pages 8, 48, 51, 54, 57, and 60)

Hassani, V.; Hespanha, J.; Athans, M.; and Pascoal, A. M., 2011. Stability analysis of robust multiple model adaptive control. In *Proceedings of The 18th IFAC World Congress*. Milan, Italy. (cited on page 48)

Hassani, V.; Sørensen, A. J.; Pascoal, A. M.; and Aguiar, A. P., 2012. Multiple model adaptive wave filtering for dynamic positioning of marine vessels. In *Proc. ACC'12 - American Control Conference*. Montreal, Canada. (cited on page 51)

He, W. G.; Kaufman, H.; and Roy, R., 1986. Multiple model adaptive control procedure for blood pressure control. *IEEE Transactions on Biomedical Engineering*, 33, 1 (Jan 1986), 10–19. (cited on pages 4, 12, 14, 15, 20, 24, and 27)

Heier, T. and Steen, P. A., 1996. Assessment of anaesthesia depth. *Acta Anaesthesiologica Scandinavica*, 40, 9 (1996), 1087–1100. (cited on page 30)

Hemmerling, T. M.; Arbeid, E.; Wehbe, M.; Cyr, S.; Taddei, R.; and Zaouter, C., 2013. Evaluation of a novel closed-loop total intravenous anaesthesia drug delivery system: a randomized controlled trial. *British Journal of Anaesthesia*, 110, 6 (2013), 1031–1039. (cited on page 5)

Hespanha, J.; Liberzon, D.; Morse, A. S.; Anderson, B. D. O.; Brinsmead, T. S.; and Bruyne, F. D., 2001. Multiple model adaptive control: Part II: Switching. *International Journal of Robust and Nonlinear Control*, 11 (2001), 479–496. (cited on pages 48 and 51)

Hoeksel, S. A.; Blom, J. A.; Jansen, J. R.; Maessen, J. G.; and Schreuder, J. J., 1999. Automated infusion of vasoactive and inotropic drugs to control arterial and pulmonary pressures during cardiac surgery. *Critical Care Medicine*, 27, 12 (Dec 1999), 2792–2798. (cited on pages 4 and 77)

Hol, J. D.; Schon, T. B.; and Gustafsson, F., 2006. On resampling algorithms for particle filters. In *IEEE Nonlinear Statistical Signal Processing Workshop*, 79–82. (cited on page 56)

Hornuss, C.; Wiepcke, D.; Praun, S.; Dolch, M. E.; Apfel, C. C.; and Schelling, G., 2012. Time course of expiratory propofol after bolus injection as measured by ion molecule reaction mass spectrometry. *Analytical and Bioanalytical Chemistry*, 403, 2 (Apr 2012), 555–561. (cited on page 31)

Hovorka, R.; Kumareswaran, K.; Harris, J.; Allen, J. M.; Elleri, D.; Xing, D.; Kollman, C.; Nodale, M.; Murphy, H. R.; Dunger, D. B.; Amiel, S. A.; Heller, S. R.; Wilinska, M. E.; and Evans, M. L., 2011. Overnight closed loop insulin delivery (artificial pancreas) in adults with type 1 diabetes: crossover randomised controlled studies. *British Medical Journal*, 342 (4 2011). (cited on page 6)

Ioannou, P. A., 2008. Robust adaptive control: The search for the holy grail. In *Proceedings of the 47th IEEE Conference on Decision and Control*, 12–13. (cited on page 3)

Isaka, S. and Sebald, A. V., 1993. Control strategies for arterial blood pressure regulation. *IEEE Transactions on Biomedical Engineering*, 40, 4 (1993), 353–363. (cited on page 12)

Jee, G.-I. and Roy, R. J., 1992. Adaptive control of multiplexed closed-circuit anesthesia. *IEEE Transactions on Biomedical Engineering*, 39, 10 (1992), 1071–1080. (cited on page 4)

Jelliffe, R. W.; Schumitzky, A.; Van Guilder, M.; Liu, M.; Hu, L.; Maire, P.; Gomis, P.; Barbaut, X.; and Tahani, B., 1993. Individualizing drug dosage regimens: roles of population pharmacokinetic and dynamic models, Bayesian fitting, and adaptive control. *Therapeutic Drug Monitoring*, 15, 5 (Oct 1993), 380–393. (cited on page 30)

Kamysek, S.; Fuchs, P.; Schwoebel, H.; Roesner, J. P.; Kischkel, S.; Wolter, K.; Loeseken, C.; Schubert, J. K.; and Miekisch, W., 2011. Drug detection in breath: effects of pulmonary blood flow and cardiac output on propofol exhalation. *Analytical and Bioanalytical Chemistry*, 401, 7 (Oct 2011), 2093–2102. (cited on pages 31, 34, and 35)

Khoo, M. C. K., 1999. *Physiological Control Systems*. John Wiley & Sons, Inc. (cited on page 1)

Krener, A., 2003. The convergence of the extended kalman filter. *Directions in Mathematical Systems Theory and Optimization*, (2003), 173–182. (cited on page 86)

Kuipers, M. and Ioannou, P., 2010. Multiple model adaptive control with mixing. *IEEE Transactions on Automatic Control*, 55 (2010), 1822–1836. (cited on pages 48, 51, and 63)

Lunze, K.; Singh, T.; Walter, M.; Brendel, M. D.; and Leonhardt, S., 2013. Blood glucose control algorithms for type 1 diabetic patients: A methodological review. *Biomedical Signal Processing and Control*, 8, 2 (2013), 107 – 119. (cited on page 6)

Magni, L., 2012. Model predictive control of type 1 diabetes. In *Proceedings of 4th IFAC Nonlinear Model Predictive Control Conference*, 99–106. (cited on page 6)

Malagutti, N., a. Open-loop real-time estimation of propofol pharmacokinetics-pharmacodynamics using particle filtering. Submitted October 2013, pending review. (cited on page 29)

Malagutti, N., b. Particle filter-based robust adaptive control for closed-loop administration of sodium nitroprusside. Submitted July 2013, final version submitted October 2013, awaiting publication. (cited on page 65)

Malagutti, N.; Dehghani, A.; and Kennedy, R., 2012a. Improved robust performance in a system for automatic administration of a vasoactive drug. In *Proceedings of BIOSTEC Biosignals Conference*. Portugal. (cited on page 68)

Malagutti, N.; Dehghani, A.; and Kennedy, R., 2012b. A robust multiple-model adaptive control system for automatic delivery of a vasoactive drug. In *Proceedings of the 9th IASTED International Conference on Biomedical Engineering*. Innsbruck, Austria. (cited on page 15)

Malagutti, N.; Dehghani, A.; and Kennedy, R. A., 2011. Safety issues in adaptive control systems for automatic administration of vasoactive drugs. In *Proceedings of 18th IFAC World Congress*. IFAC, Milan, Italy. (cited on page 12)

Malagutti, N.; Dehghani, A.; and Kennedy, R. A., 2013. Robust control design for automatic regulation of blood pressure. *IET Control Theory & Applications*, 7 (2013), 387–396(9). (cited on pages 11, 66, and 68)

Malagutti, N.; Hassani, V.; and Dehghani, A., 2012c. An adaptive multi-controller architecture using particle filtering. In *Proceedings of the 2012 Australian Control Conference.*, 392–398. Sydney, Australia. (cited on page 47)

Mansour, N. E. and Linkens, D. A., 1989. Pole-assignment self-tuning control of blood pressure in postoperative patients: a simulation study. *IEE Proceedings of Control Theory and Applications*, 136, 1 (jan 1989), 1–11. (cited on page 4)

Martin, J. F.; Schneider, A. M.; Mandel, J. E.; Prutow, R. J.; and Ty, S. N., 1986. A new cardiovascular model for real-time applications. *Transactions of the Society for Computer Simulation International*, 3, 1 (Jan 1986), 31–63. (cited on page 14)

Martin, J. F.; Schneider, A. M.; Quinn, M. L.; and Smith, N. T., 1992. Improved safety and efficacy in adaptive control of arterial blood pressure through the use of a supervisor. *IEEE Transactions on Biomedical Engineering*, 39, 4 (April 1992), 381–388. (cited on pages 14, 24, and 84)

Martin, J. F.; Schneider, A. M.; and Smith, N. T., 1987. Multiple-model adaptive control of blood pressure using sodium nitroprusside. *IEEE Transactions on Biomedical Engineering*, 34, 8 (August 1987), 603–611. (cited on pages 4, 12, 13, 20, 24, 27, 66, 89, and 90)

Masui, K.; Kira, M.; Kazama, T.; Hagihira, S.; Mortier, E. P.; and Struys, M. M., 2009. Early phase pharmacokinetics but not pharmacodynamics are influenced by propofol infusion rate. *Anesthesiology*, 111, 4 (Oct 2009), 805–817. (cited on page 45)

Meijers, R. H.; Schmartz, D.; Cantraine, F. R.; Barvais, L.; dHollander, A. A.; and Blom, J. A., 1997. Clinical evaluation of an automatic blood pressure controller during cardiac surgery. *Journal of Clinical Monitoring and Computing*, 13, 4 (1997), 261–268. (cited on pages 14 and 77)

Meline, L. J.; Westenskow, D. R.; Pace, N. L.; and Bodily, M. N., 1985. Computer-controlled regulation of sodium nitroprusside infusion. *Anesthesia & Analgesia*, 64, 1 (1985), 38–42. (cited on page 24)

Miekisch, W.; Fuchs, P.; Kamysek, S.; Neumann, C.; and Schubert, J. K., 2008. Assessment of propofol concentrations in human breath and blood by means of hs-spme-gc-ms. *Clinica Chimica Acta*, 395, 1-2 (2008), 32 – 37. (cited on page 5)

Nikolajsen, L. and Haroutiunian, S., 2011. Intravenous patient-controlled analgesia for acute postoperative pain. *European Journal of Pain Supplements*, 5, 2 (2011), 453 – 456. (cited on page 2)

Pajunen, G. A.; Steinmetz, M.; and Shankar, R., 1990. Model reference adaptive control with constraints for postoperative blood pressure management. *IEEE Transactions on Biomedical Engineering*, 37, 7 (1990), 679–687. (cited on pages 4 and 14)

Parker, R. S. and Doyle, F. J., 2001. Control-relevant modeling in drug delivery. *Advanced Drug Delivery Reviews*, 48 (2001), 211 – 228. (cited on page 84)

Parker, R. S.; Doyle, F. J.; Ward, J. H.; and Peppas, N. A., 2000. Robust h-inf glucose control in diabetes using a physiological model. *AIChE Journal*, 46, 12 (2000), 2537–2549. (cited on page 6)

Petre, J. H.; Cosgrove, D. M.; and Estafanous, F. G., 1983. Closed loop computerized control of sodium nitroprusside. *Transactions American Society for Artificial Internal Organs*, 29 (1983), 501–505. (cited on page 24)

Rao, R. R.; Aufderheide, B.; and Bequette, B. W., 2003. Experimental studies on multiple-model predictive control for automated regulation of hemodynamic variables. *IEEE Transactions on Biomedical Engineering*, 50, 3 (Mar 2003), 277–288. (cited on pages 4 and 28)

Ritchie, R. G.; Ernst, E. A.; Pate, B. L.; Pearson, J. D.; and Sheppard, L. C., 1987. Closed-loop control of an anesthesia delivery system: development and animal testing. *IEEE Transactions on Biomedical Engineering*, 34, 6 (1987), 437–43. (cited on page 4)

Russell, I. F., 2007. A similar bis value does not mean a similar depth of anaesthesia. *British Journal of Anaesthesia*, 99, 4 (2007), 592–593. (cited on page 5)

Russell, I. F., 2013. The ability of bispectral index to detect intra-operative wakefulness during total intravenous anaesthesia compared with the isolated forearm technique. *Anaesthesia*, 68, 5 (2013), 502–511. (cited on page 5)

Saeed, M.; Villarroel, M.; Reisner, A. T.; Clifford, G.; Lehman, L.-W.; Moody, G.; Heldt, T.; Kyaw, T. H.; Moody, B.; and Mark, R. G., 2011. Multiparameter intelligent monitoring in intensive care ii (mimic-ii): A public-access intensive care unit database. *Critical Care Medicine*, 39 (May 2011), 952–960. (cited on pages 14 and 85)

Safonov, M. G. and Tsao, T. C., 1997. The unfalsified control concept and learning. *IEEE Transactions on Automatic Control*, 42 (1997), 843–847. (cited on page 48)

Schiller, G. J. and Maybeck, P. S., 1997. Control of a large space structure using MMAE/MMAC techniques. *IEEE Transactions on Aerospace and Electronic System*, 33 (1997), 1122–1131. (cited on pages 48 and 51)

Schnider, T. W.; Minto, C. F.; Shafer, S. L.; Gambus, P. L.; Andresen, C.; Goodale, D. B.; and Youngs, E. J., 1999. The influence of age on propofol pharmacodynamics. *Anesthesiology*, 90, 6 (1999), 1502–1516. (cited on page 30)

Schon, T.; Gustafsson, F.; and Nordlund, P.-J., 2005. Marginalized particle filters for mixed linear/nonlinear state-space models. *IEEE Transactions on Signal Processing*, 53, 7 (2005), 2279–2289. doi:10.1109/TSP.2005.849151. (cited on pages 52 and 56)

Schon, T. B.; Gustafsson, F.; and Karlsson, R. ., 2011. The particle filter in practice. In *The Oxford Handbook of Nonlinear Filtering* (Eds. D. Crisan and B. Rozovskii). Oxford University Press, London. (cited on page 49)

Schuttler, J. and Ihmsen, H., 2000. Population pharmacokinetics of propofol: a multicenter study. *Anesthesiology*, 92, 3 (Mar 2000), 727–738. (cited on pages 31, 33, and 34)

Sheppard, L., 1980. Computer control of the infusion of vasoactive drugs. *Annals of Biomedical Engineering*, 8, 4-6 (1980), 431–444. (cited on page 4)

Skogestad, S. and Postlethwaite, I., 2006. *Multivariable Feedback Control, Analysis and Design*, chap. 8, 309–368. Wiley. (cited on pages 50 and 74)

Slate, J. B.; Sheppard, L. C.; Rideout, V. C.; and Blackstone, E. H., 1979. A model for design of a blood pressure controller for hypertensive patients. In *Proceedings of the first annual conference, IEEE Engineering in Medicine and Biology Society*. Denver, Colorado. (cited on pages 12, 13, 14, and 89)

Steil, G. M.; Rebrin, K.; Darwin, C.; Hariri, F.; and Saad, M. F., 2006. Feasibility of automating insulin delivery for the treatment of type 1 diabetes. *Diabetes*, 55, 12 (2006), 3344–3350. (cited on page 6)

Stern, K. S.; Chizeck, H. J.; Walker, B. K.; Krishnaprasad, P. S.; Dauchot, P. J.; and Katona, P. G., 1985. The self-tuning controller: comparison with human performance in the control of arterial pressure. *Annals of Biomedical Engineering*, 13, 5 (1985), 341–357. (cited on page 24)

Struys, M.; Versichelen, L.; Byttebier, G.; Mortier, E.; Moerman, A.; and Rolly, G., 1998. Clinical usefulness of the bispectral index for titrating propofol target effect-site concentration. *Anaesthesia*, 53, 1 (1998), 4–12. (cited on page 30)

Struys, M. M.; De Smet, T.; Versichelen, L. F.; Van De Velde, S.; Van den Broecke, R.; and Mortier, E. P., 2001. Comparison of closed-loop controlled administration of propofol using bispectral index as the controlled variable versus 'standard practice' controlled administration. *Anesthesiology*, 95 (2001), 6–17. (cited on page 5)

Takita, A.; Masui, K.; and Kazama, T., 2007. On-line monitoring of end-tidal propofol concentration in anesthetized patients. *Anesthesiology*, 106, 4 (Apr 2007), 659–664. (cited on pages 31, 34, and 40)

Uemura, K.; Kamiya, A.; Hidaka, I.; Kawada, T.; Shimizu, S.; Shishido, T.; Yoshizawa, M.; Sugimachi, M.; and Sunagawa, K., 2006. Automated drug delivery system to control systemic arterial pressure, cardiac output, and left heart filling pressure in acute decompensated heart failure. *Journal of Applied Physiology*, 100, 4 (2006), 1278–1286. (cited on page 4)

Van Leeuwen, P. J., 2009. Particle filtering in geophysical systems. *Monthly Weather Review*, 137, 12 (2009), 4089–4114. (cited on page 49)

Varon, J. and Marik, P. E., 2008. Perioperative hypertension management. *Vascular Health and Risk Management*, 4, 3 (2008), 615–627. (cited on pages 4, 12, and 28)

Wiczling, P.; Bienert, A.; Sobczynski, P.; Hartmann-Sobczynska, R.; Bieda, K.; Marcinkowska, A.; Malatynska, M.; Kaliszan, R.; and Grzeskowiak, E., 2012. Pharmacokinetics and pharmacodynamics of propofol in patients undergoing abdominal aortic surgery. *Pharmacological Reports*, 64, 1 (2012), 113–122. (cited on pages 31, 32, 33, 34, 38, and 44)

Woodruff, E. A.; Martin, J. F.; and Omens, M., 1997. A model for the design and evaluations of algorithms for closed-loop cardiovascular therapy. *IEEE Transactions on Biomedical Engineering*, 44, 8 (August 1997), 694–703. (cited on page 83)

Ying, H. and Sheppard, L. C., 1994. Regulating mean arterial pressure in postsurgical cardiac patients. a fuzzy logic system to control administration of sodium nitroprusside. *Engineering in Medicine and Biology Magazine, IEEE*, 13, 5 (1994), 671–677. (cited on page 4)

Yu, C.; Roy, R. J.; Kaufman, H.; and Bequette, B. W., 1992. Multiple-model adaptive predictive control of mean arterial pressure and cardiac output. *IEEE Transactions on Biomedical Engineering*, 39, 8 (Aug 1992), 765–778. (cited on page 4)

Yu, Y. C., 2006. Blood pressure, automatic control of. In *Encyclopedia of Medical Devices and Instrumentation* (Ed. J. G. Webster), 490–500. John Wiley & Sons, Inc., 2nd edn. ISBN 9780471732877. doi:10.1002/0471732877.emd039. (cited on page 12)

Zenker, S.; Rubin, J.; and Clermont, G., 2007. From inverse problems in mathematical physiology to quantitative differential diagnoses. *PLoS Computational Biology*, 3, 11 (2007), e204. (cited on pages 49, 79, and 84)

Zhou, K.; Doyle, J. C.; and Glover, K., 1995. *Robust and Optimal Control*. Prentice-Hall. (cited on pages 6 and 18)